Techniques for Measuring Supply System Impedances

by

Shijia Zhang

A thesis submitted in partial fulfillment of the requirements for the degree of

Master of Science

in

Energy Systems

Department of Electrical and Computer Engineering
University of Alberta

Abstract

The Thevenin circuit impedance of the supply system is an important data for both utility companies and their customers. The data has many uses, such as calculating short-circuit currents, verifying models of power system networks, and establishing protective relay settings. The impedance data is typically obtained using model-based short-circuit calculations. The accuracy of the results highly depends on the quality of input data and the status of equipment used in the model. This limitation has resulted in a need to develop methods that can measure supply system impedances. In this thesis, a set of novel and practical methods has been developed for impedance measurement using the waveform data collected at the customer-utility interface point.

The first technique is to use natural disturbances produced by customer loads for impedance estimation. It consists of two methods: one is the large-disturbance-based method (LD method) and the other is the small-disturbance-based method (SD method). A detection scheme was proposed for the combined and individual use of the two methods.

For sites that lack natural disturbances, a method that injects intentional disturbances for impedance estimation is proposed. This technique consists of two components: one component is a portable thyristor-based device, which is used for generating active disturbances; and the other component is the active-disturbance-based method (AD method) for impedance estimation. Statistical theories and signal processing techniques are utilized to develop the method.

Finally, the above passive and active methods are combined to form an integrated impedance measurement tool. The methods proposed in this thesis have been verified using simulation studies and extensive field data. The results show that the proposed methods can serve as useful tools to support the supply system impedance measurement task.

Preface

This thesis is an original work by Shijia Zhang. No part of this thesis has been previously published.

Acknowledgments

I really appreciate my supervisor, Professor Wilsun Xu, for giving me so much guidance and help during my MSc program. The way of thinking, the attitude towards doing things and the professional knowledge I have learned from him will all significantly benefit my future career and life.

I feel lucky to have worked with my colleagues in the PDS-LAB and I thank them for their help and company: Tianyu Ding, Bo Gao, Xi Wang, Yang Wang, Conghui Wei and Xin Li.

I would also like to acknowledge CANDURA Instruments for providing the field test validation opportunity for this research.

I dedicate this thesis to my parents, Mr. Zhaobin Zhang and Mrs. Meixian Dai, and to my girlfriend, Sijia Ye. Words cannot express how grateful I am for their love and support.

Table of Contents

List of Tables

List of Figures

List of Abbreviations

PCC	Point of Common Coupling
FFT	Fast Fourier Transform
ICA	Independent Components Analysis
DG	Distributed Generation
PQ	Power Quality
LD	Large-Disturbance-Based
SD	Small-Disturbance-Based
AD	Active-Disturbance-Based
MAM	Moving Average Method
RMS	Root Mean Square
L-G	Line to Ground
L-L	Line to Line
CPU	Central Processing Unit
N/A	Not Applicable
PLL	Phase-Lock-Loop

Chapter 1 Introduction

The Thevenin circuit impedance of the supply system is an important data for both utility companies and their customers. The data has many uses, such as calculating short-circuit currents, verifying models of power system networks, and establishing protective relay settings [1]. The impedance data is typically obtained using model-based short-circuit calculations. The accuracy of the results highly depends on the quality of input data and the status of equipment used in the model. As a result, utility companies have been looking for methods that can measure the actual system impedance at a given point in a power system. In recent years, this need has become more evident due to the concerns about power quality and the proliferation of distributed generators. The objective of this thesis is to provide feasible methods for measuring the supply system impedance.

This introductory chapter starts with an overview of system impedance measurement. Next, the existing methods of system impedance measurement are discussed. Finally, the scope and outline of this thesis are presented.

1.1 Supply System Impedance Measurement

The following section first defines the problem of system impedance measurement, and then technical challenges are presented.

1.1.1 Problem Definition

The problem of system impedance measurement to be solved by this research can be understood with the help of Figure 1.1-1.2. Figure 1.1 shows a customer's distribution system connected to the utility supply system at the service entrance point called point of common coupling (PCC). The equivalent circuit of this system is presented in Figure 1.2.

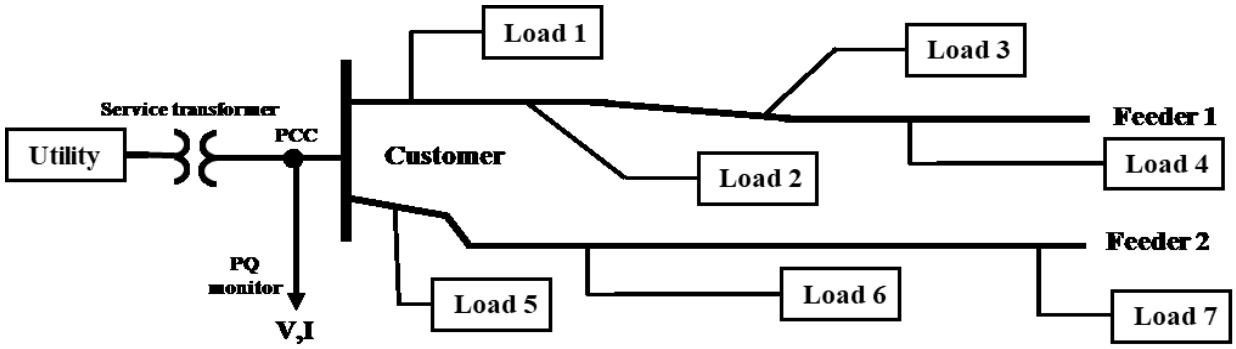

Figure 1.1 Typical distribution system

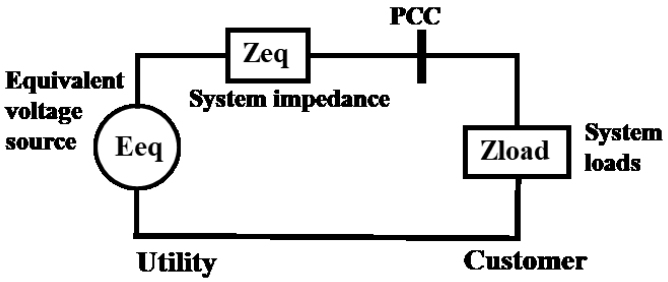

Figure 1.2 Equivalent circuit

The supply system impedance Z_{eq} is typically obtained using model-based short-circuit calculations. The accuracy of the results highly depends on the quality of input data and the status of equipment used in the model. There is always a need by the supply utility company to make sure the correct impedance data is used for facility design. Therefore, a method that can measure the impedance is desired. The objective of this research is to develop a set of methods to estimate the fundamental frequency equivalent system impedance Z_{eq} based on the voltage and current waveforms measured at PCC. The target PCCs have voltages up to 10 kV. The associated customers are those connected to utility distribution systems (10 kV to 66 kV).

The basic theory of system impedance measurement deals with analyzing the network voltage and current responses to downstream disturbances. The equivalent circuit of the distribution system for illustrating the basic theory is shown in Figure 1.3. The circuit reveals two variables in the equivalent circuit: one is E_{eq}, which is the equivalent voltage source; and

the other is Z_{eq}, which is the equivalent source impedance. Z_{eq} is the variable to be estimated. Since the upstream is a Thevenin circuit, Z_{eq} cannot be determined by using the following simple mathematical operation:

$$Z = \frac{V}{I} \tag{1.1}$$

where V and I are the voltage and current phasors measured at the monitoring point. In fact, Z represents the equivalent downstream load impedance, not the equivalent network impedance Z_{eq}, i.e., $Z_{eq} \neq Z$.

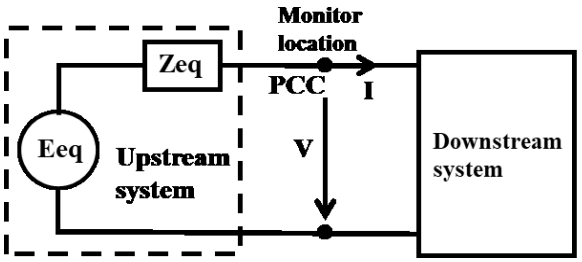

Figure 1.3 Equivalent circuit for illustrating the basic theory

Since there are two unknowns, E_{eq} and Z_{eq}, in the upstream circuit, two equations are needed to solve for Z_{eq}. To create these two equations, two measurement instants are required. In addition, the following conditions must be satisfied: one condition is that the downstream loads have some variations; and the other condition is that the upstream side is constant during this period. At cycle t_1, V_1 and I_1 phasors are measured; and at cycle t_2, V_2 and I_2 phasors are measured. The following equations can, therefore, be established.

$$\begin{aligned} E_{eq} &= Z_{eq} I_1 + V_1 \\ E_{eq} &= Z_{eq} I_2 + V_2 \end{aligned} \tag{1.2}$$

Solving the above equations leads to

$$Z_{eq} = -\frac{V_2 - V_1}{I_2 - I_1} = -\frac{\Delta V}{\Delta I} \tag{1.3}$$

In summary, a disturbance on voltage and current quantities at the measuring point is required to estimate the equivalent network impedance. The disturbance can only be caused by downstream loads or equipment.

1.1.2 Technical Challenges

Although the theory of system impedance measurement is straightforward, several theoretical and implementation problems must be solved. Three major challenges are discussed below.

The first challenge is frequency and synchronization issues. In theory, system impedances should be measured at the fundamental frequency, which is 60Hz in North America power systems. However, system frequency is not always exactly constant as 60Hz. Therefore, the phase angle's errors caused by frequency issues should be considered when applying the fast fourier transformation (FFT) algorithm. In addition, the calculation of system impedance is phasor-based, so how to synchronize the data measured at two cycles (t_1 and t_2) is an important issue. This problem can be better clarified using Figure 1.4.

Figure 1.4 shows an example of raw waveform data that is typically collected by a PQ monitor.

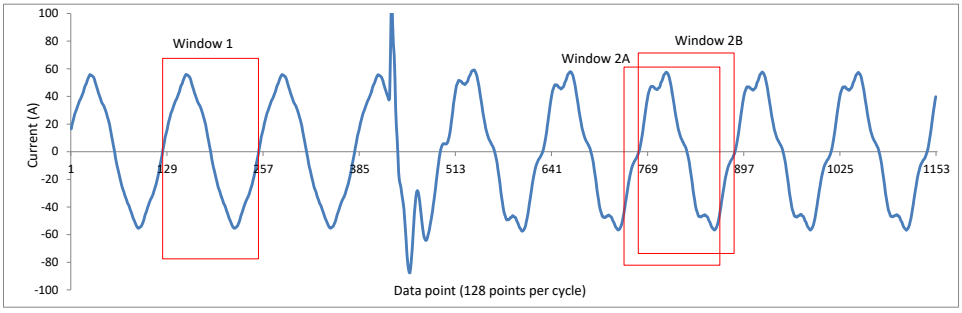

Figure 1.4 Selection of the correct post-disturbance data

As shown in Figure 1.4, there is a disturbance around the fourth cycle. Data in window 1 can be converted into the pre-disturbance phasor data using FFT. Data in window 2A or 2B could be processed to serve as the post-disturbance phasor data. It can be seen that window 2A and 2B will yield different phasor results. Therefore, how to position windows properly so that phasors are referred (or synchronized) to the same reference time is a problem.

The second challenge is how to identify voltage/current variations caused by disturbances from the downstream system. If disturbances come from the upstream system, voltage/current variations at the measuring point reflect the response of the downstream system, and analyzing these variations can only yield parameters of the load side. Therefore, only downstream disturbances should be used for system impedance estimation.

The third challenge is how to determine the degree and frequency of voltage/current variations caused by downstream disturbances that are adequate for impedance estimation. Different customers have different fluctuation levels. Voltage/current variations caused by downstream disturbances might be either sufficiently large or inadequate for the use of system impedance estimation algorithms. Thus, unified indicators are needed to guarantee the reliability of the estimated results. Also, there are various kinds of downstream disturbances in power systems, and their characteristics are different. Proper methods should be used to detect and proceed with certain disturbances that are suitable for system impedance estimation.

1.2 Overview of Existing Measurement Techniques

After many years of research efforts, two broad approaches for measuring the supply system impedance have been proposed: passive methods and active methods. Passive methods use natural disturbances in power systems. The natural disturbances mainly include variations of downstream loads and events of switching on/off downstream equipment such as shunt capacitors, motors, and lines. Active methods employ the injection of intentional disturbances to the power system. The disturbances can be generated by connecting specific devices or switching existing electric components manually.

Several passive methods have been proposed in the literature. The methods in [2] and [3] use the events of switching on/off shunt capacitors to estimate the system impedance. Capacitor switching events, however, rarely occur in power system operations. As a result, the scope

of methods in [2] and [3] is very limited. Compared to the events of switching on/off shunt capacitors, the fluctuation of downstream loads through time is much more common. Therefore, researchers pay attention to the more effective source of disturbances, which is the natural variation of downstream loads. The method proposed in [4] employs real number-based regression algorithms to estimate system impedance. The approaches in [5] and [6] use the basic algorithm as shown in (1.3) and focus on synchronization issues of continuous measurement along with the solutions. If, however, there are background variations from the system side, the methods in [4]-[6] are likely to provide poor results. The methods in [7] and [8] try to deal with this problem by evaluating the covariance characteristic of the random vector and adding the process of data selection. Nevertheless, their methods are still not robust, and practical cases used for verification are ideal. [9] and [10] use independent components analysis (ICA) to calculate harmonic impedance by assuming current sources in both the load side and the system side. Since the load side generally does not have a voltage/current source in the fundamental frequency, the assumptions of the proposed method are not valid anymore for the measurement of the fundamental frequency impedance. Therefore, for passive system impedance measurement, a more robust and efficient method is desired.

Also, some specific active methods have been proposed in the literature. The methods proposed in [11] and [12] introduce the techniques of creating intentional disturbances for system impedance measurement by switching existing electrical components. Switching existing electric components in power systems manually, however, is too complex, and this method will put too much pressure on the operation of power systems. Therefore, using separate devices to inject disturbances seems to be a better option. For example, the method in [13] proposed to inject currents into power systems for impedance measurements by using an inverter. Similarly, methods in [14] and [15] use converters for measuring the supply impedances at the distributed generation (DG) interconnection sites. Also, the method in [16] and [20] proposed a thyristor-based device to inject intentional disturbances at the measuring point by creating a small short circuit around the zero-crossing point.

Compared to passive methods, active methods could adjust disturbance energy to improve measurement accuracy for different system conditions and locations. Existing active methods, however, are still too costly with heavy and large-sized devices. Also, the use of these devices is complex and lacks flexibility. Table 1.1 is presented as follows to better illustrate the characteristics of passive methods and active methods.

Table 1.1: Comparison of passive methods and active methods

Name	Advantages	Disadvantages
Passive methods	No impact on the distribution system	Relatively low accuracy
	Flexible and convenient to use	Relatively low efficiency
	Low cost	
Active methods	High accuracy	Affect the distribution system
	More reliable results	Relatively complex to use
		Relatively high cost

1.3 Thesis Scope and Outline

This thesis aims to establish solutions for the supply system impedance measurement problem by using different disturbances and to develop an integrated system impedance measurement system. The following tasks are accomplished in this research:

- A technique of estimating the system impedance using naturally occurring downstream disturbances is proposed. One of the contributions is to combine two methods where each of them deals with large disturbances and small disturbances, respectively. Another contribution is the use of negative sequence components for (small disturbance based) impedance determination. Compared to existing passive methods, the proposed technique is more robust and has a wider range of applications.

- A technique of estimating the system impedance using intentionally injected downstream disturbances is proposed. This technique is intended for customer facilities that have very little load fluctuations. The main idea is to use a portable thyristor-based device to create a controlled short-circuit downstream and extract the impedance based on this unique disturbance. The novelty of this work is that the signal injection device can be located in any locations downstream of PCC. Compared to existing active methods, the proposed technique is more flexible to use with a portable low-cost disturbance generator.

- An integrated impedance measurement system is established by combining the previous two techniques. The system consists of software embedded with algorithms and a portable thyristor-based device. This system is designed to estimate the supply system impedance at the PCC by inputting the waveform data collected by power quality (PQ) monitors.

The remainder of the thesis is organized as follows:

Chapter 2 describes the proposed method for passive system impedance measurement in detail. The proposed method mainly consists of two components: the LD method and the SD method. Practical issues encountered in the field are discussed along with proposed solutions. Finally, the LD method and the SD method are combined through a detection scheme.

Chapter 3 presents the assessment results when the proposed passive method is tested using extensive lab and field tests. The estimated results are verified directly or indirectly by comparing them with those determined from other sources. In addition, the performance characteristics of the proposed passive method are analyzed and summarized.

Chapter 4 describes the proposed method for active system impedance measurement in detail. A novel measurement scheme by connecting portable thyristor-based devices into downstream sockets to inject specific disturbance signals is proposed. The AD method,

which estimates system impedance by utilizing injected disturbances, is clarified. Practical issues encountered in the field are investigated along with proposed solutions. Finally, the proposed method is summarized in a step-by-step procedure.

Chapter 5 documents performance studies for the proposed active method. The assessments are done through computer simulations with practical settings for parameters. The existing method in [20] and the proposed method are compared.

Chapter 6 presents an integrated impedance measurement system, which consists of software embedded with algorithms and a portable device. How to combine passive and active methods is explained and the prototype device is designed.

Chapter 7 summarizes the main conclusions of this study and makes recommendations for future research.

Chapter 2 Methods for Passive System Impedance Measurement

For passive system impedance measurement, natural disturbances in the network are used for estimation. In practical systems, there are mainly two types of natural disturbances. One type is the events of switching on/off typical electrical equipment accompanied by large transients, such as motor starting and capacitor switching. For this type of disturbance, pre-disturbance steady-state cycles and post-disturbance steady-state cycles are used to estimate the system impedance, which is called the large-disturbance-based method (LD method) in this thesis. The other type is smaller but more frequent disturbances caused by natural load variations. For this type of disturbance, a statistical method is used to estimate system impedance. It is named the small-disturbance-based method (SD method).

2. 1 Large-Disturbance-Based Method

Capacitor switching and motor starting are two important disturbances for passive system impedance measurement. These two events are not difficult to be detected and the frequency of occurrence may be high depending on the type of customers. More importantly, these two events can cause significant variations in voltage and current. The system-side variation is generally much smaller than these types of load-side disturbances with respect to magnitude. Thus, it can be assumed that the system side is constant during the measurement period. Therefore, for motor starting or capacitor switching cases, (1.3) with some modifications can be used to estimate system impedance.

2.1.1 Basic Algorithm

Supply system impedance is the fundamental frequency source impedance seen from the measuring point. For its measurement, both steady-state pre-disturbance cycles and post-

disturbance cycles of three-phase voltage and current waveforms should be selected first. The selection methods will be discussed in section 2.3. Next, the fundamental frequency quantities can be obtained by implementing FFT on the chosen cycles. In addition, voltages and currents may have considerable imbalances in the three-phase system, which will lead to inaccurate results of impedance estimation. In order to avoid this situation, the sequence transformation is used to convert the voltage and current phasors into the positive, negative and zero-sequence quantities as follows.

$$\begin{bmatrix} G_+ \\ G_- \\ G_0 \end{bmatrix} = \frac{1}{3}\begin{bmatrix} 1 & \alpha & \alpha^2 \\ 1 & \alpha^2 & \alpha \\ 1 & 1 & 1 \end{bmatrix}\begin{bmatrix} G_a \\ G_b \\ G_c \end{bmatrix} \tag{2.1}$$

where $\alpha = e^{j2\pi/3}$ and G can be either a voltage or current phasor. The desirable disturbances are generally caused by three-phase inductor motors or capacitor banks where positive-sequence quantities dominate. Thus, only the positive-sequence quantities are used.

In order to minimize error, (1.3) is modified as follows. Positive-sequence quantities of 10 cycles before disturbance are averaged to be pre-disturbance quantities V_1, I_1. Positive-sequence quantities of the i^{th} cycle after disturbance is used as post-disturbance quantities $V_2(i)$, $I_2(i)$. The impedances are then calculated by using (2.2).

$$Z(i) = -\frac{V_1 - V_2(i)}{I_1 - I_2(i)},\ i = 1,2,\mathrm{L}\ ,100 \tag{2.2}$$

Figure 2.1 is presented as follows for a better illustration of (2.2). The reduction of the results of (2.2) into one final estimated value is discussed later in section 2.1.2.

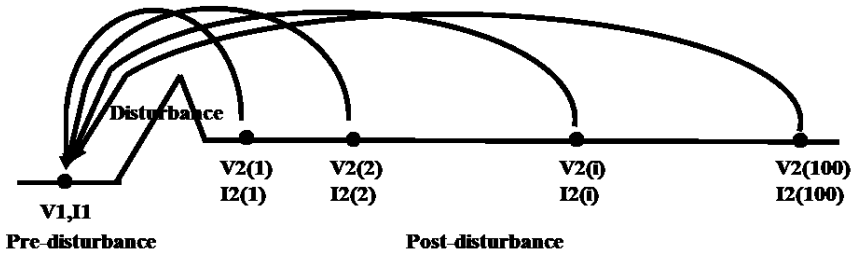

Figure 2.1 Selection of the correct post-disturbance data

To further illustrate the theory of the LD method, a simulation case is built by MATLAB Simulink as shown in Figure 2.2. For this simulation case, a small load is supplied by an 11 kV feeder and an 11 kV-Yg/575 V-Yg transformer. An induction motor and a capacitor bank are also connected through contactors. The detailed parameters of components in simulation and the reference value of system impedance at the transformer's secondary side are listed in Table 2.1. The reference value is obtained by adding the internal impedance of the source feeder and the equivalent impedance of the transformer.

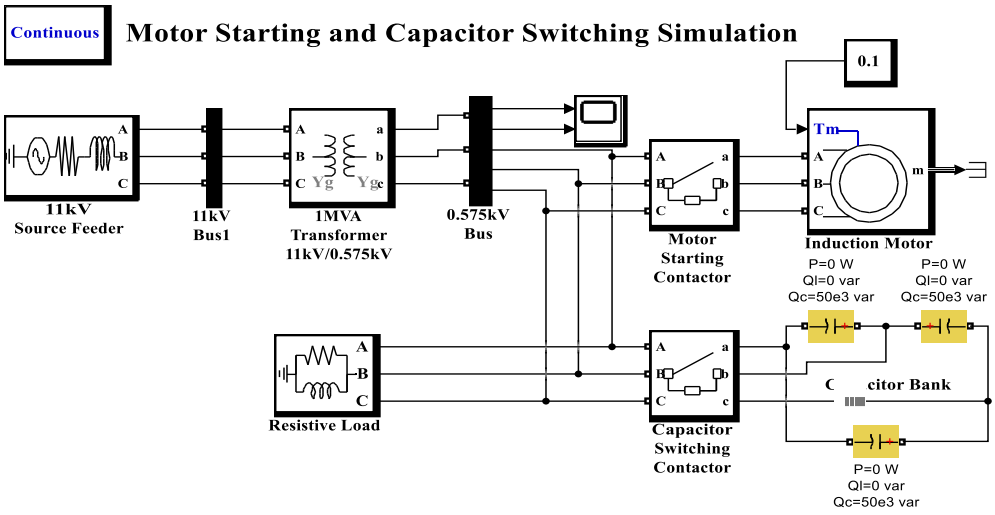

Figure 2.2 Overview of the simulation system

Table 2.1: Parameters of components in simulation

No.	Name	Parameter
1	Induction motor	100 HP 575 V 60 Hz 1780 RPM
2	Capacitor bank	575 V 150 kVar
3	11 kV source feeder	0.2+2j Ohms
4	Transformer	1 MVA
5	Load	500 kW + 300 kVar
6	The reference value of system impedance	0.0319 Ohms

1) Motor-starting simulation. At first, the induction motor and the capacitor bank are both disconnected. After 0.1 s, the induction motor is connected and started. Three-phase voltage and current waveforms at the service transformer's secondary side are shown in Figure 2.3.

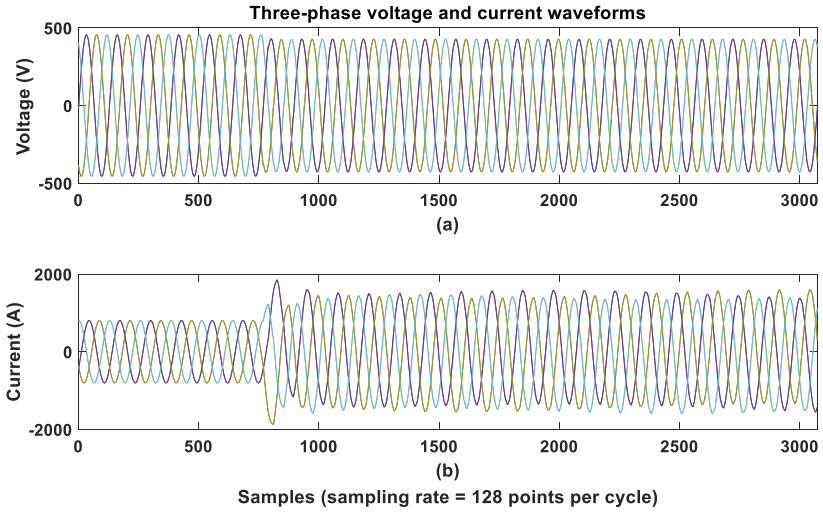

Figure 2.3 Three-phase voltage and current waveforms

The estimated results of the LD method are shown in Figure 2.4. The averaged value of the estimated system impedance is 0.0319 Ohms, which is consistent with the reference value. The induction motor's model is not very accurate, so waveforms are not perfectly stable. However, some subtle fluctuations of results do not influence the accuracy.

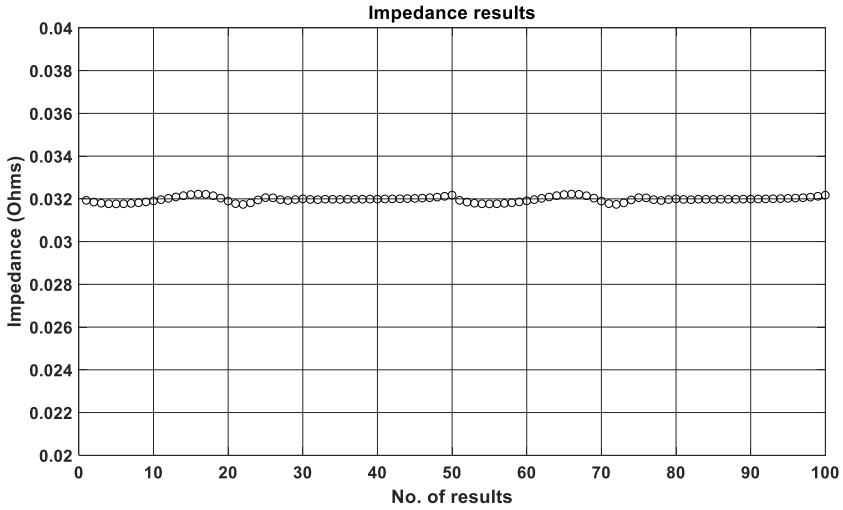

Figure 2.4 Impedance results of the LD method

2) Capacitor-switching simulation. Similarly, the induction motor and the capacitor bank are disconnected first. After 0.1 s, the capacitor bank is connected. Three-phase voltage and current waveforms are presented in Figure 2.5.

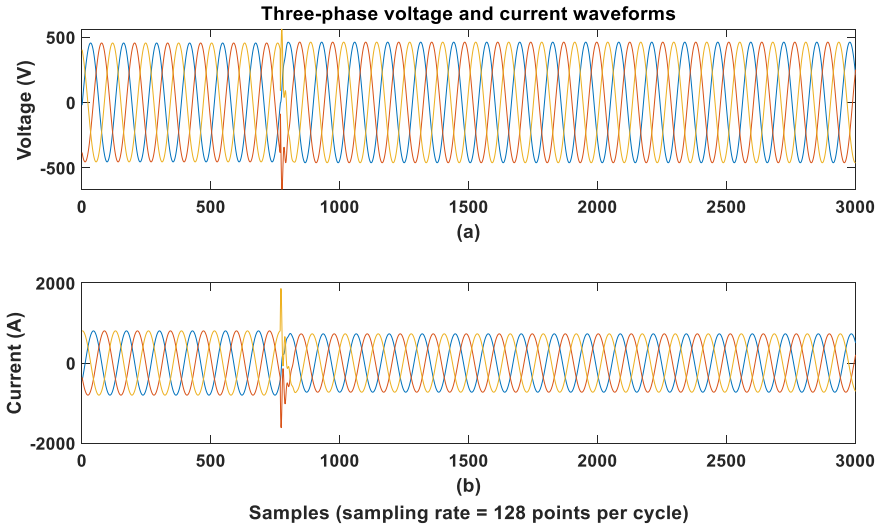

Figure 2.5 Three-phase voltage and current waveforms

Impedance results are shown in Figure 2.6. The averaged value of the estimated system impedance is 0.0319 Ohms, which is consistent with the reference value. From the results of the above two case studies, the LD method performs well on simulated events of motor starting and capacitor switching.

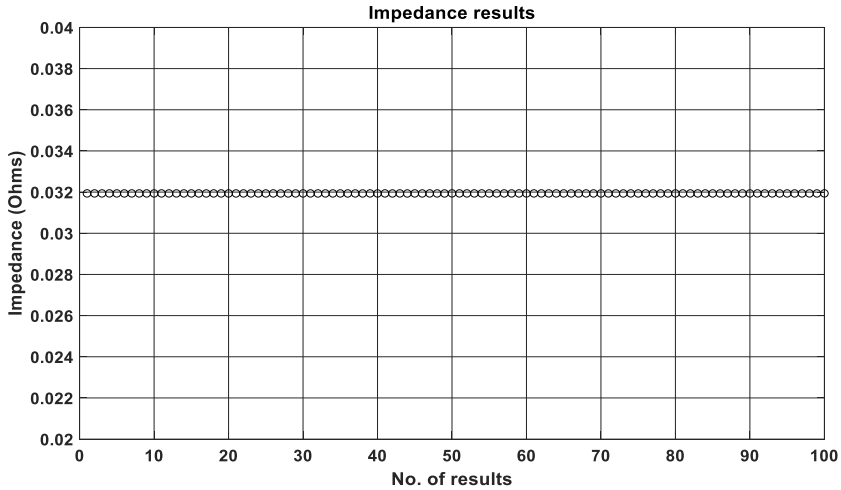

Figure 2.6 Impedance results of the LD method

2.1.2 Practical Considerations

For practical use, the following issues need to be considered to avoid erroneous results.

1) Frequency. In practice, system frequency is not always perfectly constant and may vary with time. However, after investigating several practical cases, it has been found that system frequency variation is always insignificant for a long period and large changes are not frequent. The proposed method uses no more than 100 consecutive cycles, which is much smaller than the period of significant changes within system frequency [6]. It is possible that chosen cycles may contain large changes of frequency by coincidence, but this misleading result can be detected and removed by the results reliability test, which will be discussed in section 2.1.2. Therefore, it is reasonable to assume that the frequency is constant in the process of synchronization.

The other concern is phase angle drift. The slip between real system frequency (e.g., 59.9 Hz) and sampling frequency of PQ monitors (e.g., 60 Hz) may result in a drift of measured phase angles. Figure 2.7 illustrates such a scenario. As shown in Figure 2.7, the frequency is not exactly 60 Hz, and an obvious phase angle drift exists. This will result in large errors between measured phase angles and real phase angles. Therefore, a feasible method for phase angle drift correction is proposed as follows.

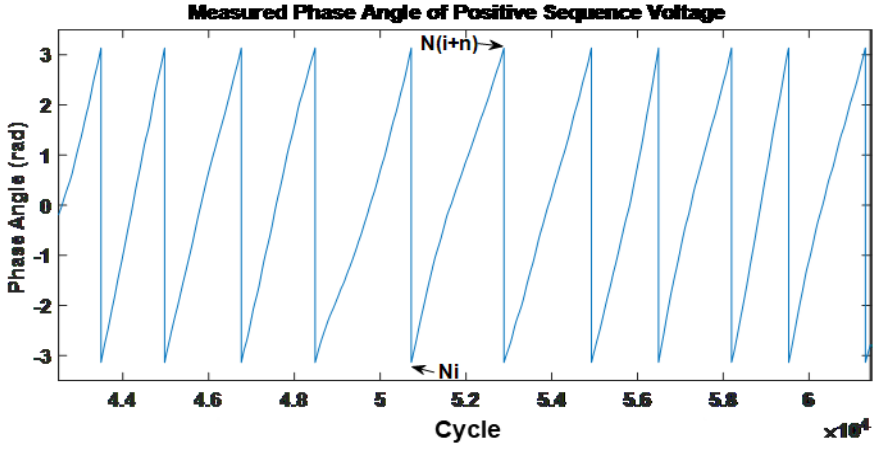

Figure 2.7 Measured phase angle of positive-sequence voltage

The method can be explained by using Figure 2.8. A and C are pre-disturbance and post-disturbance cycles respectively. B is the cycle where a disturbance occurs and the phase angle change can be caused by motor-starting events. Cycles between A and B are selected to estimate phase angle shift per cycle, as shown in (2.3).

$$Phase\ angle\ shift\ per\ cycle = \frac{\pi - 2.7693}{N_2 - N_1}\ rad \tag{2.3}$$

Next, the phase angle drift between B (before motor starting) and C (after motor starting) can be calculated using (2.4). Finally, the measured phase angle of C is compensated by the calculated phase angle drift, as shown in (2.5).

$$Phase\ angle\ shift\ between\ B\ and\ C = (N - N_2) \times \frac{\pi - 2.7693}{N_2 - N_1}\ rad \tag{2.4}$$

$$|\mathrm{V}|e^{j\theta_{corrected}} = |\mathrm{V}|e^{j\theta_{measured}} \times e^{j(N-N_2)\times\frac{\pi-2.7693}{N_2-N_1}} \tag{2.5}$$

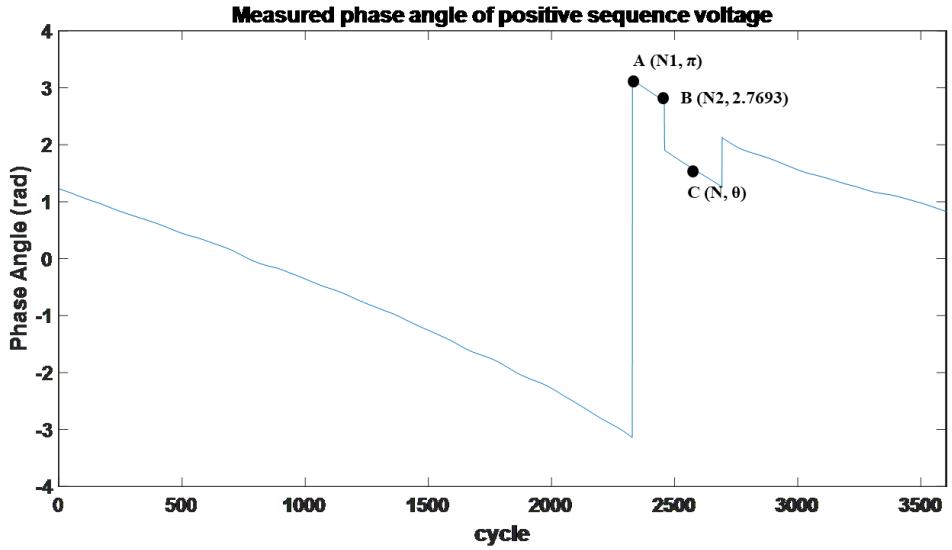

Figure 2.8 Illustrative figure to clarify the proposed phase angle drift correction method

2) The threshold of voltage change. The second issue is the level of voltage change caused by motor-starting or capacitor-switching events. It is possible that the fluctuations and noise of the system may overwhelm the voltage changes caused by the disturbance in some cases. This may occur if the system capacity is much larger than the disturbance source. Therefore, the size of voltage change ρ_v must be larger than a certain threshold δ, as shown in (2.6).

$$\rho_v = \left|\frac{V_2 - V_1}{V_1}\right| > \delta, \tag{2.6}$$

Where V_2 is the averaged value of 10 post-disturbance voltage phasors' magnitudes; and V_1 is the averaged value of 10 pre-disturbance voltage phasors' magnitudes.

How to determine the threshold δ is explained as follows. Different systems have different noise levels that are closely related to the threshold δ. For example, if noise levels are higher, the threshold δ should be larger. Therefore, a statistical index ρ_E called system variation level is defined in (2.7) to evaluate the fluctuations and noise of the system.

$$\rho_E = \frac{\sqrt{\sum_{i=1}^{n} \frac{(V_i - \sum_{i=1}^{n} \frac{V_i}{n})^2}{n}}}{\sum_{i=1}^{n} \frac{V_i}{n}} \tag{2.7}$$

Where V_i is the magnitude of the i^{th} pre-disturbance voltage phasor; n is the number of used voltage phasors. Based on the analysis of measurement data obtained from practical systems, 100 cycles of data can ensure a meaningful statistical index for system variation level. Using ρ_E, several cases have been evaluated and results are listed in Table 2.2.

Table 2.2: System variation level of different practical cases

No.	Case Name	ρ_E
1	WoodChipper	0.26%
2	EVChargerConquilam	0.76%
3	RecCentre	0.3%
4	EVChargerSurrey	0.07%
5	ATCO flyingshot	0.57%
6	Grande Prairie	0.65%
7	Industrial and Commercial	0.1%

Including ρ_E's effect, the threshold δ can be expressed as (2.8).

$$\delta = \beta \rho_E \tag{2.8}$$

Where β is called the voltage-system ratio here. To determine the reasonable value of β, a Monte-Carlo simulation is conducted and the details are provided in Appendix C. It can be found that the relationship between the error level of system impedance measurement and voltage-system ratio can be established by the curve-fitting method as shown in (2.9).

$$Error\ level\ (\%) = \frac{29.79\beta^2 - 40.6\beta + 20.45}{\beta^3 - 1.097\beta^2 + 0.5127\beta - 0.02026}, \tag{2.9}$$

Using (2.9), the value of β can be adjusted according to the desired error level. For example, if the margin of error level is 10%, 5% and 1%, β should be 2.6404, 5.6575 and 29.5169, respectively. Then δ can be obtained by (2.8) using the corresponding β and ρ_E. The above techniques are used in section 2.3 as voltage change level detection.

3) Results reliability test. As discussed earlier, there is still the chance of a sudden change in system frequency. It can cause the results of the LD method to diverge from the true value. Figure 2.9 (a) shows impedance results when system frequency decreases suddenly, and Figure 2.9 (b) shows impedance results when system frequency increases suddenly.

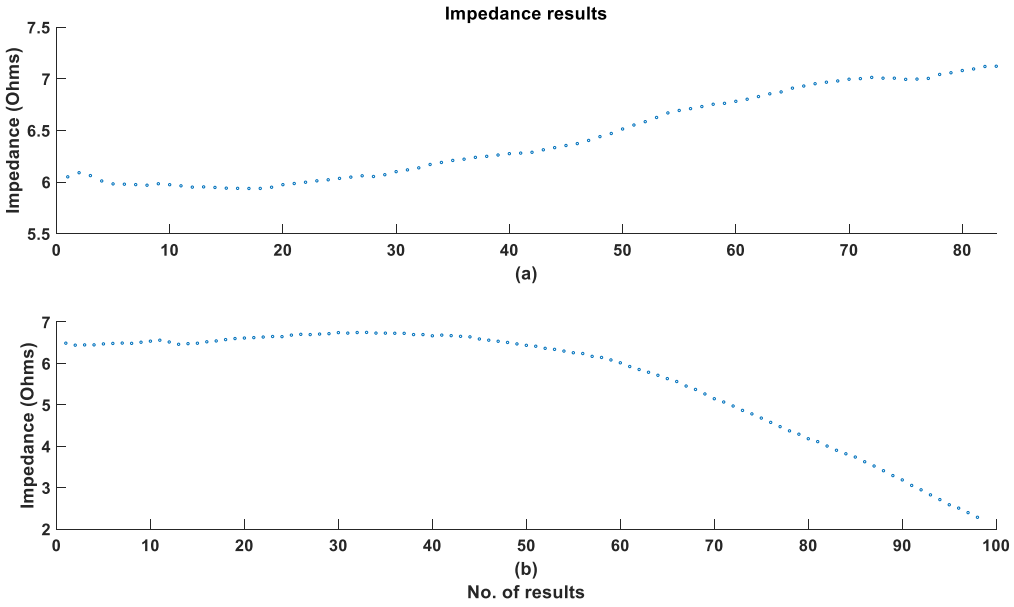

Figure 2.9 Impedance results with frequency change at the turning point

Moving average method (MAM) is selected to deal with this problem and guarantee the reliability of the proposed method. The MAM uses 10 consecutive impedance results, and the average value is calculated according to (2.10).

$$M(n) = \frac{\sum_{i=n}^{n+9} Z_i}{10}, n = 1, 2, \cdots, 91 \tag{2.10}$$

Where Z_i is the i[th] result of the estimated impedance. In addition, index D is defined using (2.11). If $D(i)$ is larger than 10%, the results after Z_{i+9} (i.e., Z_{i+10}, Z_{i+11}, $\cdots$, Z_{100}) are abandoned.

$$D(i) = \frac{|M(i) - M(1)|}{M(1)}, i = 1, 2, \cdots, 91 \tag{2.11}$$

Please note that $M(1)$ uses the first 10 results and works as the base value of the $D(i)$ calculation. It is possible that there could be a significant frequency change in the first 10 results, but it would not have an influence on the performance of the above methods.

2.1.3 Flow Chart of Proposed Method

How to detect such disturbances and how to determine if the disturbance has ended will be explained in sections 2.3.1 and 2.3.2, and is called disturbance detection. Combining the above circuit theory and practical considerations, the proposed method is implemented according to the following steps:

Step 1 Capture three-phase voltage and current waveforms continuously with proper sampling rate, for example, 64 samples per cycle.

Step 2 Convert each cycle of the waveforms to the frequency domain using FFT.

Step 3 Convert the resulting three-phase voltage and current phasors to positive-sequence, negative-sequence, and zero-sequence quantities by using the sequence transformation in (2.1).

Step 4 Correct the phase drift of the positive-sequence quantities by using the proposed method in 2.1.2.

Step 5 After disturbance detection and voltage-change-level detection, estimate impedances by using (2.12). Positive-sequence quantities of 10 cycles before

disturbance are averaged to be pre-disturbance quantities V_1, I_1. Positive-sequence quantities of the i^{th} cycle after disturbance are used as post-disturbance quantities $V_2(i)$, $I_2(i)$.

$$Z(i) = -\frac{V_1 - V_2(i)}{I_1 - I_2(i)},\ i = 1,2,\mathrm{L}\ ,100 \tag{2.12}$$

Step 6 Results reliability tests are implemented on impedance results by using the method in 2.1.2.

Step 7 Remaining results are averaged and outputted.

The flowchart of this process is shown in Figure 2.10.

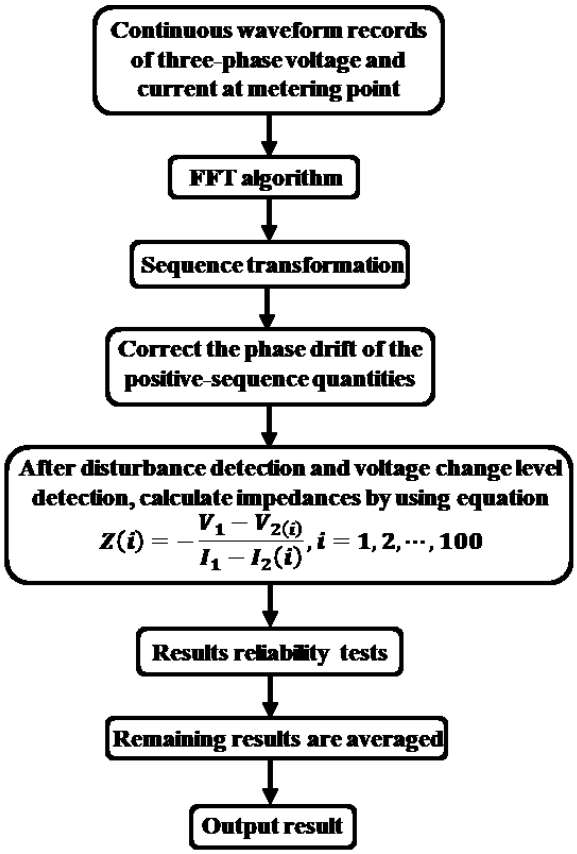

Figure 2.10 Flowchart of the LD method

2. 2 Small-Disturbance-Based Method

Compared to the events of motor starting and capacitor switching, disturbances caused by natural variations of loads are more common. Although the size of induced disturbance is smaller, statistical algorithms can be implemented due to the high frequency of occurrence.

2.2.1 Basic Algorithm

The proposed SD method is built on the work presented in [8]. Assuming the system remains constant for a group of data (i.e., *N* samples),

$$\begin{cases} E_{eq} = Z_{eq} \times I_1 + V_1 \\ E_{eq} = Z_{eq} \times I_2 + V_2 \\ \cdots \\ E_{eq} = Z_{eq} \times I_N + V_N \end{cases} \tag{2.13}$$

Where V_i and I_i are positive-sequence or negative-sequence measured voltage and current phasors at fundamental frequency; E_{eq} and Z_{eq} are unknown equivalent source voltage and equivalent source impedance, respectively. N is generally set as 10 in practical applications according to industrial experience. Complex number-based linear least-square regression can be performed to obtain the system impedance. The objective function of the regression is given by

$$\min f(Z_{eq}, E_{eq}) = \sum_{i=1}^{N} \left| V_i + Z_{eq} \times I_i - E_{eq} \right|^2 \tag{2.14}$$

The solution of (2.14) is

$$\begin{bmatrix} Z_{eq} \\ E_{eq} \end{bmatrix} = (X^T X)^{-1} X^T Y \tag{2.15}$$

where $\mathrm{X} = \begin{bmatrix} -I_1 & -I_2 & \cdots & -I_N \\ 1 & 1 & \cdots & 1 \end{bmatrix}^T$ and $\mathrm{Y} = [V_1 \quad V_2 \quad \cdots \quad V_3]^T$.

Through the comparative study of existing work, the SD method finally selects linear regression as the basic algorithm due to the following considerations. One consideration is that the linear regression technique does not require the system side to be perfectly constant, and the least-square algorithm can reduce the impact of the system variations. The other consideration is that the linear regression technique is a simple but mature statistical

algorithm. Several indices have been developed to check the reliability of the estimates. However, it has been shown that purely using a linear regression technique may not yield satisfactory results for practical cases. Therefore, several improvements are proposed to enhance accuracy and reliability in real implementation, and will be discussed later.

To further illustrate the theory of the SD method, a simulation case is built by MATLAB Simulink as shown in Figure 2.11. For this simulation case, several loads are supplied by an 11 kV feeder and an 11 kV-Yg/575 V-Yg transformer. The detailed parameters of components in simulation and the reference value of system impedance at the transformer's secondary side are listed in Table 2.3.

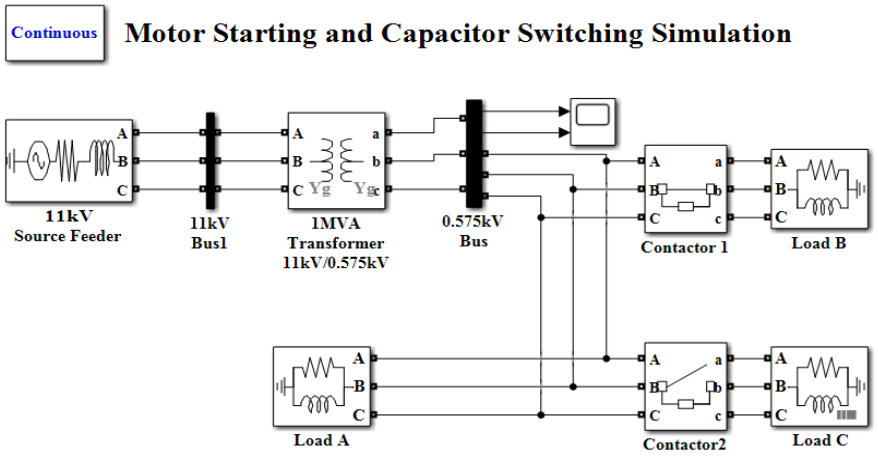

Figure 2.11 Overview of the simulation system

Table 2.3: Parameters of components in simulation

No.	Name	Parameter
1	11 kV source feeder	0.2+2j Ohms
2	Transformer	1 MVA
3	Load A	500 kW + 300 kVar

4	Load B	25 kW + 15 kVar
5	Load C	50 kW + 30 kVar
6	The reference value of system impedance	0.0319 Ohms

Load A and Load B are connected first. After 0.2 s, Load B is disconnected to simulate load reduction. Then, Load C is connected after 1 s to simulate load increase. Three-phase voltage and current waveforms at the secondary side of the transformer are presented in Figure 2.12. The estimated results of the SD method are shown in Figure 2.13.

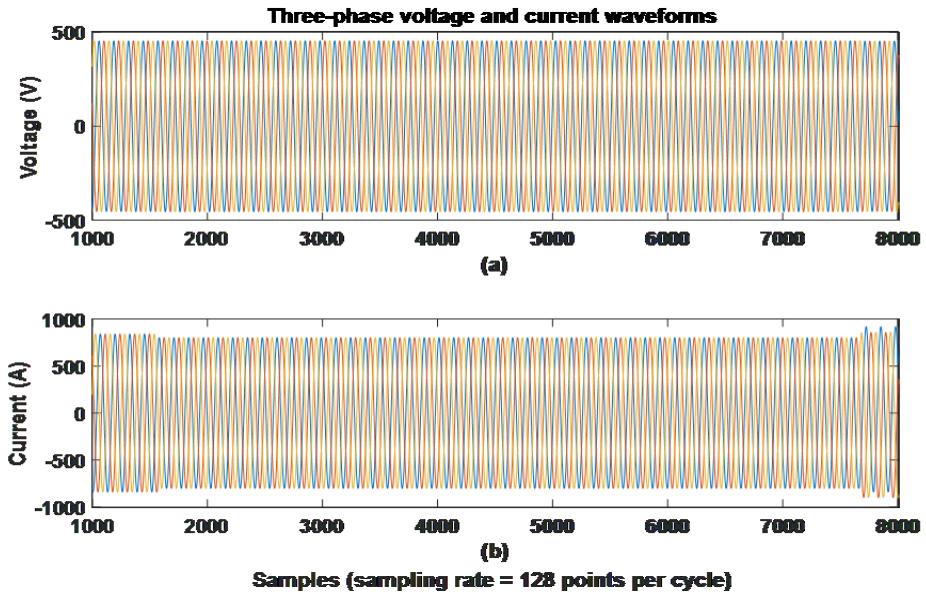

Figure 2.12 Three-phase voltage and current waveforms

As shown in Figure 2.13, the SD method only yields results at a specific time. When there is no load variation in 10 consecutive cycles used for linear regression, no reliable results can be obtained. It is reasonable that results lie in the time intervals with load variations such as 0.2 s and 1 s. The averaged value of measured system impedance is 0.0319 Ohms, which is consistent with the reference value.

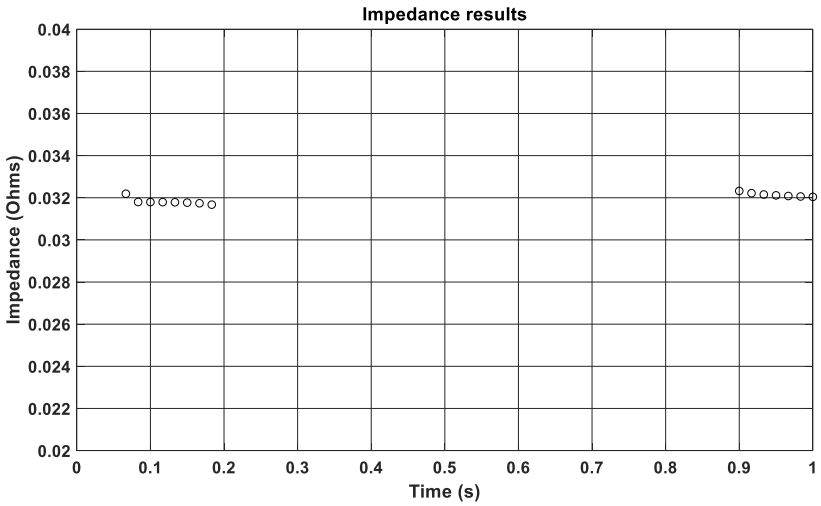

Figure 2.13 Impedance results of the SD method

2.2.2 Estimation Based on Negative-Sequence Components

Conventionally, positive-sequence phasors are used for system impedance estimation as the power system is inherently dominated by positive-sequence quantities. However, it should be realized that the negative-sequence system impedance is almost identical to that of the positive sequence in most cases. Therefore, it is theoretically possible to estimate the supply system impedance based on negative-sequence phasors as well. In fact, field tests have revealed that estimation based on the negative sequence may have better performance than that based on the positive sequence. The main reasons for this are explained as follows.

1) Low synchronization requirements. One advantage of using the negative-sequence quantities is that it leads to lower synchronization requirements. According to (1.2), the expression of Z_{eq} can be rewritten as (2.16) when there is a synchronization error ΔE. It can be seen that the error term ΔE will directly show up in the estimated Z_{eq}.

$$Z_{eq} = \frac{\Delta E - \Delta V}{\Delta I} \tag{2.16}$$

Assuming the measurement is taken at the 14.4 kV (L-G) substation and there is a 0.1 degree synchronization error, ΔE can be 25 V as shown in (2.17).

$$|\Delta E| = |14.4 - 14.4\angle 0.1°|kV = 25V \quad (2.17)$$

Such an error could be significant for the SD method as the natural load fluctuation is generally small. On the other hand, if the negative-sequence voltage is 2% of the nominal voltage and there is also a 0.1 degree synchronization error, ΔE is only 0.5 V. It is clear that the synchronization error has a much smaller impact on negative sequence. As a result, the synchronization issue can be satisfactorily addressed by many existing methods such as resampling methods [17] or adaptive filter methods [18]. In this thesis, synchronization is realized by using the positive-sequence voltage phasor as shown in (2.18) and (2.19). By doing so, the phase drift caused by varying system frequency is compensated, and different measurement sets are then synchronized. Compared to other synchronization methods, this method is simpler but yet reliable.

$$V^{-}_{corrected} = |V^{-}|e^{j(\angle V^{-} - \angle V^{+})} \quad (2.18)$$

$$I^{-}_{corrected} = |I^{-}|e^{j(\angle I^{-} - \angle V^{+})} \quad (2.19)$$

Where V^{-} is the negative-sequence voltage phasor and $\angle V^{-}$ is the respective phase angle; I^{-} is the negative-sequence current phasor and $\angle I^{-}$ is the respective phase angle; $\angle V^{+}$ is the phase angle of positive-sequence voltage phasor.

2) Small influence from the system side. Another advantage of using negative-sequence quantities is that the variation of the negative-sequence equivalent source voltage is likely to be smaller than that of the positive sequence in most cases. In general, the variations of E_{eq} come from the upstream load fluctuations. If a single-phase load causes a phase A voltage variation ΔE_A, the variation will show up equally in positive-sequence, negative-sequence, and zero-sequence as $\Delta E_A/3$ according to (2.1). In terms of three-phase loads, the variation will only show up in the positive sequence. Since the positive-sequence E_{eq} is much larger than that of the negative sequence, its voltage variation is also larger. Table 2.4 shows the system voltage variations for the positive sequence and the negative sequence. The numbers in the table are obtained by using the voltage data when the calculated load impedance keeps constant (no load changes). It is clear that the negative-sequence voltage has a smaller variation than the positive-sequence voltage for all substations.

Table 2.4: System voltage variations measured at 25 kV substations

25 kV substations	#1	#2	#3	#4	#5	#6	#7	#8
Positive sequence	5.4 V	5.6 V	4.7 V	4.6 V	5.0 V	3.5 V	2.9 V	6.8 V
Negative sequence	2.0 V	1.4 V	1.4 V	1.8 V	1.3 V	1.7 V	1.0 V	2.0 V

Based on the above two findings, it is recommended to estimate the system impedance based on negative-sequence quantities when the load current has sufficient negative-sequence quantities. By using both positive-sequence and negative-sequence quantities, a cross-check of results can be performed. When the deviation of these two results is too large, both results are discarded as reliability in this case cannot be guaranteed.

However, in some practical cases, loads are almost all three-phase and there is no sufficient negative-sequence component. In such cases, too small variations of negative-sequence components will have an influence on the accuracy of the proposed linear regression algorithm. Insisting on using negative-sequence components may lead to large errors for the estimated system impedance. To solve this problem, the percentage of negative-sequence components in the load current is calculated. The threshold level is set as 2% based on the analysis performed on measurement data obtained from practical systems. When the percentage of negative-sequence components in load current is under 2%, the system impedance estimation of these cases will only utilize positive-sequence components.

2.2.3 Data Preprocessing

To guarantee the robustness and efficiency of the SD method, several data preprocessing techniques are discussed as follows.

1) Remove undesirable transients. As discussed before, complex number-based linear least square regression is used as the basic algorithm. FFT is the basis, which requires steady-state waveforms. When transients last more than one cycle, they will lead to wrong results. For

this reason, a proper method is proposed to remove these transients by comparing the magnitude of the current phasors. FFT is applied for the selected three consecutive cycles, and the variation ratios of the consecutive two quantities are calculated as follows.

$$\left|\frac{I_{i+1}-I_i}{I_i}\right| < 1\% \ \wedge \ \left|\frac{I_{i+2}-I_{i+1}}{I_{i+1}}\right| < 1\% \tag{2.20}$$

Where I_i is the magnitude of the first cycle's current phasor, I_{i+1} is the magnitude of the second cycle's current phasor and I_{i+2} is the magnitude of the third cycle's current phasor. If the variation ratios in (2.20) are both less than 1%, I_{i+1} is considered as a steady-state value. If not, I_i is eliminated, and the next three consecutive cycles I_{i+1}, I_{i+2}, I_{i+3} are considered.

2) Disturbance side detection. In (2.14), it is assumed that all disturbances are from downstream. However, this assumption may not hold true in practice, and this is the main reason that simply using a linear regression technique cannot yield reliable results in many field cases. Therefore, a disturbance side detection method is required to judge whether the disturbance is from upstream or downstream.

The main idea is that if disturbances are from downstream, (1.3) will yield the upstream impedance with positive resistance and reactance value; and if disturbances are from upstream, (1.3) will yield the opposite number of the downstream impedance with negative resistance and reactance value. Also, since the supply system impedance is unlikely to change significantly within a short time, such as within 100 cycles, it is unnecessary to constrain the linear regression for consecutive measurements.

This subsection proposes a disturbance side method to find groups of data with downstream disturbances. The method is described in the following steps:

Step 1 Select one data sample k (k starts from 1) in the basic unit as the target sample. The default basic unit is set as 100 cycles.

Step 2 For the rest of the samples in the outputted unit, filter out the sample j does not satisfy (2.21). The remaining data samples are called companion samples and stored for linear regression analysis later.

$$\begin{cases} R = real\left(Z_{eq}(k,j)\right) > 0 \\ X = imag\left(Z_{eq}(k,j)\right) > 0 \end{cases}, where\ Z_{eq}(k,j) = -\frac{V(k) - V(j)}{I(k) - I(j)} \tag{2.21}$$

Step 3 Once the data regrouping is done for the target data k, select k+1 data as the target data and go to Step 2.

2.2.4 Selection of Good Estimates

After implementing linear regression, several statistical techniques are used to check the reliability of impedance estimates and further improve the accuracy of the final results.

1) The goodness of fit. If one regression group has an approximately equal E_{eq} and Z_{eq}, there should be a strong linear correlation between the measured voltage and current. Hence, the corresponding impedance results can be selected as useable results; otherwise, these results should be discarded. The goodness of fit is a statistical index developed to measure how strong the linear relationship is between the two studied variables, which is defined as

$$R^2 = 1 - \frac{\sum_{i=1}^{N} \left| V_i - \frac{1}{N} \sum_{i=1}^{N} V_i \right|^2}{\sum_{i=1}^{N} \left| \hat{E}_{eq} - I_i \hat{Z}_{eq} - V_i \right|^2} \tag{2.22}$$

The stronger the linear relationship is, the closer the value of R^2 is to one. When R^2 is closer to one, the estimated impedance is more accurate [8]. In practice, estimation results satisfying R^2>0.9 are commonly regarded as useable results.

2) R-X ratio criterion. In addition to the above statistical filtering, practical data selection criteria that consider the actual characteristics of power systems are also adopted. Field

measurements have shown that the following conditions can further improve the quality of estimated impedance data for PCC-based measurements.

① X>0

② R>0

③ 1<X/R<10

④ E>0

Where X is the imaginary part of estimated impedance; R is the real part of estimated impedance; E is the magnitude of estimated source voltage phasor.

3) The fluctuation of current quantities. The reliability of R^2 relies on the variance of the input data. In the linear regression problem, y=ax+b, the regression coefficient a is determined by studying the inter-dependency between the variation of explanatory variables x and their response on the response variable y. If the fluctuation of x is very small, its response on y becomes ambiguous, so it is difficult for the linear regression algorithm to determine the correlation between x and y, and R^2 may give the wrong result. A simple diagram in Figure 2.14 is plotted below for better illustration.

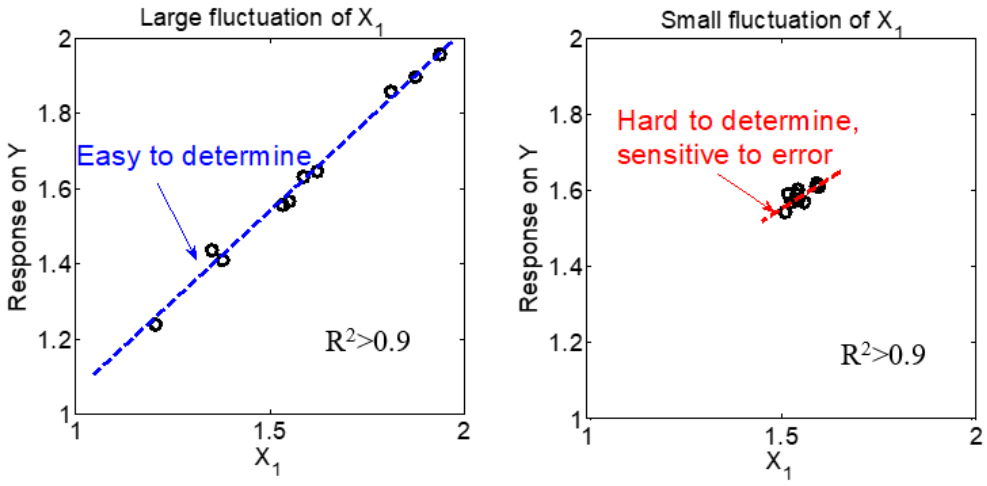

Figure 2.14 The impact of the fluctuation of X_1 on the correlation determination

The above analysis indicates the useable estimates with a larger variance of the current, denoted as var(I), are considered to be more reliable. Through the data regrouping technique

proposed in the previous section, it is possible to obtain thousands of useable estimates. In this thesis, 10% of good estimates with the largest var(I) are selected as the candidate results.

4) Statistical test and confidential level. The above candidate results are finally checked by a statistical test and a confidential level is given. By defining the maximum acceptable error, the confidence level of a set of data is defined as follows.

$$Confidence\ Level\ (CL) = \frac{N(\mu \pm e\%)}{N} \tag{2.23}$$

Where μ is the mean value, and $e\%$ is the maximum acceptable error level. N is the total number of candidate impedances, and $N(\mu \pm e\%)$ is the number of candidate impedances that are in the range of $[\mu(1-e\%), \mu(1+e\%)]$ [1].

As an example, resistance R and reactance X of candidate impedances are plotted in Figure 2.15.

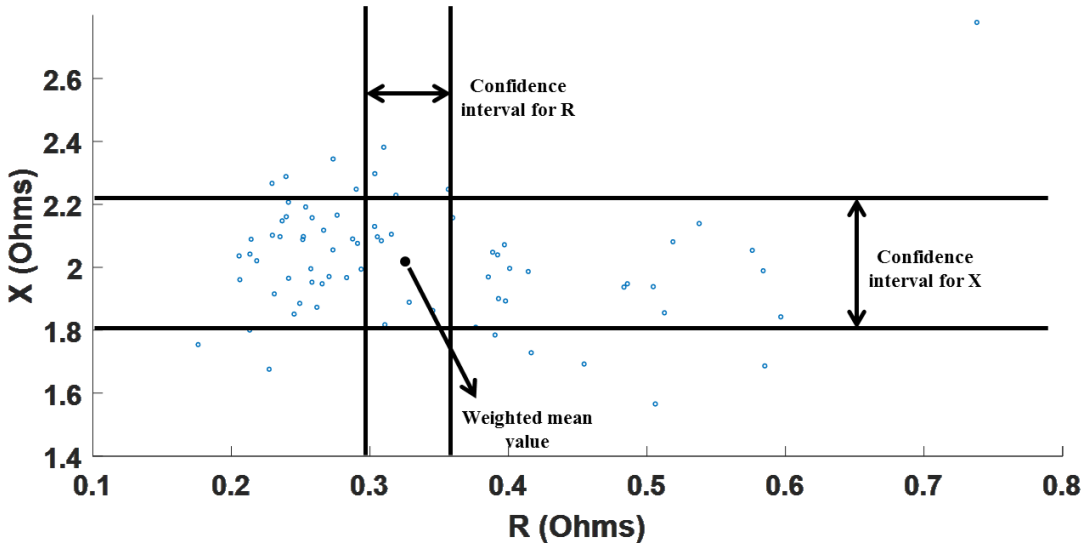

Figure 2.15 Confidence interval for R and confidence interval for X

In this case, a total number of 45 candidate impedances is obtained and the weighted mean value is shown with a black point. Figure 2.15 also shows the confidence interval for R and

X. The maximum acceptable error is 10% and specified with rectangles. For each parameter, the confidence level is the ratio of data number in the rectangle to the total data number [1]:

$$CL(R) = \frac{12}{45} \times 100 = 27\% \tag{2.24}$$

$$CL(X) = \frac{39}{45} \times 100 = 87\% \tag{2.25}$$

If the confidential level is high enough, it can be concluded that those candidate results are reliable, and their weighted mean value can be trusted. Otherwise, the algorithm will tell the user that there is no reliable estimated result that can be given for this case.

2.2.5 Flow Chart of Proposed Method

Combining the above circuit theory and practical considerations, the proposed SD method is implemented according to the following steps:

Step 1. Capture three-phase voltage and current waveforms continuously with a proper sampling rate, for example, 64 samples per cycle.

Step 2. Select 100 consecutive cycles and do the following:

- Step 2.1. Convert each cycle of the waveforms to frequency domain using FFT.
- Step 2.2. Convert the resulting three-phase voltage and current phasors to positive-sequence, negative-sequence, and zero-sequence quantities.
- Step 2.3. Correct the phase drift of the positive-sequence quantities and negative-sequence quantities.
- Step 2.4. Calculate the percentage of negative-sequence components in load current. If the percentage is larger than 2%, both positive-sequence components and negative-sequence components are used for calculation; if the percentage is smaller than 2%, only positive-sequence components are used for calculation.
- Step 2.5. Remove transients based on the method discussed in section 2.2.3. If the number of remaining samples is less than 10, select the next 100 cycles and

go to Step 2.1.

Step 2.6. Select one data sample k (k starts from 1) as the target sample. For the rest of the samples in this basic unit, filter out the phasors that do not satisfy the conditions in (2.21). The remaining samples are called companion samples, and the number of companion samples is c.

Step 2.7. If c is less than nine, select sample k+1 as the target point and go to Step 2.6.

Step 2.8. Select nine samples at a certain interval n (n=1, 2, ⋯,⌊c/9⌋) from companion samples.

Step 2.9. The linear regression analysis is performed for every group of nine companion samples with the target sample k.

Step 2.10. If the impedance estimates do not satisfy R^2>0.9 or R-X ratio criterion, reject the result. The rest of the impedance estimates are regarded as preliminary results.

Step 2.11. If k is larger than 91, select the next 100 cycles and go to Step 2.1. If not, select the sample k+1 as the target point and go to Step 2.6.

Step 3. Select 10% of the preliminary results with the largest variance of the current as the candidate results. Those candidate results are again checked by a statistical test and a confidential level is given.

Step 4. The final results are averaged by weights and outputted.

The flowchart illustrating these steps is shown in Figure 2.16.

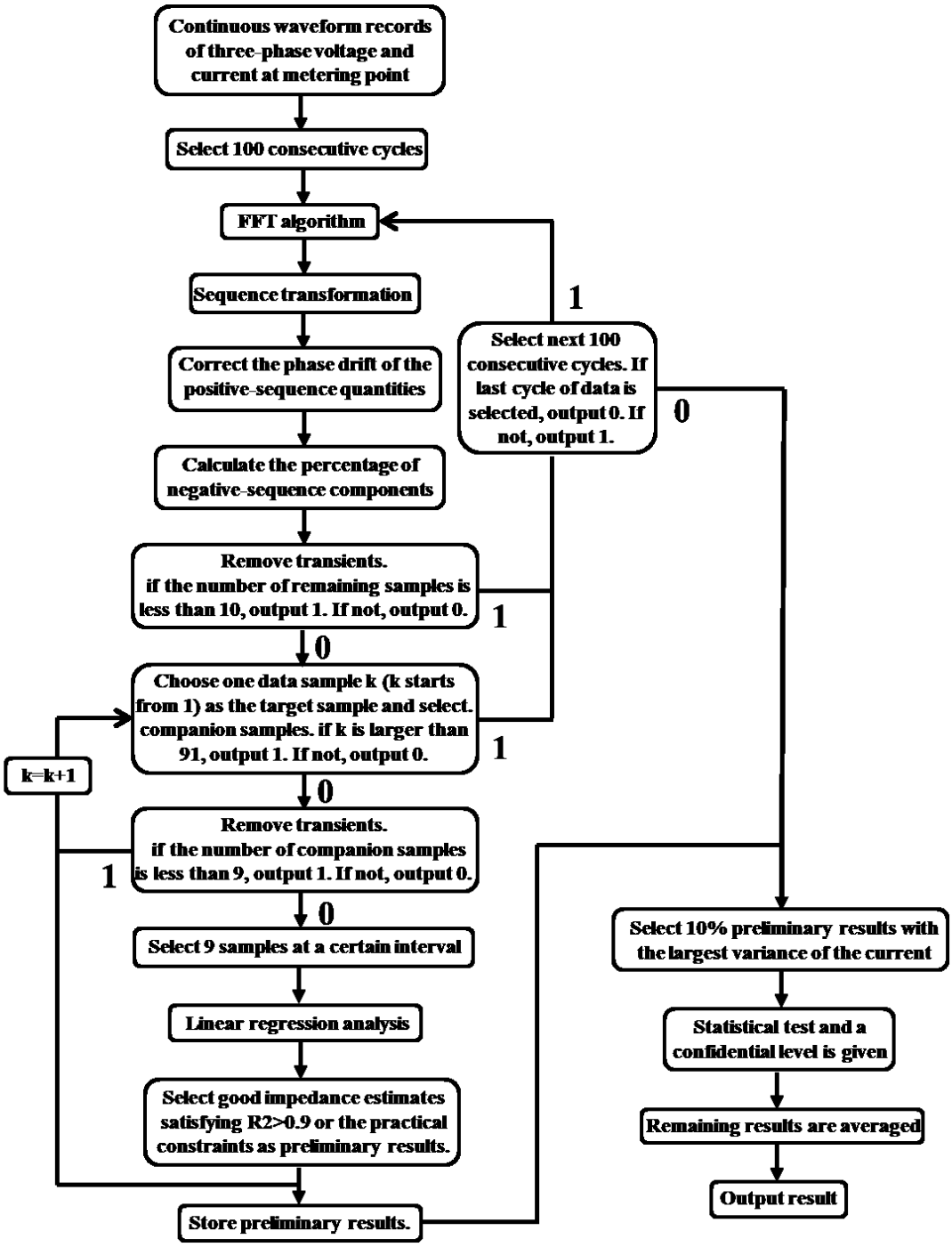

Figure 2.16 Flowchart of the SD method

2. 3 Combined Use of Large-Disturbance-Based Method and Small-Disturbance-Based Method

As discussed in previous sections, there are two types of methods suitable for different disturbances in the passive system impedance measurement. To automatically identify which scenarios are applicable to the LD method or the SD method, a detection scheme is proposed in the following sections. The basic idea of the detection scheme is to first identify cases suitable for the LD method and then to proceed with the SD method for the rest of the cases.

2.3.1 Current Abnormality Detection

Noise in power systems can be modelled by Gaussian distribution [19]. The characteristics of the Gaussian distribution can be utilized to detect outliers in current quantities. The mean value and variance of these current quantities are calculated as follows:

$$\begin{aligned} \mu &= \sum_{i=1}^{n} \frac{x_i}{n} \\ \sigma^2 &= \sum_{i=1}^{n} \frac{(x_i - \mu)^2}{n} \end{aligned} \tag{2.26}$$

Where n is the number of current quantities; x_i is the magnitude of the i^{th} cycle's current phasor. On the assumption of Gaussian distribution, $\mu \pm 3\sigma$ contains 99.7% data. Therefore, if one value's disturbance from the mean value μ exceeds 3σ, this point can be marked as an outlier. These outliers are identified and regarded as possible points of abnormal events. This step serves as a preliminary screening.

2.3.2 Steady-State Detection

As discussed before, the LD method requires steady-state waveforms of both pre-disturbance quantities and post-disturbance quantities. Motor-starting and capacitor-switching cases

always include large transients; thus, a method is proposed to identify the steady-state cycles after disturbance.

The method is based on a comparison of current phasors' magnitudes. FFT is applied for the selected three consecutive cycles and the variation ratios of the consecutive two quantities are calculated as follows:

$$\left|\frac{I_{i+1} - I_i}{I_i}\right| < 1\% \ \wedge \ \left|\frac{I_{i+2} - I_{i+1}}{I_{i+1}}\right| < 1\% \tag{2.27}$$

Where I_i is the magnitude of the first cycle's current phasor, I_{i+1} is the magnitude of the second cycle's current phasor, and I_{i+2} is the magnitude of the third cycle's current phasor. If the variation ratios in (2.27) are both less than 1%, I_{i+1} is considered as a steady-state value. If not, I_i is eliminated, and the next three consecutive cycles I_{i+1}, I_{i+2}, I_{i+3} are considered. If no steady-state cycle is identified after 100 cycles from the detected abnormal current point, detection is ended due to synchronization issues.

2.3.3 Voltage Change Level Detection

As discussed in 2.1.2, the size of voltage change ρ_v must be larger than a certain threshold δ, as shown in Equation (2.28).

$$\rho_v = \left|\frac{V_2 - V_1}{V_1}\right| > \delta = \beta\rho_E, \tag{2.28}$$

Where V_2 is the averaged value of 10 post-disturbance voltage phasors' magnitudes; V_1 is the averaged value of 10 pre-disturbance voltage phasors' magnitudes. The value of β is determined by the input acceptable error level.

There are two reasons for adding this detection. One reason is that sometimes only using the current phasors' magnitudes can be misleading because other events will also lead to large changes in current. For example, woodchippers can cause big and frequent spikes in the current waveform, and preliminary screening will include this undesired disturbance. As a result, we need voltage phasors' magnitudes to make sure there is voltage sag or swell. The

other reason is that it is possible that the system capacity is much larger than the disturbance source such as induction motors or capacitor banks. The switch on/off events of induction motors or capacitor banks cannot induce significant voltage change in such a scenario. Therefore, the size of voltage change must be large enough to be used by the LD method.

By adding the detection scheme, the complete flow chart of the proposed passive method is presented as follows:

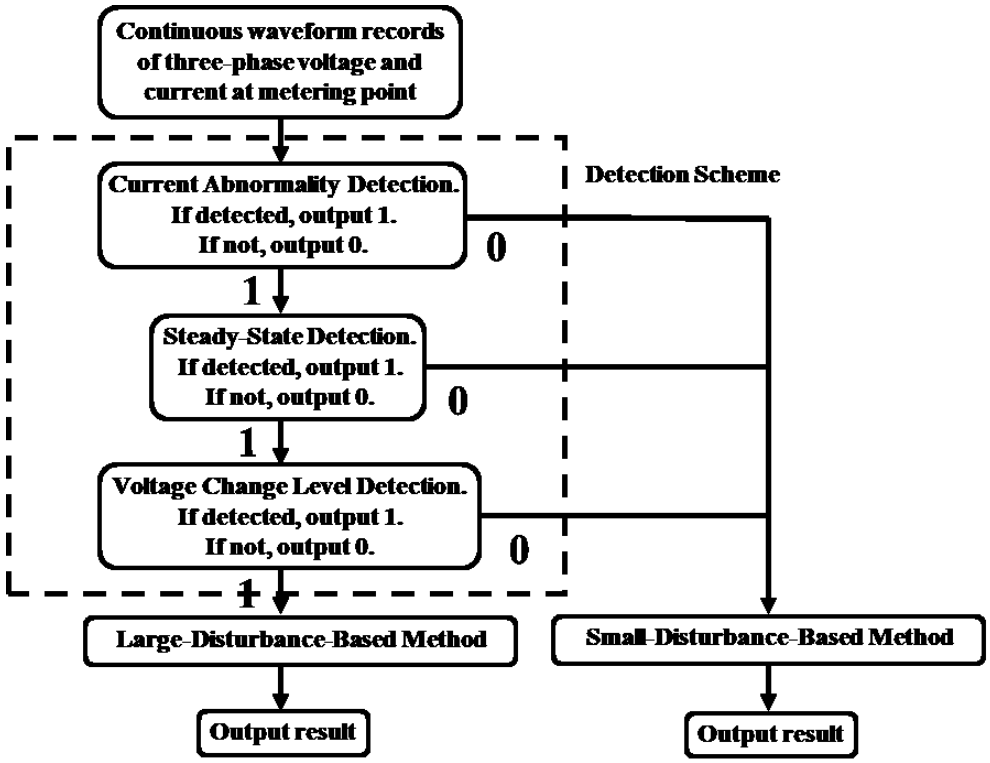

Figure 2.17 Flowchart of the proposed passive method

2.4 Summary

This chapter has comprehensively presented improved methods for passive system impedance measurement. Firstly, the problem of system impedance measurement was formulated. Then, two methods were proposed to deal with different disturbances. Section 2.1 explained the details of the LD method, which is suitable for the switch on/off events of

electrical equipment such as motor starting and capacitor switching. Section 2.2 clarified the details of the SD method, which performs well on disturbances caused by natural load variations. Simulations were conducted to illustrate the theory of the LD method and the SD method. In addition, practical considerations and respective solutions were presented. Finally, detailed flowcharts were depicted for the whole scheme of passive system impedance measurement.

Chapter 3 Performance of the Proposed Passive Method

To evaluate the performance of the proposed passive system impedance measurement method, several lab experiments and field tests are conducted for verification. In this chapter, the results obtained from lab experiments and practical cases are presented. A discussion and summary are provided as well.

3.1 Lab Experiment

The lab experiments aim to test the proposed method by creating motor-starting and capacitor-switching events in a laboratory environment. The results of the experiments are used to evaluate the proposed detection scheme and the LD method.

3.1.1 Experiment Design

An overview of the experiment design in a single line diagram is shown in Figure 3.1. The actual experimental setup is shown in Figure 3.2. The parameters of the components used in the experiment are listed in Table 3.1. All voltage and current waveforms are continuously measured by *PQPro*™ developed by CANDURA with a 7.68 kHz sampling rate.

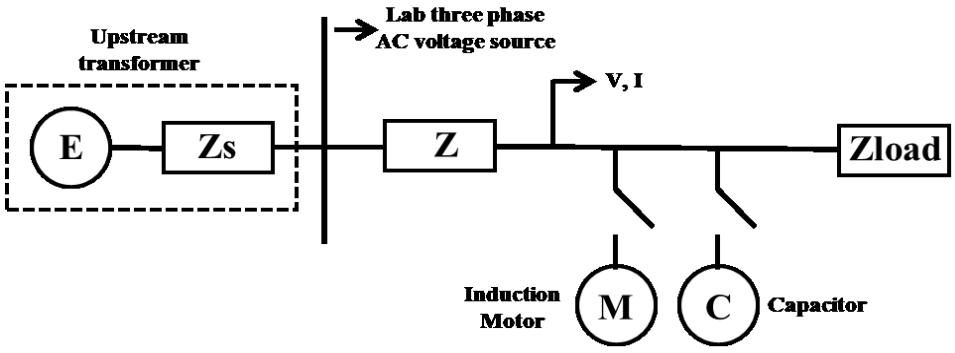

Figure 3.1 Design of lab experiment

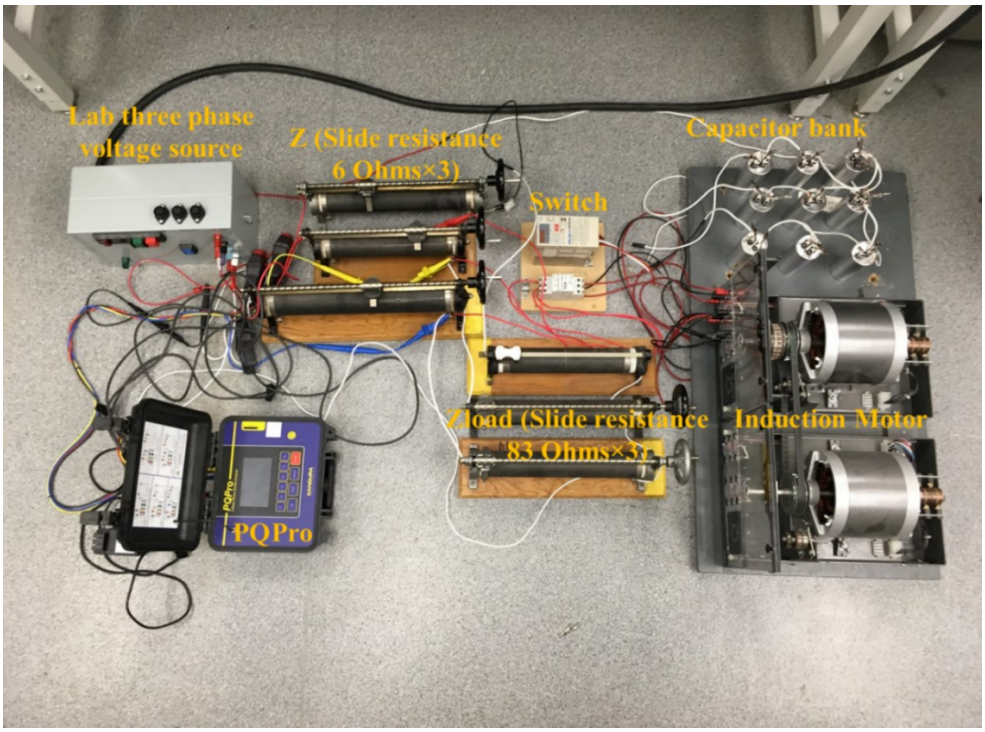

Figure 3.2 Picture of the lab experiment

Table 3.1: Parameters of components in the lab experiment

Sign	Actual Equipment	Value
M	Induction Motor×1	175 W×1
C	Capacitor×9	50 μF×9
Z	Slide Resistance×3	6 Ω×3
Zload	Slide Resistance×3	83 Ω×3
E	60 Hz three-phase AC voltage source×1	120 V(L-G)×1

The 60 Hz three-phase AC voltage source shown in Table 3.1 is supplied by an upstream transformer (600 V to 120 V). The upstream transformer's capacity is much larger than that of the induction motor. Therefore, the disturbance caused by motor starting cannot induce obvious changes on the voltage RMS waveforms, as shown in Figure 3.3. As a result, the

proposed method yields no results. In addition, the parameters of the upstream transformer are unknown. Thus, it is hard to obtain a reference value to verify the results of lab tests.

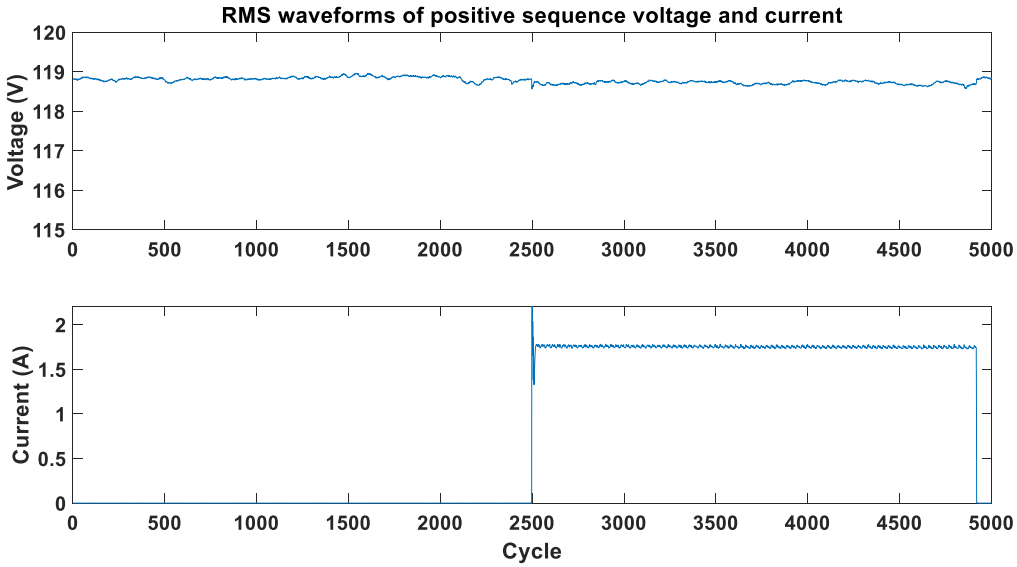

Figure 3.3 RMS waveforms of positive-sequence voltage and current

Thus, there are two challenges for this lab experiment. One challenge is that the parameters of the upstream transformer are unknown and the reference value for verification is hard to obtain. The other challenge is that the system side is too strong for the existing induction motor in the lab. In order to solve these two problems, an impedance Z, which is much larger than Zs, is added between the three-phase AC voltage source and loads. Due to its small size compared to Z, Zs can be omitted. In this way, the three-phase AC voltage source in the lab can be regarded as an ideal source, and the added impedance Z can be regarded as a new system impedance.

The modification of the lab experiment through the addition of Z comes with two advantages. One advantage is that the system side is not strong anymore so that motor starting can cause significant voltage sag at the measurement point. The other advantage is that the true value of the added impedance can be obtained. For this experiment, Z is determined as 6.5040 Ohms by the method described in Appendix A. This value is regarded as the reference value

to verify the test results. The experiment is carried out for both motor starting and capacitor switching, one at a time. Details of disturbance creation and results of the proposed algorithm are discussed below.

3.1.2 Experiment of Motor Starting

The disturbance is created by connecting the induction motor after 40 s and the capacitor bank is disconnected all the time. The waveforms of voltage and current are recorded, and the RMS of the positive-sequence voltage and current are calculated. The RMS values are shown in Figure 3.4. System impedances are estimated as shown in Figure 3.5.

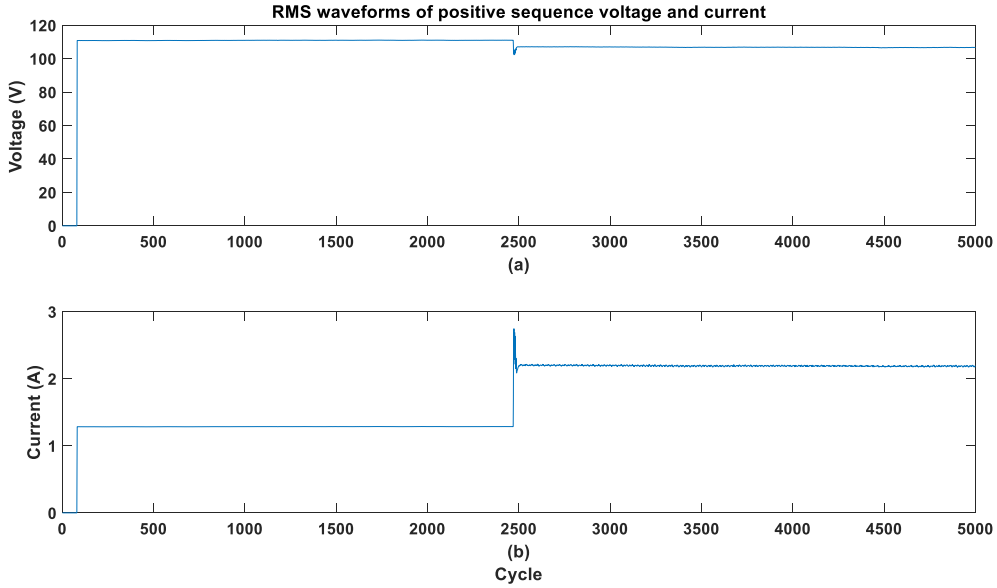

Figure 3.4 RMS waveforms of positive-sequence voltage and current

As shown in Figure 3.5, the results are almost constant. The averaged value is 6.3895 and the error level is 1.76%, both of which are acceptable. The main reason for the differences among these results is frequency variation. This is due to the phase angle compensation in Appendix B that assumes the frequency is almost constant during the measurement period.

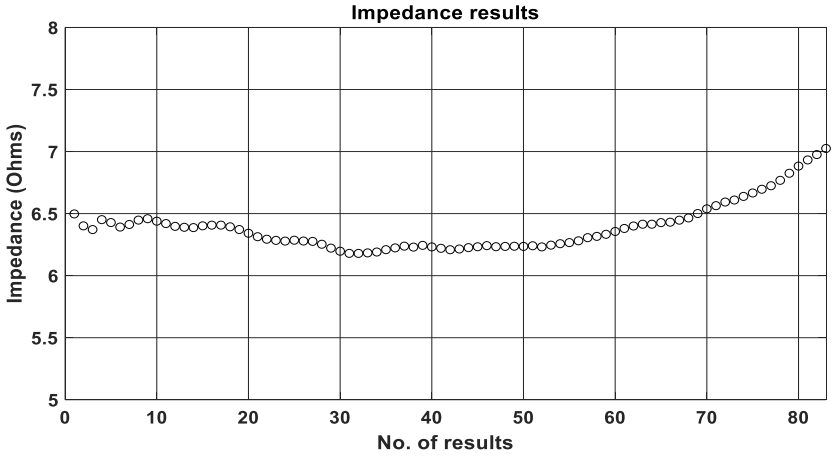

Figure 3.5 Estimated impedances

3.1.3 Experiment of Capacitor Switching

The disturbance is created by connecting the capacitor bank after 40 s, and the induction motor is disconnected all the time. The waveforms of voltage and current are recorded, and the RMS of the positive-sequence voltage and current are calculated. The RMS values are shown in Figure 3.6. The calculated system impedance is shown in Figure 3.7. The averaged value is 6.5682 and the error level is 0.99%.

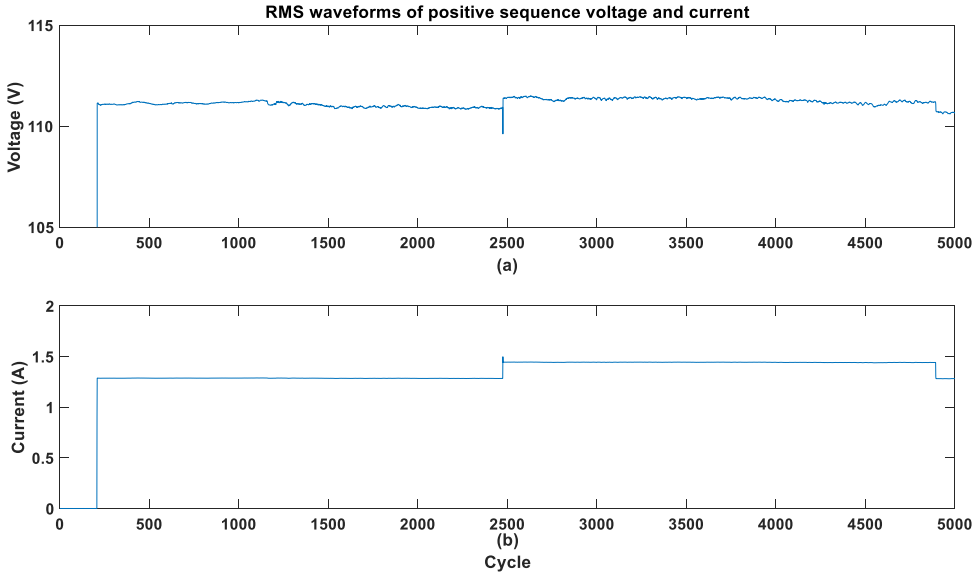

Figure 3.6 RMS waveforms of positive-sequence voltage and current

3.1.4 Conclusions and Discussions

Although the induction motor and the capacitor bank used in this experiment have small capacities, the proposed method of passive system impedance measurement performs well for motor starting and capacitor switching in lab experiments. The error level is acceptable.

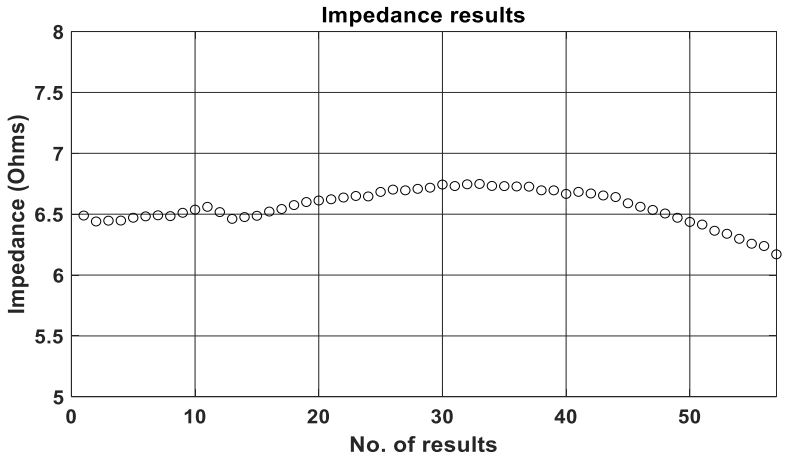

Figure 3.7 Estimated impedances

Please note that the phase-lock-loop (PLL) function in the PQ monitor should be disabled during the measurement period. The reason is that the PLL might confuse phase angle change and frequency change, which would lead to significant errors in the results of the proposed algorithm.

Assuming system impedance is constant during the concerned period, large transients caused by motor starting and capacitor switching can result in a certain phase angle change on voltage and current phasers. For example, the phase angles of pre-disturbance V_1 and post-disturbance V_2 in Equation (2.5) are generally different. If the PLL function in PQ monitors is used, the phase angle change will be regarded as frequency change and removed. The reason is that the PLL function will change the internal frequency of the crystal oscillator to keep the phase angles of reference phaser unchanged. The details of PLL's error analysis are discussed in Appendix B.

3.2 Field Measurement Result

This section documents the testing and application of the proposed passive method on field measurement data. Field measurements are presented in two categories: substation measurements and PCC measurements. The estimation results are compared with reference values calculated using the PSS/E short-circuit program.

3.2.1 Substation Measurements

Field measurements were conducted at three load-serving substations: Substation One, Substation Two and Substation Three. The instrument set-up and field results are presented below.

1) Instrument setup. For Substation One and Substation Two, the national instrument NI-6020E 12-bit data-acquisition system with a 15.36 kHz sampling rate was used for the recording. By using this data-acquisition system, we obtained 256 samples per cycle for each channel of the waveform: Va, Vb, Vc, Ia, Ib, Ic. The captured waveforms were three-phase voltages, and the currents were at the point of the metering in the load-serving substations. All measuring points were at 14.4 kV; therefore, CTs and PTs were used to step down the currents and voltages, respectively, to measurable values. The measurements were taken as 12 cycles per 12 seconds and 12 cycles per 5 seconds for Substation One and Substation Two, respectively. For Substation Three, the waveforms of three-phase voltage and the currents were measured by the power quality analyzer *PQPro*^{TM} with continuous measurement mode, i.e., 60 cycles per second. The sampling rate was 64 samples per cycle.

2) Verification results. Measurement activities and estimated system impedances for each substation are presented as follows.

- **Substation One**

Site One is a 14.4 kV substation mainly serving residential loads. The single-line diagram of the substation and measurement points are shown in Figure 3.8.

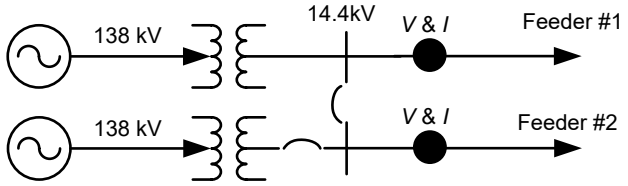

Figure 3.8 Single-line diagram of Substation One

The data were collected as 12 cycles per 12 seconds over one day. The three-phase waveforms of each measurement point are transformed into the frequency domain by FFT. Then, the positive-sequence and negative-sequence voltages/currents are calculated by using the sequence transformation. The variation of the RMS values of the positive- and negative-sequence voltage/current for Feeder One is shown in Figure 3.9.

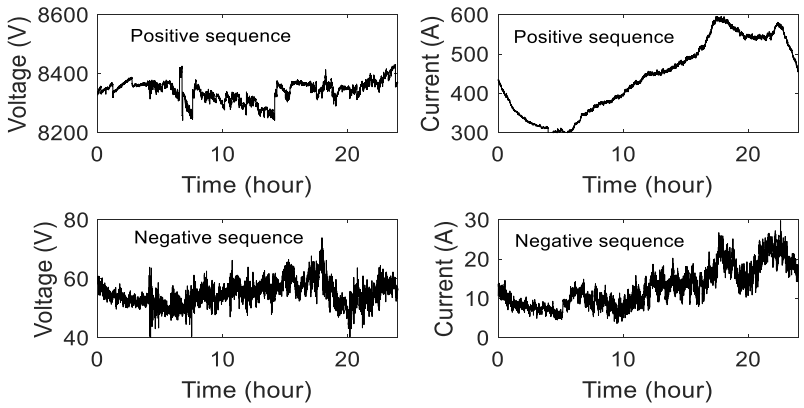

Figure 3.9 Variations of voltage and current of Feeder One, Substation One

The positive-sequence and negative-sequence system impedances are estimated by a group of 10 samples and screened according to the criteria developed in Chapter 2. The outputted results are plotted in Figure 3.10. The results show the estimated impedance data. It can be seen that both positive-sequence quantities and negative-sequence quantities are able to yield reliable results. In addition, it is clear that using negative-sequence quantities leads to much

more estimates than that of the positive sequence; thus, using negative-sequence quantities is more suitable for online tracking.

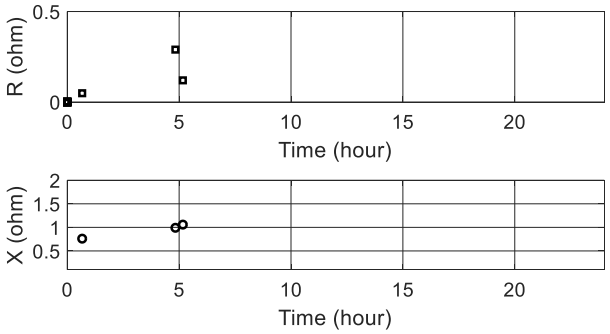

(a) Estimated by positive sequence

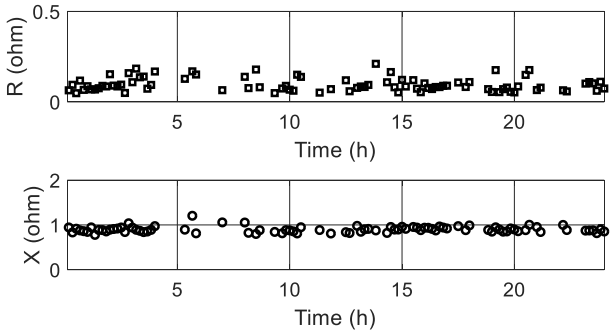

(b) Estimated by negative sequence

Figure 3.10 System Impedances of Feeder One, Substation One

The same procedure is applied for Feeder Two, and the average values of the calculated impedances for the measurement period are calculated for both feeders. The results are compared with each other. The feeders are expected to result in the same system impedance. This comparison is shown in Table 3.2. It can be seen there is an acceptable agreement between the two results. The slight difference is likely caused by the loads in each feeder. The feeder loads are expected to affect the network impedance in this measurement setup since the unmetered feeder is considered as a part of the supply system. Note that the algorithm estimates the driving point impedance upstream of the metering point. The results are verified with the network impedance calculated from the short-circuit function of the PSS/E program. It can be seen that the impedance results are close to each other.

Table 3.2: System impedance data of Substation One

Feeder	Estimated by Positive Sequence	Estimated by Negative Sequence	PSS/E
# 1	0.10+0.90j	0.15+0.93j	0.073+ j0.85
# 2	0.21+0.87j	0.10+0.89j	

- **Substation Two**

The second substation is a 14.4 kV substation mainly serving commercial loads. The single-line diagram of the substation and measurement points are shown in Figure 3.11.

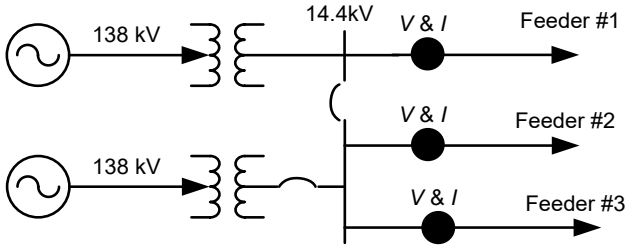

Figure 3.11 Single-line diagram of Substation Two

The measurements were taken from all three feeders at this substation. The three-phase waveforms of each measurement point are transformed into the frequency domain by FFT. Then, the positive- and negative-sequence voltages/currents are calculated by using the sequence transformation. The variations of the RMS values of the positive- and negative-sequence voltage and current for Feeder One are shown in Figure 3.12.

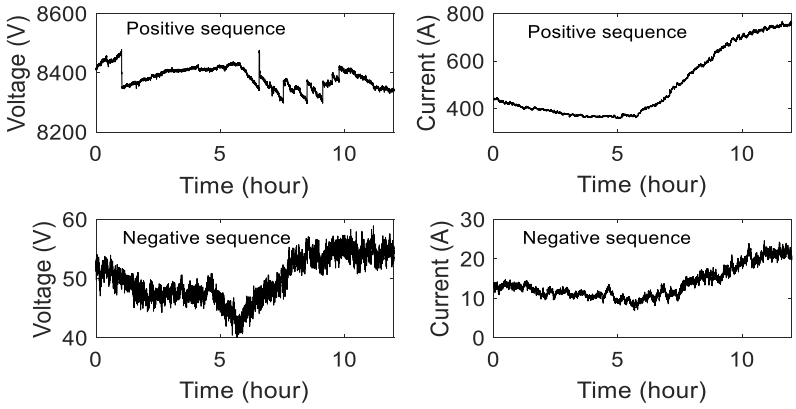

Figure 3.12 Variation of voltage and current of Feeder One, Substation Two

The system impedances are then estimated by the proposed method. The outputted results are plotted in Figure 3.13. Likewise, estimation based on negative-sequence quantities leads to more estimates than that of the positive sequence. The proposed algorithm is applied to all the feeders in Substation Two. The results are shown in Table 3.3; the average values of the calculated impedances are compared with those derived from the PSS/E model. The agreement is quite acceptable considering the proposed method only uses naturally occurring small disturbances for impedance estimation.

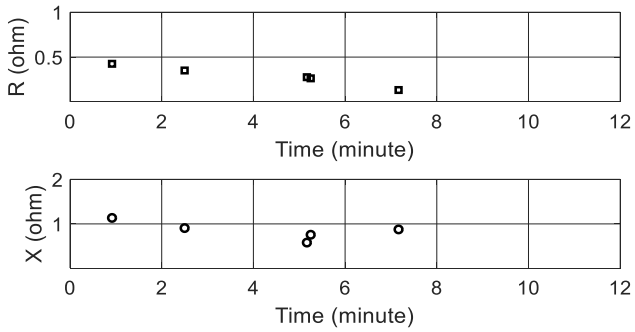

(a) Estimation based on positive-sequence quantities

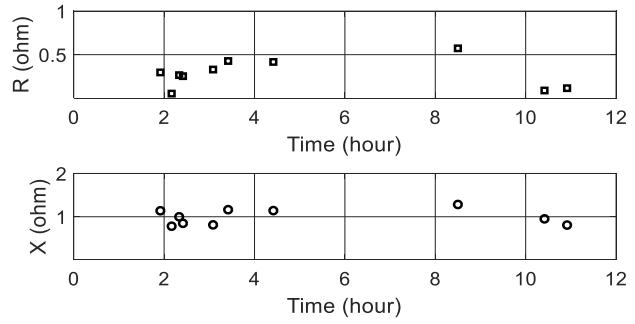

(b) Estimation based on negative-sequence quantities

Figure 3.13 Positive-sequence parameters of Feeder One, Substation Two

Table 3.3: Substation Two, impedance data

Feeder	Estimated by Positive Sequence	Estimated by Negative Sequence	PSS/E
# 1	0.32+0.88j	0.28+0.95j	0.12+0.85j
# 2	0.20+0.80j	0.16+0.84j	
# 3	NA	0.25+0.93j	

- **Substation Three**

The third substation is a 25 kV load-serving substation. The single-line diagram of the substation and the measurement points is shown in Figure 3.14.

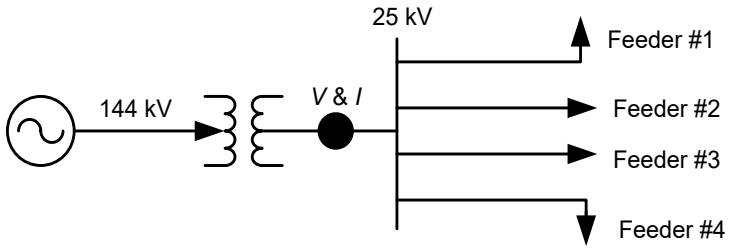

Figure 3.14 Single-line diagram of Substation Three

For Substation One and Substation Two, the measurements were taken from feeders, while for Substation Three, the measurements were taken from the 25 kV substation side, which means that the measured current is the total current of four feeders and the estimated impedance will be true system impedance. Three-phase voltages and currents were captured at a rate of sixty seconds per minute for around 160 minutes. The variations of the RMS values of the positive- and negative-sequence voltage and current are shown in Figure 3.15.

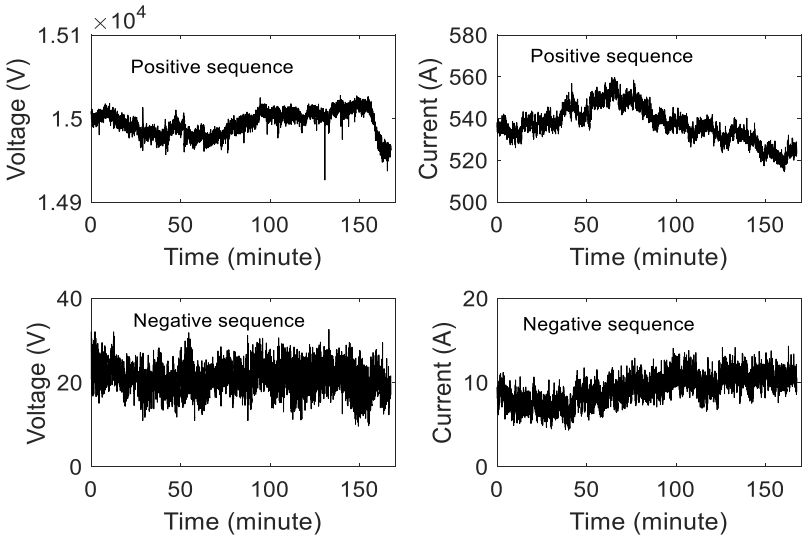

Figure 3.15 Variation of voltage and current at Substation Three

The system impedances are then estimated by the proposed method. The outputted results are plotted in Figure 3.16. Likewise, estimation based on negative-sequence quantities leads to more estimates than estimation based on the positive sequence.

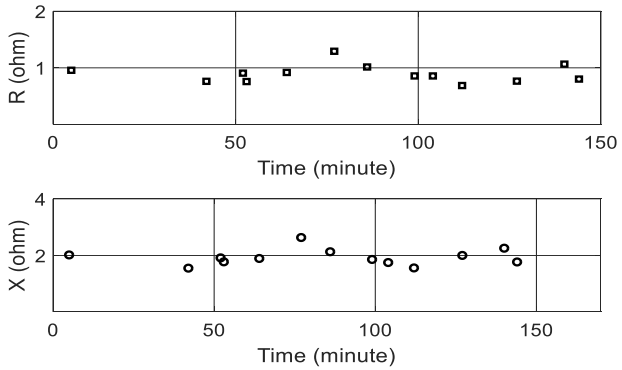

(a) Estimated by positive-sequence phasors

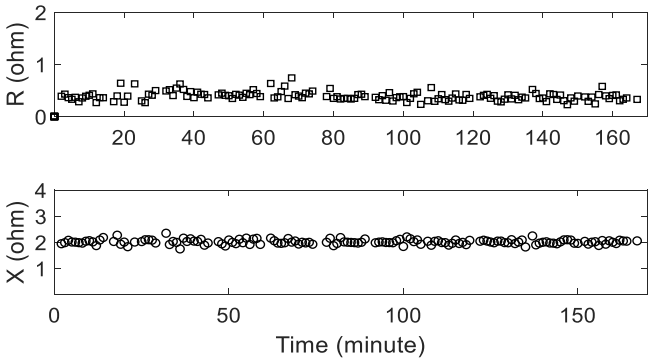

(b) Estimated by negative-sequence phasors

Figure 3.16 Positive-sequence parameters of Substation Three

The average values of the calculated impedances are compared with those derived from the PSS/E model. The agreement is quite acceptable.

Table 3.4: System impedance data of Substation Three

Feeder	Estimated by Positive Sequence	Estimated by Negative Sequence	PSS/E
# 1	0.78+1.91j	0.45+2.01j	0.38+1.97j

3.2.2 PCC Measurements

Field measurements were conducted at two sites, namely PCC One and PCC Two. The instrument set-up and field results are presented below.

1) Instrument setup. For PCC One, the measurements were carried out at an oil sand site for around 45 minutes. There were certain load variations during the measurement period that were mainly caused by the pumpjack operation. The waveforms of three-phase voltage and the currents were captured by the power quality analyzer *PQPro*™ with continuous measurement mode, i.e. 60 cycles per second. The sampling rate was 256 samples per cycle. For PCC Two, the measurements were carried out at a commercial building for around 84 minutes. There were certain load variations during the measurement period that were probably caused by a chiller or air conditioner. The waveforms of three-phase voltage and the currents were captured by the power quality analyzer *PQPro*™ with continuous measurement mode, i.e. 60 cycles per second. The sampling rate was 128 samples per cycle.

2) Verification results. Measurement activities and estimated system impedances for each PCC are presented as follows. For PCC One, the results are verified using the characteristics of harmonic impedance. For PCC Two, the results are verified using the reference value provided by the utility.

- **PCC One**

The variation of the RMS values of the positive- and negative-sequence voltage/current at the oil sand site is shown in Figure 3.17. The system impedances are then estimated by the proposed method with a group of 10 samples and screened according to the criteria developed earlier. The outputted results are plotted in Figure 3.18, which shows a stream of estimated impedance data. Estimation based on negative-sequence quantities again leads to more estimates than estimation based on the positive sequence.

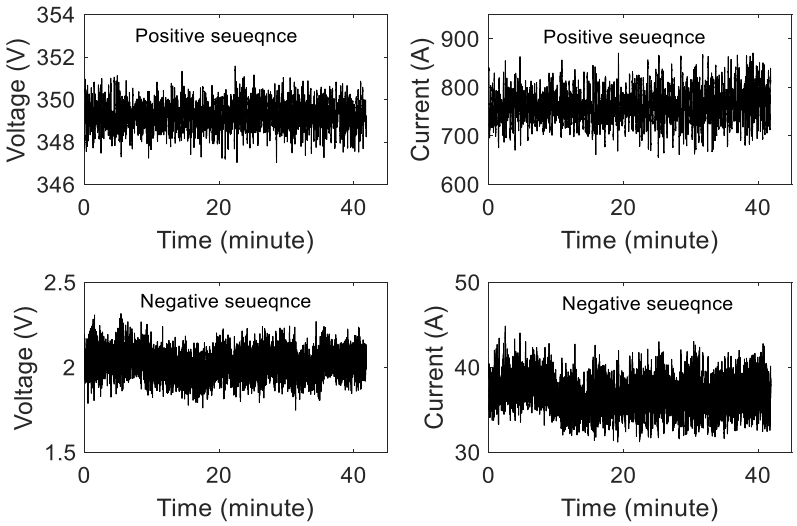

Figure 3.17 Variation of voltage and current at the oil sand site

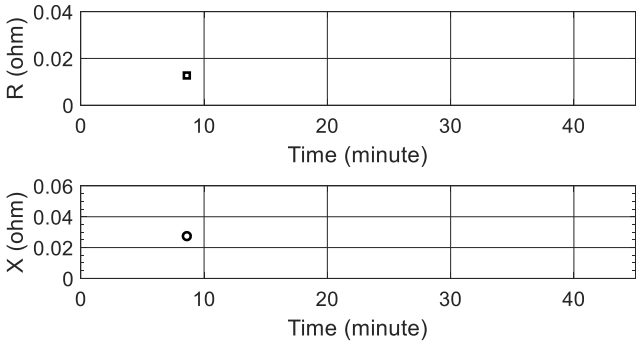

(a) Estimated by positive sequence

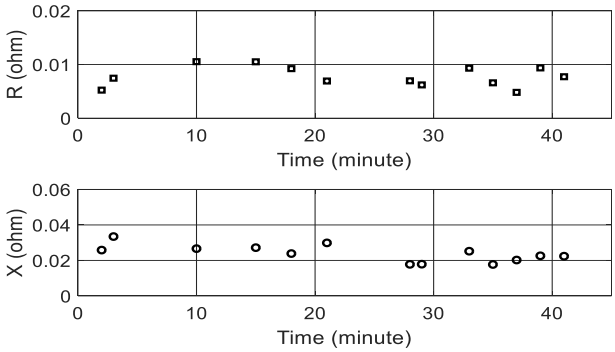

(b) Estimated by negative sequence

Figure 3.18 System impedances of the oil sand site

The average values of the calculated impedance parameters are presented in Table 3.5. Since the PSS/E program does not have a detailed secondary distribution system model, the estimated system impedances are validated through the comparison with harmonic impedances. It is observed that the load current contains high fifth and seventh harmonic components. By using the method presented in [1], the site's average 5th harmonic impedance and 7th harmonic impedance are estimated as 0.012+0.110j and 0.015+0.170j, respectively. The results suggest that the reference value of the system impedance at the fundamental frequency can be regarded as $Z_s=R_{5th}+X_{5th}/5=0.012+0.022j$ or $Z_s=R_{7th}+X_{7th}/7=0.012+0.023j$. The agreement is generally good with the estimated values.

Table 3.5: System impedance data of the oil sand site

	Estimated by negative sequence	Estimated by positive sequence	Reference value (5th)	Reference value (7th)
System impedance	0.011+0.025j	0.008+0.024j	0.012+0.022j	0.015+0.023j

- **PCC Two**

The variation of the RMS values of the positive-sequence voltage/current at the commercial building is shown in Figure 3.19.

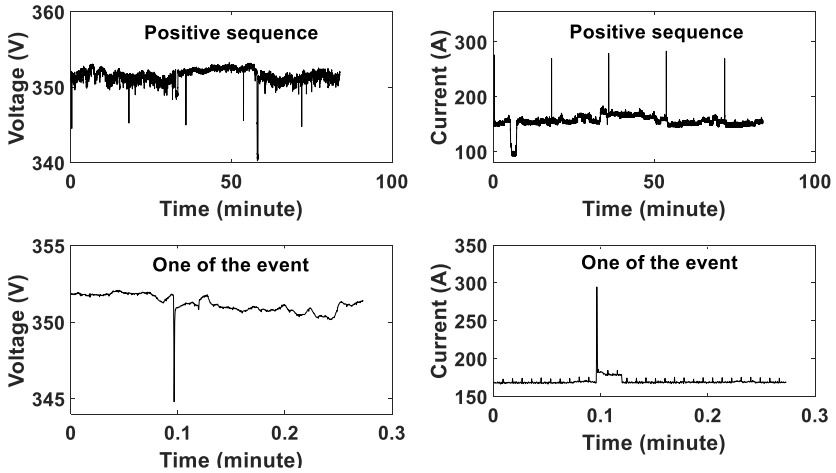

Figure 3.19 Variation of voltage and current at the commercial building

As shown in Figure 3.19, there are five events of motor starting caused by a chiller or air conditioner. The events are detected, and the system impedances are then estimated by the LD method developed earlier. The outputted results were plotted in Figure 3.20, and the averaged value is 0.0586 Ohms, which is consistent with the reference value 0.0583 Ohms.

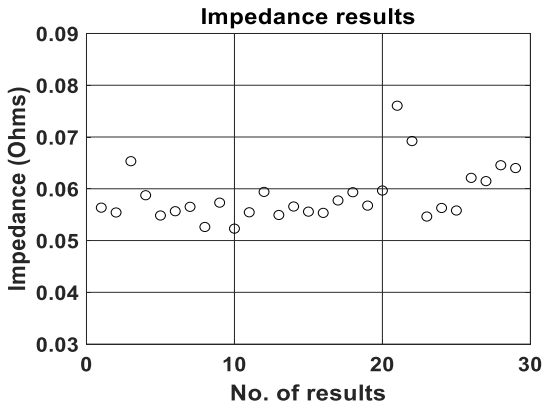

Figure 3.20 System impedances of the commercial building

3.2.3 Conclusions and Discussions

Verification studies have been conducted for the proposed passive system impedance measurement using extensive field data. The results show that the proposed method can estimate system impedances for the majority of cases adequately. The main findings are summarized and discussed as follows:

- Much of the field data used are short-term measurements, such as 120 minutes. Even for such a relatively short period, a number of impedance results have been obtained. This suggests that if one can monitor a site for 24 hours or a few days, many impedance estimates can be obtained and more reliable results can be determined. Since the system impedance does not change a lot over time, it can be concluded that the proposed method has the potential to be used in practical applications.

- In view of the fact that the network positive-sequence impedance is generally equal to its negative-sequence impedance, this research has investigated the use of negative-

sequence components as an additional source of data to improve the positive-sequence impedance estimation. The results are satisfactory as more reliable estimates are obtained in most field cases. The recommendation is to rely on the negative-sequence components when the load has sufficient negative-sequence currents.

- Load variations that are useful for the proposed passive methods do not occur at all times. Thus, the best strategy for impedance estimation is to do long-term monitoring. The recommended monitoring period is several days to 1 week. This is especially applicable for cases where load fluctuations are not frequent.

- Although the proposed method is designed for measuring the system impedance seen from PCC points, it also has a good performance on substation cases. Thus, the application of the proposed method can be extended to measure the system impedance seen from substations.

3.3 Summary

This chapter has presented several experimental tests and practical case studies. The estimated results and reference values are generally in good agreement.

However, the performance of the proposed method depends on the degree of voltage and current variations at the measurement point. A higher level of variations is beneficial for more reliable impedance estimation. Particularly, it is found that estimating system impedance based on negative-sequence quantities may have much better performance than estimating system impedance based on the positive sequence. This is mainly due to the small variation of the negative-sequence voltage at the system side. The main requirements for using the proposed method are summarized below:

- Quantities to measure: three-phase voltage and current waveforms;

- Data sampling rate: 64 samples per cycle or higher;
- Continuous waveform snapshots: 12 cycles or higher;
- The gap between two snapshots: 0;
- Duration of measurement: multiple hours or days depending on the degree of current and voltage variations.

By satisfying the requirements summarized above, the proposed method can be used to provide reliable results of system impedance measurement.

Chapter 4 Methods for Active System Impedance Measurement

As mentioned before, methods for passive system impedance measurement rely on natural disturbances in the customer system. However, some customers such as data centres or computer centres have stable loads. In such cases, there are no sufficient downstream disturbances at the measuring point, and methods for passive system impedance measurement therefore cannot yield results. To deal with this problem, methods for active system impedance measurement can be used by intentionally involving an injection of proper disturbances from the customer side. In this chapter, an improved active system impedance measurement method is proposed based on analyzing existing methods and considering practical conditions.

4.1 Description of Active Methods

The problem of active system impedance measurement methods can be understood with the help of Figure 4.1.

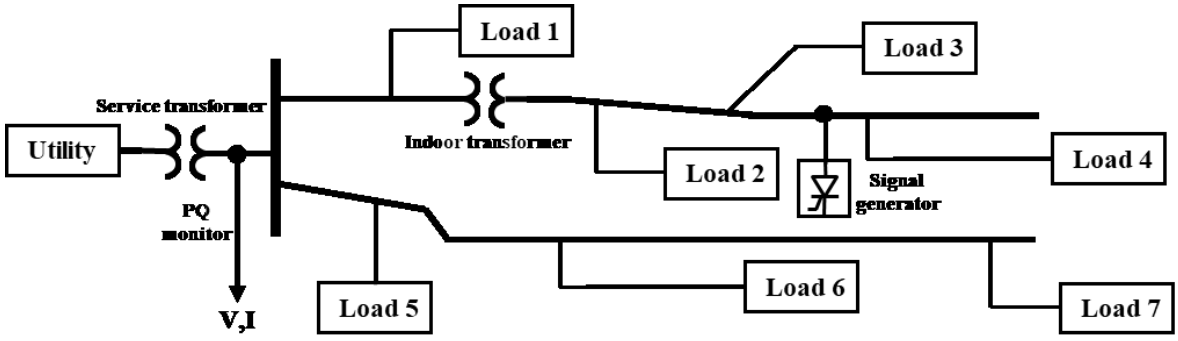

Figure 4.1 The topology of a commercial building

Figure 4.1 presents the topology of a commercial building with stable loads (e.g., a computer centre). Similarly, the supply system impedance at the PCC is to be determined. The main

idea of active methods is connecting a signal generator into a downstream network to generate proper disturbances, as shown in Figure 4.1. Consequently, PQ monitors at the PCC collect three-phase voltage and current waveforms containing disturbances, and these waveforms will be used to estimate the system impedance.

The active method consists of three major activities:

1. Disturbance generation. To generate intentional disturbances, a power electronic device should be designed and added at downstream locations (120 V-600 V).

2. Disturbance detection. PQ monitors are generally placed at the secondary side of the service transformer to record three-phase voltage and current waveforms. The recorded data by PQ monitors should be processed by detection techniques to detect and select cycles with injected disturbances.

3. System impedance estimation. Proper methods should be implemented on the chosen cycles to estimate system impedance.

4.2 Review of Existing Techniques

There are several existing techniques proposed to improve the active method in terms of disturbance generation, disturbance detection, and impedance estimation. In the following section, typical existing techniques are reviewed and the deficiencies are discussed.

4.2.1 Disturbance Generation

Existing disturbance generation methods mainly consist of switching existing electric components [11]-[12] and using separate power electronic devices [13]-[16], [20]. Since switching existing electric components in power systems manually is too complex and will

lead to too much pressure on the operation of power systems, using separate devices to inject specific disturbances seems to be a better option. The methods in [13]-[15] proposed injecting currents into power systems for impedance measurements by using inverters or converters, but these methods are complex and costly. Thus, the methods in [16] and [20] proposed a better way of connecting a simpler thyristor-based device to inject intentional disturbances by creating a small short circuit around the zero-crossing point, and this injection technique is patented as the Zero-Crossing-Distortion technique [22]-[23]. This thyristor-based device is designed to be connected to the PCC. Therefore, there will be large disturbance energy injected at the PCC, and the performance of methods in [16] and [20] is good. However, there are two drawbacks. One drawback is that the PCC is usually the secondary side of the service transformer; thus, the PCC may not be accessible in practical use. The second drawback is that the voltage level of the PCC is at least 600 V, so high-voltage-level thyristors are required, which will lead to devices that are of a heavy weight and large size. Therefore, a better device for disturbance generation is desired.

4.2.2 Disturbance Detection

The Zero-Crossing-Distortion technique is a mature and widely used technique for disturbance generation. The proposed active method, which will be explained later, also uses this technique, so only detection algorithms for disturbances of the Zero-Crossing-Distortion technique is discussed here.

There are three main types of detection algorithms: RMS-based signal detection algorithm, spectrum-based signal detection algorithm and template-based signal detection algorithm [20]. All three algorithms require voltage waveforms from the subtraction of two consecutive cycles. For each cycle of subtracted waveform (i.e., 0-360º), the waveform data between 150º-360º is used for analysis: RMS-based signal detection algorithm calculates RMS values using these samples; spectrum-based signal detection algorithm calculates RMS_h as shown in (4.1); template-based signal detection algorithm calculates RMS_t by covariances with

templates as shown in (4.2). If the calculated index is larger than the threshold, disturbance signals are detected. More details can be found in [20].

$$RMS_h = \sqrt{M_{h4}^2 + M_{h6}^2 + M_{h8}^2 + M_{h10}^2} \tag{4.1}$$

Where M_{hi} is the magnitude of the i^{th} harmonic phasor.

$$\begin{aligned} v_{template\_i} &= \eta_i \sin(2\pi f_i t), f_i = 5,6,7,8,9 \\ RMS_t &= \sqrt{CR_{t5}^2 + CR_{t6}^2 + \mathrm{L} + CR_{t9}^2} \end{aligned} \tag{4.2}$$

Where CR_{ti} is the covariance with the i^{th} template; each template is normalized with η_i so that it has an RMS value of 1.

According to [20], the accuracy and reliability of the spectrum-based signal detection algorithm and the template-based signal detection algorithm are slightly higher than the RMS-based signal detection algorithm, but the quantity and complexity of computation are much higher. In practical use, the RMS-based signal detection algorithm can greatly improve the efficiency of algorithms with acceptable accuracy and reliability.

4.2.3 Impedance Estimation

After detection, disturbance signals are utilized for estimating system impedance. The widely used approach is the method proposed in [20]. It extracts disturbance signals by the subtraction of two consecutive cycles first. Voltage quantities are used to give an example, as shown in Figure 4.2. FFT is then applied to calculate the fundamental frequency components of the extracted voltage and current disturbances. The system impedance can be estimated by (4.3).

$$\mathrm{Z} = \frac{\Delta V}{\Delta I} \tag{4.3}$$

Where ΔV and ΔI are the fundamental frequency phasors of the extracted voltage and current disturbances. Z is the estimated system impedance.

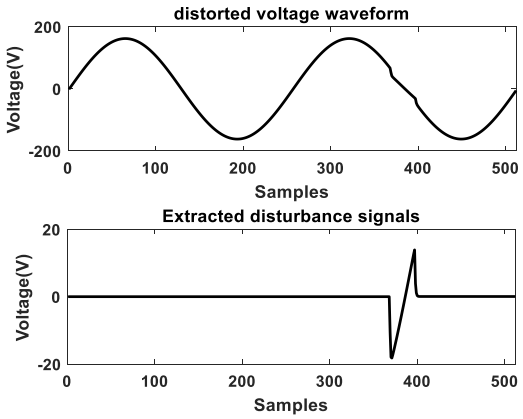

Figure 4.2 Disturbance signals extraction

The performance of this method is good when large disturbance energy is injected in the PCC. However, when injected disturbance energy is smaller (e.g., the disturbance is injected in downstream sockets), the performance of this method is not satisfactory. The reason is that (4.3) assumes that the system side is constant during two consecutive cycles. But the injected disturbance energy is very small compared to system capacity in the active scheme. The fundamental frequency component's variations from the system side cannot be ignored, or it will have an influence on the estimated results' accuracy.

Therefore, there is a need to improve the impedance estimation method. Since system variations and intentionally generated disturbances are independent, this thesis proposes to use independent components analysis (ICA) to improve the impedance estimation method. ICA is the statistical signal processing technique to recover the latent independent variables or source signals from observed mixtures without knowing the way the source signals are mixed [24], [26]-[28]. It can be extended to the separation of complex-valued signals, which facilitates the power system analysis in the frequency domain [25]. Details of ICA are presented in Appendix F.

4.3 Proposed Active Method

In this section, a new active method is proposed. The proposed method consists of two improvements with respect to disturbance generation and system impedance estimation:

1. A portable low-cost device applicable to 120 V single-phase socket and 208 V three-phase socket.

2. An improved system impedance estimation method called the active-disturbances-based method (AD method), which uses the theory of ICA. For disturbance detection, the RMS-based signal detection algorithm is used for higher efficiency.

4.3.1 The Proposed Scheme for Disturbance Generation

To generate intentional disturbances, the proposed idea is to connect a thyristor-based device in a user-selected location inside the customer's facility. The device creates a small short-circuit disturbance actively, as shown in Figure 4.3.

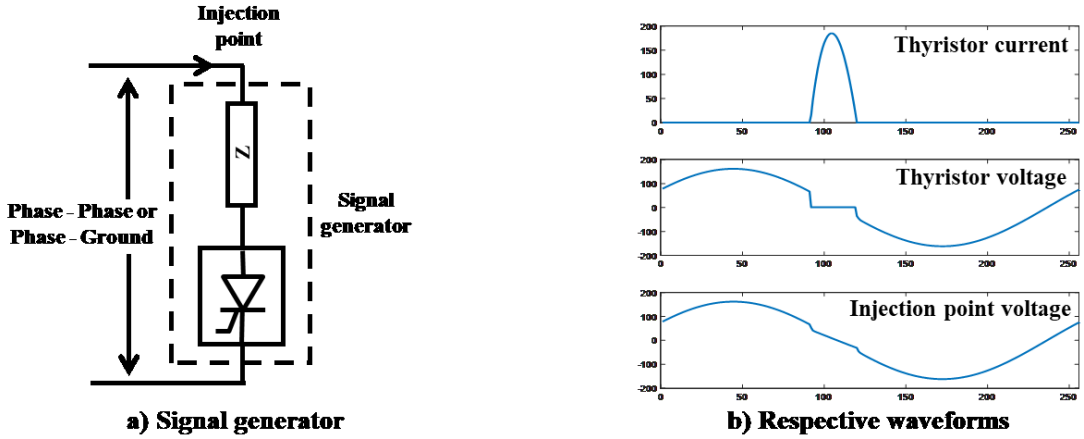

Figure 4.3 Illustration of the proposed signal generator

The disturbance signals are controlled through the firing angle of the thyristor to produce a voltage distortion and a pulse current. The firing angle is controlled to ensure that the generated disturbance does not cause power quality problems or trigger the protection devices of the system, and how to control the firing angle will be clarified in section 4.4.2.

In order to facilitate the use of the proposed method, the device is designed for connection into sockets at any downstream location. There are two available injection modes: One is the one-phase injection mode (L-G), which is applicable to a 120 V single-phase socket; and the other is the two-phase injection mode (L-L), which is applicable to a 208 V three-phase socket. The details of these two injection modes will be explained in section 4.4.1. The proposed signal pattern is shown in Figure 4.4.

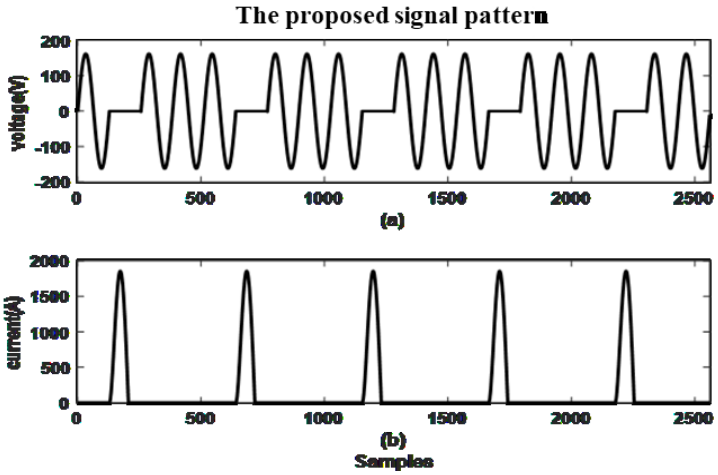

Figure 4.4 The voltage and current quantities across the thyristor

The firing angle is set as 0º here for illustration, and the disturbance signals are designed to be injected every three cycles five times, which means that the disturbance signals will last for 1/3 second (20 cycles) for one measurement activity. There are two reasons for the design of the proposed signal pattern. One reason is that ICA is a statistical algorithm, which needs a number of samples for analysis. After testing, injecting disturbance signals five times is an efficient way. If the number of times is smaller than five, the signal pattern will have an influence on the accuracy and reliability of estimated results. Meanwhile, if the number of times is larger than five, the impact of power quality and safety issues will be aggravated. The other reason is that ICA needs sources with fluctuations to indicate features, so the disturbance signal is injected with a certain time interval (i.e., three cycles).

4.3.2 Impedance Estimation Using the Active-Disturbance-Based Method

Considering the unexpected fundamental frequency component's variations from the system side, (4.3) no longer holds and the new problem is redefined as follows.

1) Problem reformulation. The utility side and signal generator side can be modelled with their Thevenin equivalent circuits during the measurement period, as shown in Figure 4.5.

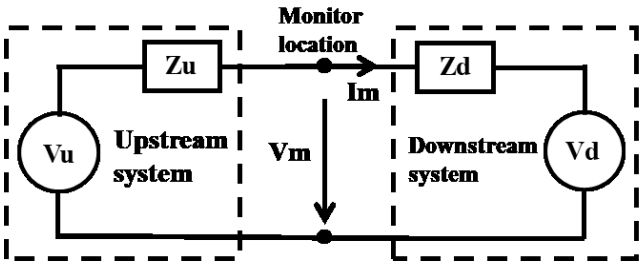

Figure 4.5 Thevenin equivalent circuits representation

After applying the superposition law, voltage and current phasors at the measurement point are defined as follows.

$$\boldsymbol{O} = \boldsymbol{ZS} \tag{4.4}$$

Where $\boldsymbol{O}$ is the matrix of observed quantities; $\boldsymbol{Z}$ is the mixed matrix; $\boldsymbol{S}$ is the source quantities on the system side and customer side. Details are presented as follows.

$$O = \begin{bmatrix} V_m \\ I_m \end{bmatrix} \tag{4.5}$$

$$Z = \begin{bmatrix} \dfrac{Z_d}{Z_u + Z_d} & \dfrac{Z_u}{Z_u + Z_d} \\ \dfrac{1}{Z_u + Z_d} & -\dfrac{1}{Z_u + Z_d} \end{bmatrix} \tag{4.6}$$

$$S = \begin{bmatrix} V_u \\ V_d \end{bmatrix} \tag{4.7}$$

Where V_m and I_m are the positive-sequence or negative-sequence voltage and current phasors at the measuring point. V_u and Z_u are the Thevenin equivalent voltage source and the Thevenin equivalent impedance from the system side. Likewise, V_d and Z_d are the Thevenin

equivalent voltage source and Thevenin equivalent impedance from the load side. V_m and I_m are known variables here since they can be measured by PQ monitors. V_u, V_d, Z_u and Z_d are unknown variables, thus, there are more unknown variables than the number of valid equations. One significant characteristic of these two Thevenin equivalent voltage sources is that their variations are independent. Therefore, we can utilize this feature to solve this problem by ICA [21]. Namely, the ICA will find the unknowns Z_u and Z_d by solving the above equation through iterations.

2) Implementation of ICA. After injecting disturbances by the proposed devices, 20 cycles of the resulting voltage and current waveforms at the measuring point are recorded. Ten cycles of new waveforms are obtained by the subtraction of two consecutive cycles (2nd cycle – 1st cycle, 4th cycle – 3rd cycle, …) as shown in Figure 4.6. Phase A is selected to give an example here.

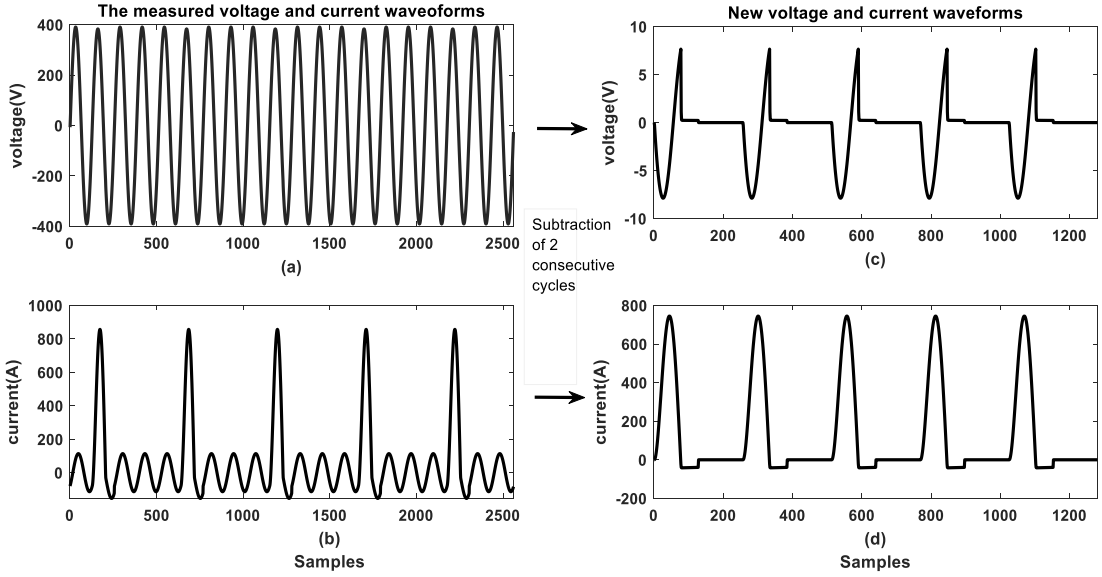

Figure 4.6 The measured voltage and current waveforms and new waveforms (phase A)

Afterward, the FFT algorithm is applied to each cycle of new waveforms to extract the fundamental frequency components. The extracted fundamental frequency components of voltage and current quantities are collected in matrix ***O***, as shown in (4.8).

$$O = \begin{bmatrix} V(1) & V(2) & \text{L} & V(10) \\ I(1) & I(2) & \text{L} & I(10) \end{bmatrix} \tag{4.8}$$

Where V(i) is the fundamental frequency component of the i^{th} cycle's new voltage waveform. I(i) is the fundamental frequency component of the i^{th} cycle's new current waveform.

Consequently, Complex ICA is applied to matrix $\boldsymbol{O}$ to estimate the separating matrix $\boldsymbol{W}$. The simplified illustration of ICA's mixing and separation process is shown in Figure 4.7.

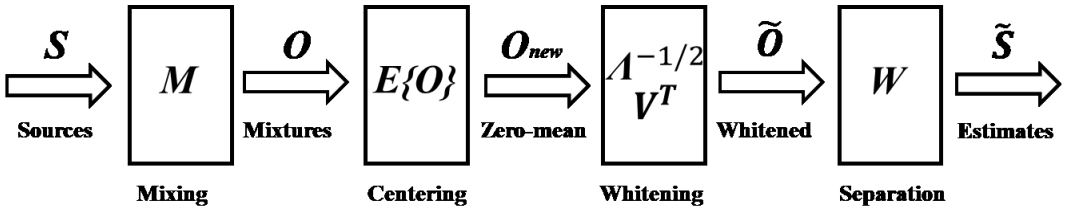

Figure 4.7 The mixing and separation process of ICA

Please note that matrix $\boldsymbol{O}$ must be preprocessed by centring and whitening first [26]. Details of centring and whitening can be found in Appendix F. The separating matrix $\boldsymbol{W}$ can then be used to recover source signals as in the following equations.

$$\hat{\boldsymbol{S}} = \boldsymbol{HO} \tag{4.9}$$

$$\hat{S} = \begin{bmatrix} \hat{V}_u \\ \hat{V}_d \end{bmatrix} \tag{4.10}$$

$$H = W^T \Lambda^{-1/2} V^T = \begin{bmatrix} h_{11} & h_{12} \\ h_{21} & h_{22} \end{bmatrix} \tag{4.11}$$

Where $\hat{\boldsymbol{S}}$ is the matrix of estimated source signals; $\boldsymbol{H}$ is the estimated mixing matrix; $\boldsymbol{\Lambda}$ is the diagonal matrix of eigenvalues of E$\{\boldsymbol{OO}^{\text{T}}\}$; and $\boldsymbol{V}$ is the orthogonal matrix of eigenvectors of E$\{\boldsymbol{OO}^{\text{T}}\}$; Symbol E denotes the statistical expectation. Note that ICA has scaling indeterminacy and ordering indeterminacy [29] and the details are explained in Appendix F.

Therefore, two complex correction factors c_u and c_d are added to represent these properties, as shown in (4.12).

$$\begin{bmatrix} \hat{V}_u \\ \hat{V}_d \end{bmatrix} = \begin{bmatrix} c_u V_u \\ c_d V_d \end{bmatrix} \tag{4.12}$$

Substituting (4.12) in (4.9) gives

$$\begin{bmatrix} V_u \\ V_d \end{bmatrix} = \begin{bmatrix} \frac{h_{11}}{c_u} & \frac{h_{12}}{c_u} \\ \frac{h_{21}}{c_d} & \frac{h_{22}}{c_d} \end{bmatrix} \begin{bmatrix} V_m \\ V_m \end{bmatrix} \tag{4.13}$$

Meanwhile, from (4.4) we have

$$\begin{bmatrix} V_u \\ V_d \end{bmatrix} = \begin{bmatrix} 1 & Z_u \\ 1 & -Z_d \end{bmatrix} \begin{bmatrix} V_m \\ V_m \end{bmatrix} \tag{4.14}$$

Comparing (4.13) with (4.14), the system impedance can be obtained as follows.

$$Z_u = \frac{h_{12}}{h_{11}} \tag{4.15}$$

3) Statistical check. The proposed disturbance signals are injected five times for one complete measurement activity. It is possible that there are occasional large fluctuations caused by other electrical components during the measurement period (20 cycles in total), as shown in Figure 4.8, which may lead to large errors in final results.

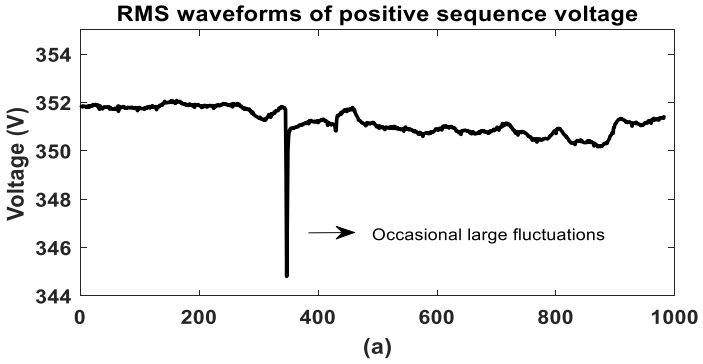

Figure 4.8 Occasional large fluctuations during the measurement period

In order to prevent this occasional error from happening, more measurement activities should be conducted to statistically check the results. It is recommended to take more than ten measurement activities. The statistical check consists of two steps: removing outliers by the Z-Score technique [30]-[33] and providing a confidential level. For example, the estimated results of ten measurement activities are shown in Figure 4.9. The seventh result is obviously one outlier, and it can be removed by the Z-Score technique.

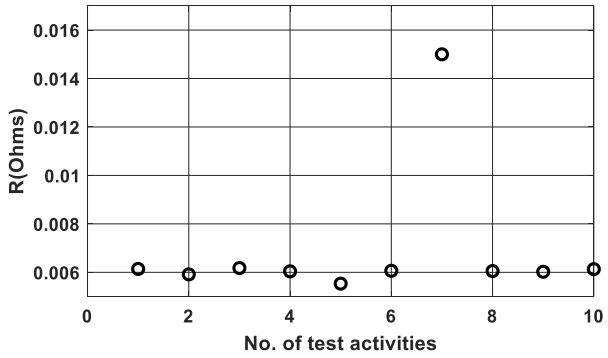

Figure 4.9 The estimated results of ten measurement activities

The determination of the confidence level for the estimated results is similar to the method described in section 2.2.4. The confidence interval for impedance results is plotted in Figure 4.10, and the confidential level is calculated in (4.16). The remaining results are averaged as the final result with the corresponding confidential level.

$$CL = \frac{9}{9} \times 100\% = 100\% \tag{4.16}$$

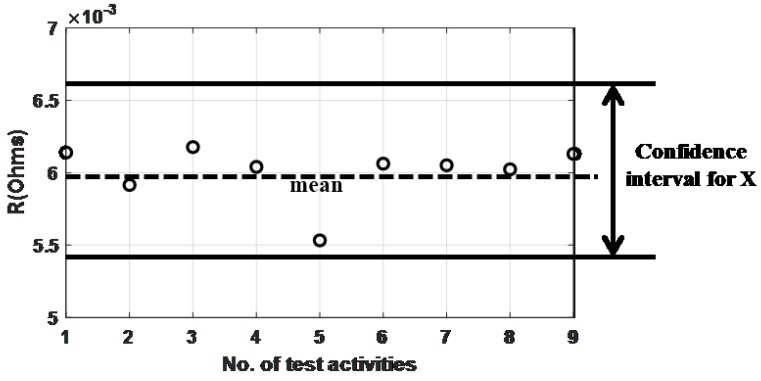

Figure 4.10 Confidence interval for impedance results

4.3.3 Flowchart of Proposed Active Method

Combining the above theories and discussions, the proposed AD method is implemented according to the following steps.

Step 1 Capture three-phase voltage and current waveforms at the measuring point continuously with proper sampling rate, for example, 64 samples per cycle.

Step 2 Detect the proposed disturbances and select 20 cycles after the start time of disturbance injection for each measurement activity.

Step 3 Extract new waveforms by the subtraction of two consecutive cycles.

Step 4 Convert each cycle of new waveforms to the frequency domain using FFT.

Step 5 Convert the resulting three-phase voltage and current phasors to positive-sequence, negative-sequence, and zero-sequence quantities.

Step 6 Correct the phase drift of the positive-sequence quantities and negative-sequence quantities.

Step 7 Formulate the matrix equation (4.4) and implement ICA to solve it. System estimates can be obtained from (4.15).

Step 8 System impedance estimates are statistically checked.

Step 9 Remaining results are averaged and outputted.

The flowchart of these steps is summarized in Figure 4.11.

4.4 Practical Considerations

In practice, injecting certain signals is a complex task, and many practical issues need to be considered. Injection mode is discussed by evaluating the efficiency of the proposed method and the accessibility of the distribution system. Then, the power quality issues and the possible action of overcurrent protection devices are considered and the corresponding limits of the firing angle are determined.

4.4.1 Injection Mode

As discussed in section 4.3, the proposed device is designed to be plugged into the sockets of the load side. In most cases, the single-phase socket and three-phase socket are both accessible. Therefore, the injection mode is quite flexible, and disturbance signals can be injected through one phase, two phases or three phases.

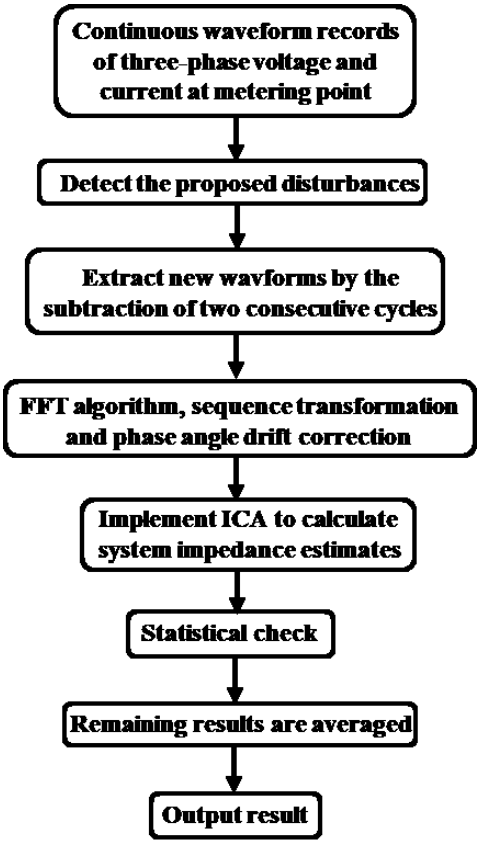

Figure 4.11 Flowchart of the AD method

But in this thesis, the three-phase injection of disturbance signals is not considered because of the following reasons. One reason is that, as discussed in Chapter 2, the influence of system variation is much smaller in the negative-sequence network. Therefore, injecting negative-sequence disturbance is more desired. As the three-phase injection mode contains no

negative-sequence components, the reliability and accuracy of results in this mode are much lower than in the other two injection modes. The other reason is that the three-phase injection mode injects more disturbance energy, which is risky and more likely to cause power quality issues or the action of protective devices. Compared to the two-phase injection mode, the three-phase injection mode has no advantage. In this way, two-phase injection can totally replace the three-phase injection mode with additional advantages. Therefore, the one-phase injection mode and the two-phase injection mode are selected for further investigation as follows.

1) One-phase injection mode. As for the one-phase injection mode, the signal generator is connected between one phase and the ground. For example, a small short circuit can be created in phase A. According to the superposition theorem, we can regard this small short circuit as a superposition of short-time voltage source -va and the original power supply va [34]-[35]. The effect of this -va voltage source on the voltage waveforms is presented in Figure 4.12.

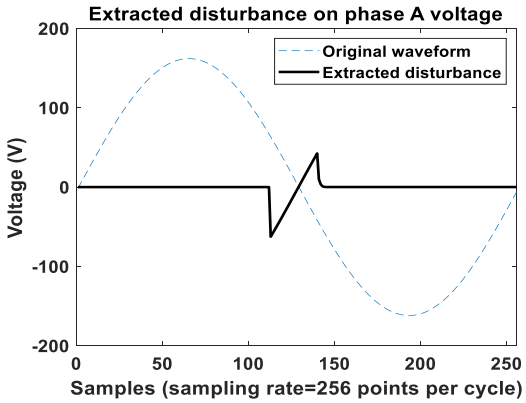

Figure 4.12 Extracted disturbance on phase A voltage

After implementing the FFT algorithm on the short-time voltage source -va for one complete cycle, the fundamental frequency component can be obtained and marked as ΔVa. From the perspective of the frequency domain, ΔVa is the actual added voltage source in the fundamental frequency network. Then the effect of ΔVa in the sequence domain can be evaluated through sequence transformation, as shown in (4.17). The desired negative-

sequence disturbance accounts for one-third, and the other one-third, namely positive-sequence disturbance, can also be used in system impedance measurement for cross-checking. Thus, the efficiency of one-phase injection is 66.7%.

$$\begin{bmatrix} V_+ \\ V_- \\ V_0 \end{bmatrix} = \frac{1}{3}\begin{bmatrix} 1 & e^{j120^\circ} & e^{j240^\circ} \\ 1 & e^{j240^\circ} & e^{j120^\circ} \\ 1 & 1 & 1 \end{bmatrix}\begin{bmatrix} V_a \\ V_b \\ V_c \end{bmatrix}$$

$$\begin{bmatrix} \Delta V_+ \\ \Delta V_- \\ \Delta V_0 \end{bmatrix} = \frac{1}{3}\begin{bmatrix} 1 & e^{j120^\circ} & e^{j240^\circ} \\ 1 & e^{j240^\circ} & e^{j120^\circ} \\ 1 & 1 & 1 \end{bmatrix}\begin{bmatrix} \Delta V_a \\ 0 \\ 0 \end{bmatrix} = \begin{bmatrix} \frac{1}{3}\Delta V_a \\ \frac{1}{3}\Delta V_a \\ \frac{1}{3}\Delta V_a \end{bmatrix} \tag{4.17}$$

2) Two-phase injection. As for the two-phase injection mode, the signal generator is connected between one phase and the other phase. For example, a small short circuit can be created between phase B and phase C. As shown in Figure 4.13, this small short circuit can be regarded as the superposition of the original network, and two short-time voltage sources (*-Vbc/2*, *Vbc/2*) are added in phase B and phase C, respectively.

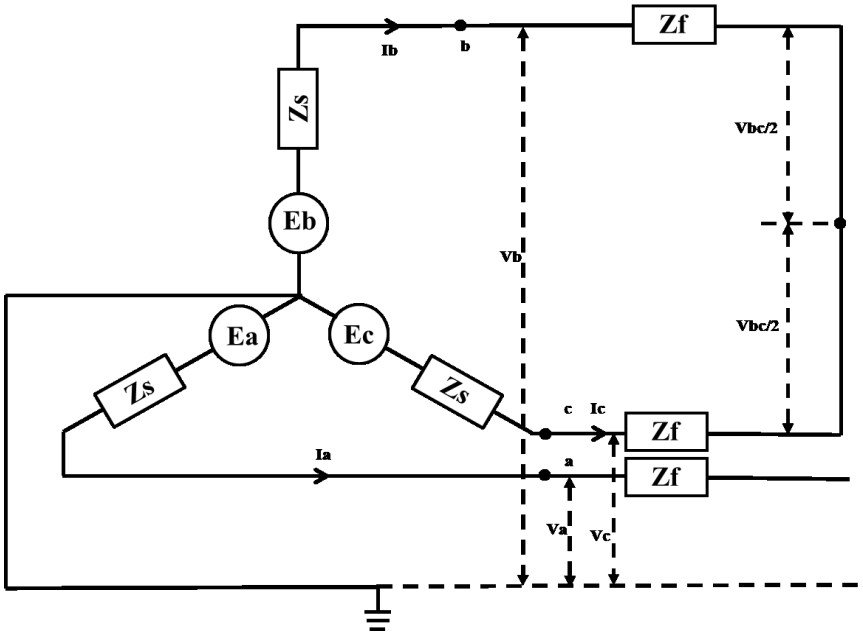

Figure 4.13 Illustration for two-phase injection mode

Vbc is the difference between phase B voltage and phase C voltage, as shown in (4.18). Likewise, the fundamental frequency components of *Vbc/2* are calculated and marked as *ΔVbc*. Then, the effect of this added voltage source in sequence domain can be evaluated through sequence transformation, as shown in (4.19). The desired negative-sequence disturbance accounts for 50%, and the other 50%, namely positive-sequence disturbance, can also be used in system impedance measurement for cross-checking. As a result, the efficiency of the two-phase injection is 100%.

$$Vbc = Vb - Vc \tag{4.18}$$

$$\begin{bmatrix} V_+ \\ V_- \\ V_0 \end{bmatrix} = \frac{1}{3}\begin{bmatrix} 1 & e^{j120^\circ} & e^{j240^\circ} \\ 1 & e^{j240^\circ} & e^{j120^\circ} \\ 1 & 1 & 1 \end{bmatrix}\begin{bmatrix} V_a \\ V_b \\ V_c \end{bmatrix}$$
$$\begin{bmatrix} \Delta V_+ \\ \Delta V_- \\ \Delta V_0 \end{bmatrix} = \frac{1}{3}\begin{bmatrix} 1 & e^{j120^\circ} & e^{j240^\circ} \\ 1 & e^{j240^\circ} & e^{j120^\circ} \\ 1 & 1 & 1 \end{bmatrix}\begin{bmatrix} 0 \\ -\Delta V_{bc} \\ \Delta V_{bc} \end{bmatrix} = \begin{bmatrix} \Delta V_{bc} e^{j270^\circ} \\ \Delta V_{bc} e^{j90^\circ} \\ 0 \end{bmatrix} \tag{4.19}$$

In summary, the one-phase injection mode and two-phase injection mode both have their advantages and disadvantages. For one-phase injection, the device is more convenient for use because of more common single-phase sockets. For the two-phase injection mode, the efficiency is higher and the capacity of available disturbance energy is larger.

4.4.2 Signal Strength

As discussed previously, the firing angle can be changed to adjust signal strength. But the signal strength of the generated disturbance signals should not be too large due to power quality issues and safety considerations. The issues are investigated from the perspective of voltage and current limit violations.

1) Power quality issues. The power quality issues mainly focus on voltage quantities. According to the CBEMA curve shown in Figure 4.14, the RMS of the proposed signal pattern should locate in "No Interruption in Function Region" to prevent the interruption of

delicate devices. Since the proposed signal pattern lasts for 20 cycles, the acceptable lower limit is 70% from the CBEMA curve. Thus, the respective limit of the firing angle is determined based on this parameter. The acceptable firing angle can be determined by iteratively setting the firing angle starting from 0º. Figure 4.15 shows the waveform of the proposed signal at 0º firing angle. The new RMS value is calculated by (4.20) as 86.6% of the original value. This RMS value is higher than the lower limit even for the worst case (i.e., 0º firing angle). Therefore, the firing angle can also range from 0º to 180º.

$$RMS^{new} = \sqrt{3 \times \frac{1}{8\pi} \int_0^{2\pi} (V_m \sin t)^2 \, dt} = \frac{\sqrt{3}}{2} \times \frac{V_m}{\sqrt{2}} = 0.866 RMS^{old} \tag{4.20}$$

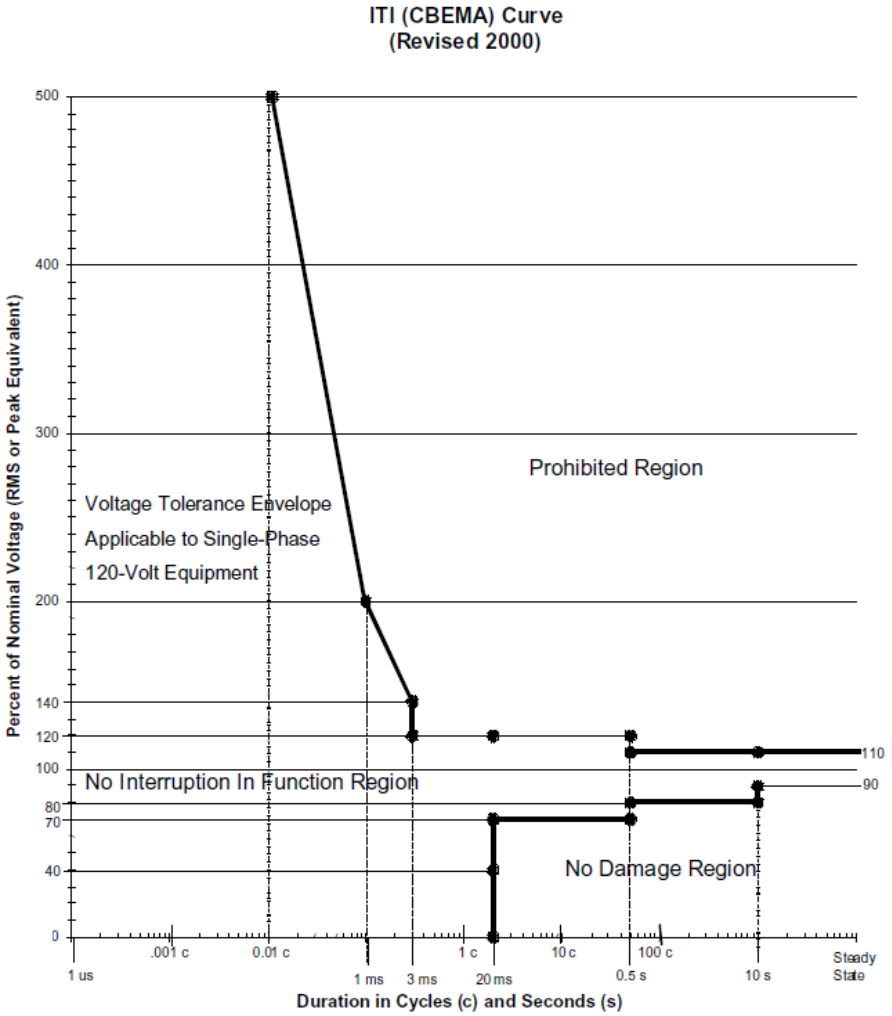

Figure 4.14 ITI (CBEMA) Curve

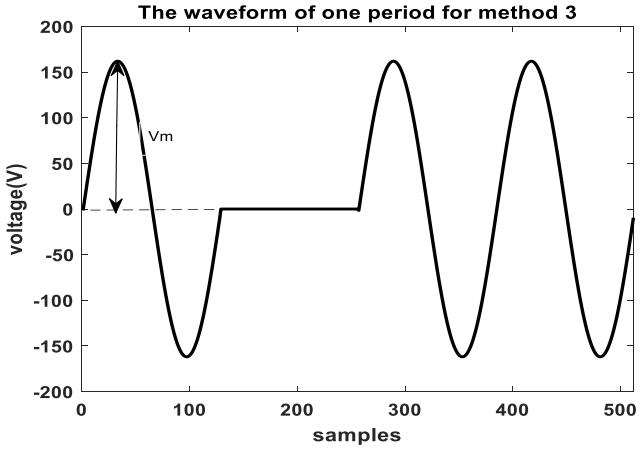

Figure 4.15 The waveform of one period for the proposed signal pattern (firing angle=0º)

2) Safety problems. The safety problems mainly focus on current quantities to prevent the action of overcurrent protection devices. According to [40], the rated current of a 120 V indoor transformer in commercial buildings is around 200 A. The transformer secondary overcurrent protection devices should be 1.25 times the rated current based on design standards. Therefore, the 250 A (200 A×1.25) fuse is considered here and the time-current curve is presented in Appendix D. Here, we use a simulation case to evaluate the possibility of a fuse blown by comparing the disturbance-caused pulse current waveform with the 250 A fuse's time-current curve. For one-phase injection, the worst case with the firing angle as 0º is considered, and the resulting current waveform is shown in Figure 4.16.

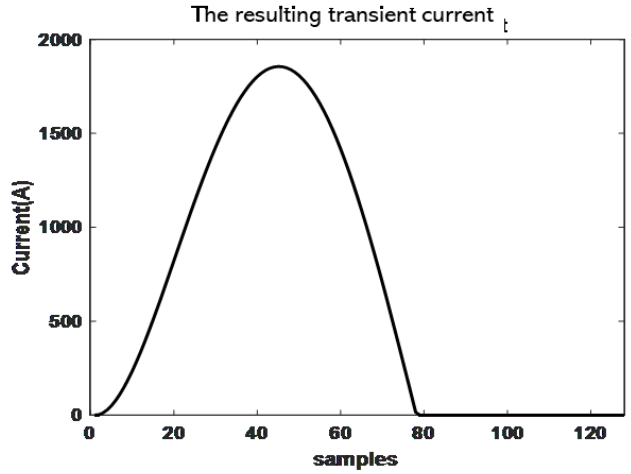

Figure 4.16 The waveform of one period for one-phase injection (firing angle=0º)

The peak value is 1864 A and the duration of the pulse current waveform is about 0.01 s. From the time-current curve (250 A for the simulation case), the peak value is 7000 A for the current lasting 0.01 s, which is much larger than that of the resulting current waveform. Thus, the requirement for avoiding the action of overcurrent protection devices is met.

For two-phase injection, we still consider the worst case with the firing angle as 0º. The resulting current waveform in the simulation case is shown in Figure 4.17. The peak value is 2310 A and the duration is about 0.01 s. From the time-current curve, the peak value is 7000 A for the transient current lasting 0.01 s, which is much larger than that of the resulting current waveform. Thus, the requirement for avoiding the action of overcurrent protection devices is also met.

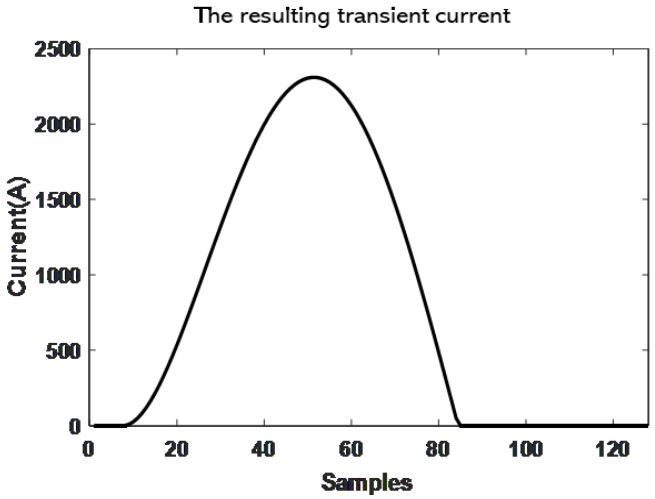

Figure 4.17 The waveform of one period for two-phase injection (firing angle=0º)

In conclusion, the minimum firing angles of one-phase injection and two-phase injection can theoretically be 0º for the main application scenarios. However, in practical application, the situation of the real system is complicated. The limitations of voltage quantities and current quantities might change according to the standards or requirements of the proposed device's target market. So, it is recommended to gradually reduce the firing angle from 180º to 0º to increase the resulting pulse current until the corresponding threshold is reached, which is called the firing angle screening in the thesis. For example, the firing angle is gradually

reduced by 10º per cycle from 180º to 0º, namely the firing angle of the first cycle is 180º, the firing angle of the second cycle is 170º and so on. As shown in Figure 4.18, when the firing angle gradually decreases, the resulting pulse current goes up. If the resulting current's magnitude is above 90% of the threshold, the firing angle screening ends, and the firing angle of the previous cycle is used to inject intentional disturbances by the proposed signal pattern. Here 10% of the threshold is to leave a certain margin for measurement errors and possible safety issues.

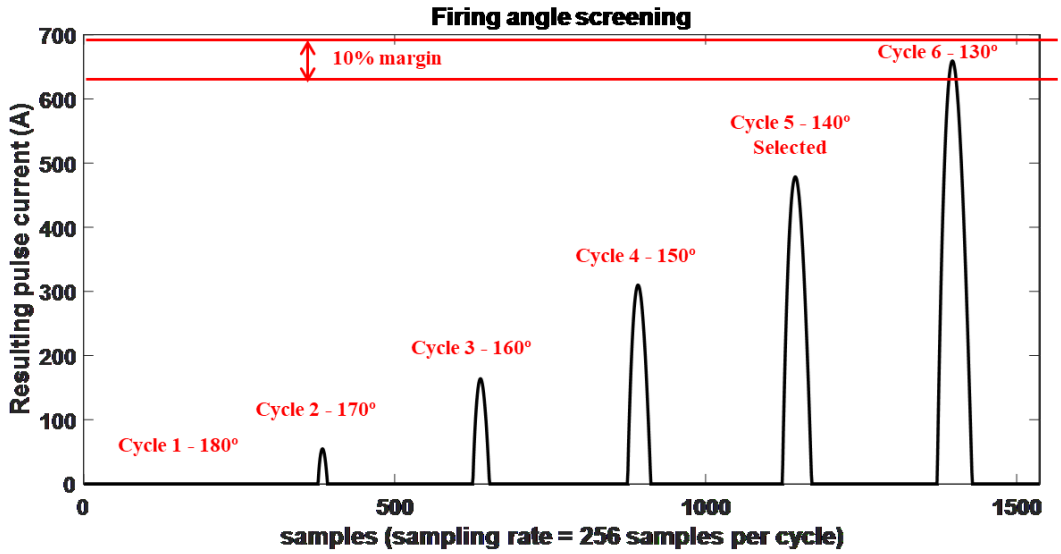

Figure

Figure 4.18 Illustration of the firing angle screening

4.5 Summary

This chapter has comprehensively presented a novel active system impedance measurement method. The proposed active method employs a flexible way of generating intentional disturbances. The portable device can be directly plugged into any one of the downstream sockets, and this way is convenient for users. But the disturbance energy of this method propagated to the PCC is smaller than that of injecting directly at the PCC. Therefore, a new method called the AD method is proposed to estimate system impedance by using ICA, and it is theoretically more accurate and reliable than existing methods.

Chapter 5 Performance of Proposed Active Method

In this chapter, computer simulations are performed to evaluate the performance of the proposed active method. Conclusions are provided based on the results obtained.

5.1 Design of Simulation System

Simulations were carried out in a 4.16 kV distribution system to test the proposed active method. The topology and parameters are presented as follows.

5.1.1 Topology of Simulation System

The simulation is built on an IEEE 13 Node Test Feeder [37] and a 10-Node Unbalanced Commercial Distribution System [38], as shown in Figure 5.1.

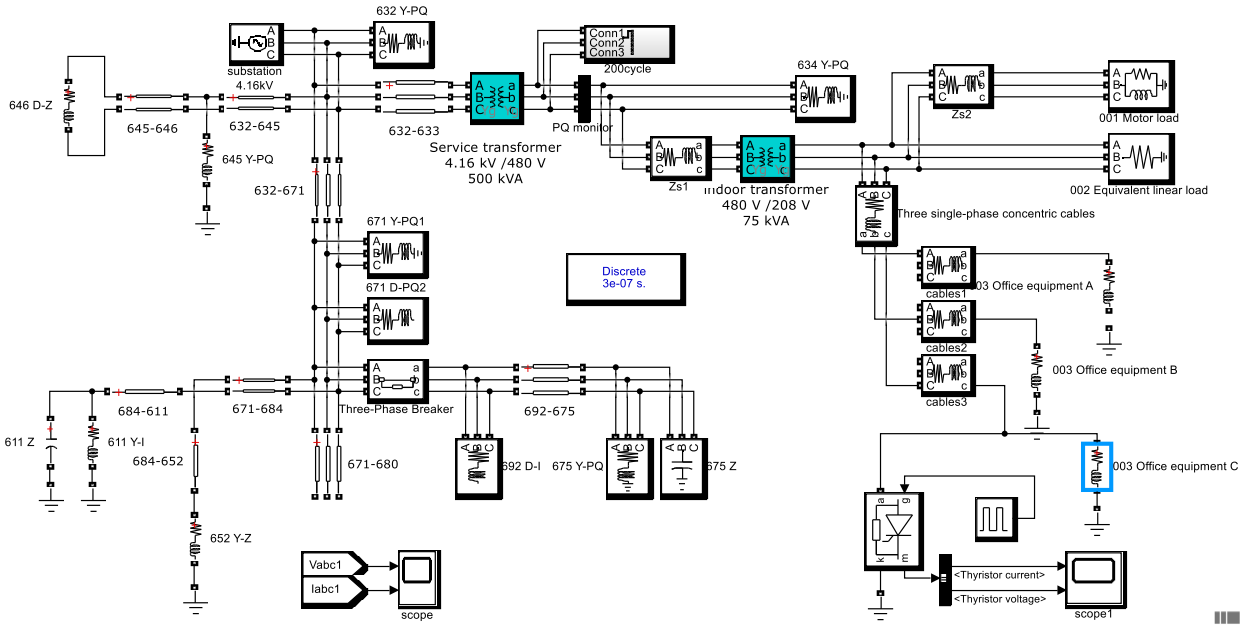

Figure 5.1 Overview of the simulation system

In this simulation, the distribution system is supplied by a 5 MVA (115 kV D/4.16 kV Yg) substation transformer. There is a 500 kVA (4.16 kV Yg/0.48 kV Yg) service transformer and a 75 kVA (480 V Yg/208 V Yg) indoor transformer for a commercial building. In addition, a block is added to simulate system-side variations.

5.1.2 System Parameters

The parameter information of the distribution system is presented in the following tables.

Table 5.1: Overhead and underground line configuration data

Config.	Phasing	Phase (ACSR)	Neutral (ACSR)	Spacing
601	B A C N	556,500 26/7	4/0 6/1	500
602	C A B N	4/0 6/1	4/0 6/1	500
603	C B N	1/0	1/0	505
604	A C N	1/0	1/0	505
605	C N	1/0	1/0	510
606	A B C N	250,000 AA, CN	None	515
607	A N	1/0 AA, TS	1/0 Cu	520

Table 5.2: Line segment data

Node A	Node B	Length (ft.)	Config.
632	645	500	603
632	633	500	602
633	634	0	XFM-1
645	646	300	603
650	632	2000	601
684	652	800	607
632	671	2000	601
671	684	300	604

671	680	1000	601
671	692	0	Switch
684	611	300	605
692	675	500	606

Table 5.3: Transformer data

No.	kVA	kV-high	kV-low	R - %	X - %
Substation	5,000	115 - D	4.16 - Gr. Y	1	8
Service transformer	500	4.16 - Gr. Y	0.48 - Gr. Y	1.1	2
Indoor transformer	75	0.48 - Gr. Y	0.208 - Gr. Y	1.96	2.27

Table 5.4: Capacitor data

Node	Ph-A (kVAr)	Ph-B (kVAr)	Ph-C (kVAr)
675	200	200	200
611	0	0	100

Table 5.5: Load data

Node	Model	Ph1(kW)	Ph1(kVAr)	Ph2(kW)	Ph2(kVAr)	Ph3(kW)	Ph3 (kVAr)
632	Y-PQ	17	10	66	38	117	68
634	Y-PQ	160	110	120	90	120	90
645	Y-PQ	0	0	170	125	0	0
646	D-Z	0	0	230	132	0	0
652	Y-Z	128	86	0	0	0	0
671	D-PQ	385	220	385	220	385	220
671	Y-PQ	17	10	66	38	117	68
675	Y-PQ	485	190	68	60	290	212
692	D-I	0	0	0	0	170	151

001	D-PQ	1.7	0.5	1.7	0.5	1.7	0.5
002	Y-PQ	3	0	2	0	3.5	0
003	Y-PQ	15	2	0	0	0	0
003	Y-PQ	0	0	9.4	1.4	0	0
003	Y-PQ	0	0	0	0	12	2.4

The determination of the line configuration between the indoor transformer and the socket is explained as follows. The system-side variation block is also introduced.

1) Line configuration between the indoor transformer and the socket. According to practical experience, the length of the single-phase line from indoor transformer to socket should be less than 250 ft. For this reason, here we choose 250 ft to assume the worst case. Since the cable between the service transformer and indoor transformer is three-phase, its maximum allowed distance is roughly double that of the cable in single-phase [39], i.e. 500 ft. The typical types of cables used in the commercial system are determined according to the examples in [40]. The corresponding parameters of the cable's impedance information can be found in Appendix E.

2) System-side variation block. This block is used to simulate system-side variations. The main idea is to investigate voltage and current quantities' variations of a practical case with stable loads first. Then, many new loads are added at the measuring point and switched on/off to create similar voltage and current quantities' variations. The details of determining the size of these loads and the control of the switches are explained in Appendix G. For this simulation, a practical case, "Industrial and commercial load data-Drumheller Bitfury," is selected. The loads are mainly computer and data centres, and three-phase voltage and current waveforms are recorded at the PCC point. Then a system-side variation block consisting of 400 breakers and 400 loads is added to create similar voltage and current quantities' variations. The resulting voltage and current RMS values at the measuring point are presented

in Figure 5.2. The variations of negative-sequence quantities are apparently much smaller than those of positive sequence.

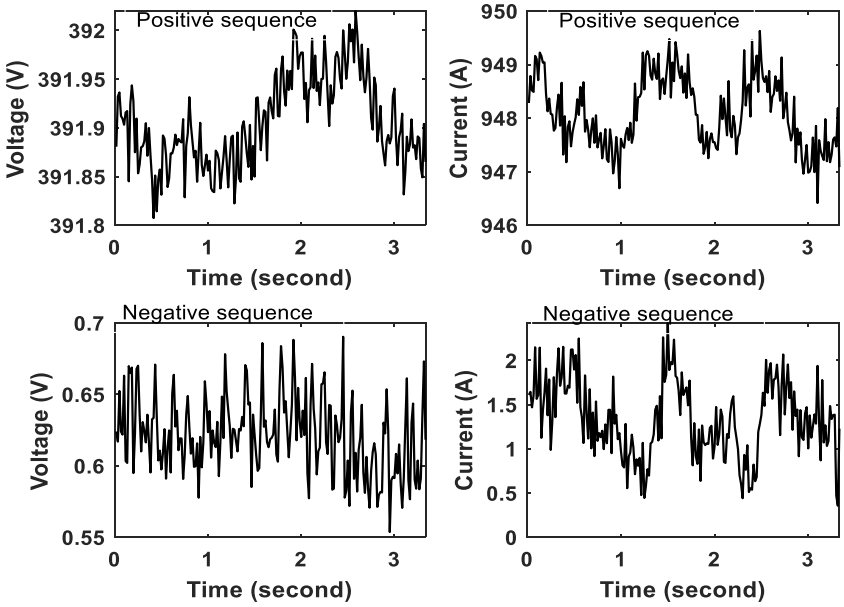

Figure 5.2 Three-phase voltage and current RMS values at the measuring point

5.2 Performance Evaluation

In this section, the performances of the one-phase injection mode and the two-phase injection mode are evaluated. The impedance estimates from using both the positive-sequence and negative-sequence quantities are presented. A comparative study based on the proposed method and the existing method in [20] is provided as well.

5.2.1 One-Phase Injection Mode

A total of ten measurement activities are conducted for this injection mode. For each measurement activity, the firing angle is set as ten degrees and the disturbance signals are injected every three cycles. The resulting three-phase voltage and current RMS values at the

measuring point are presented in Figure 5.3. The corresponding voltage and current waveforms of the thyristor-based signal generator are shown in Figure 5.4.

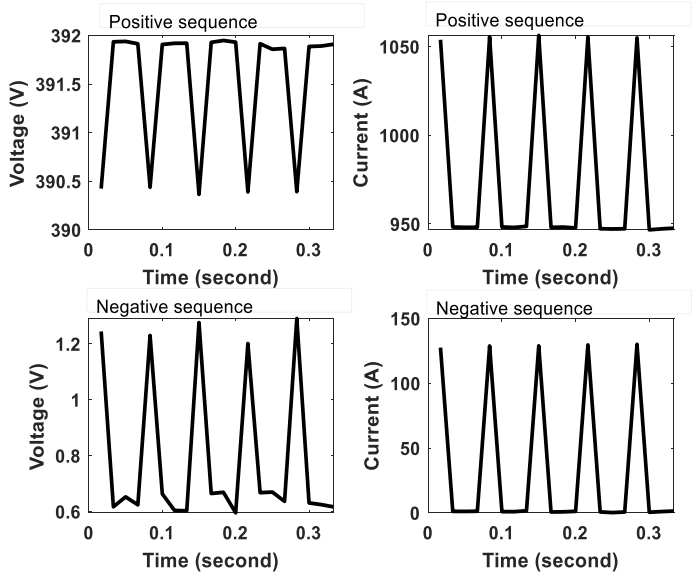

Figure 5.3 The resulting three-phase voltage and current RMS of one test activity

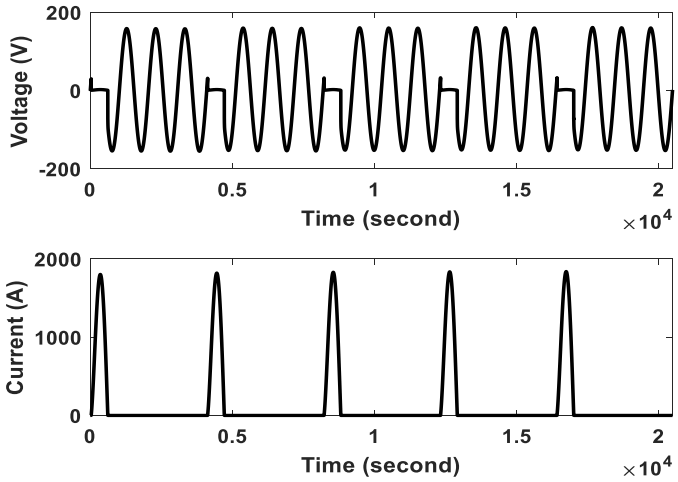

Figure 5.4 Voltage and current waveforms of the thyristor-based signal generator

The system impedances are then estimated by the proposed method with a group of ten samples. The outputted results are shown in Figure 5.5 and Figure 5.6. As can be observed

from Figure 5.6, the estimation based on negative-sequence quantities leads to better convergence than that based on the positive sequence.

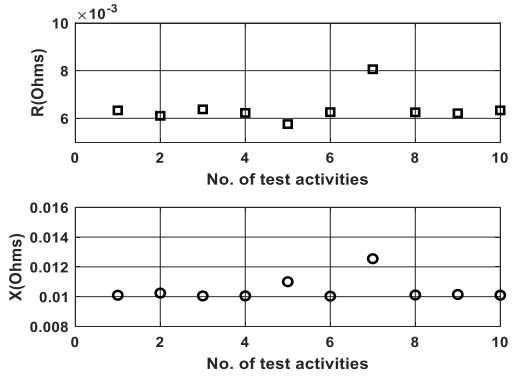

Figure 5.5 Impedance results estimated by positive-sequence quantities

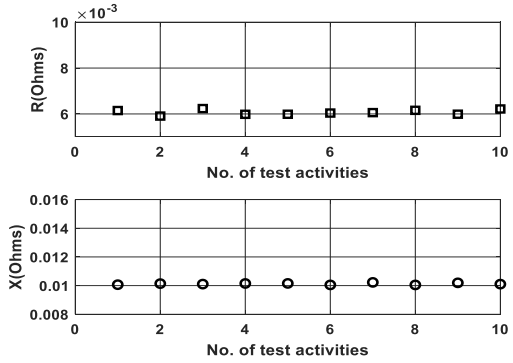

Figure 5.6 Impedance results estimated by negative-sequence quantities

After the statistical check is applied, the average values of the estimated impedances are presented in Table 5.6. The reference value derived from the short-circuit test is shown in Table 5.6 as well.

Table 5.6: System impedance results with one-phase injection mode

Estimated by Positive Sequence	Estimated by Negative Sequence	Reference Value
0.0064+0.0104j (CL 80%)	0.0061+0.0101j (CL 100%)	0.0059 + 0.0101j

As can be seen from the table, there is a good agreement between the estimated values and the reference value. It can also be observed that the impedance result estimated by negative-sequence quantities is more accurate than that estimated by the positive-sequence quantities.

5.2.2 Two-Phase Injection Mode

A total of ten measurement activities are conducted for this mode of injection. For each measurement activity, the firing angle is set as ten degrees, and the disturbance signals are injected every three cycles. The resulting three-phase voltage and current RMS values at the measuring point are presented in Figure 5.7. The corresponding voltage and current waveforms of the thyristor-based signal generator are shown in Figure 5.8.

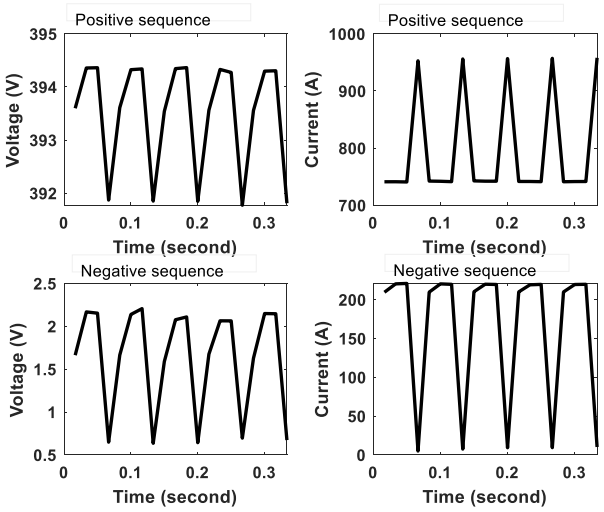

Figure 5.7 The resulting three-phase voltage and current RMS of one test activity

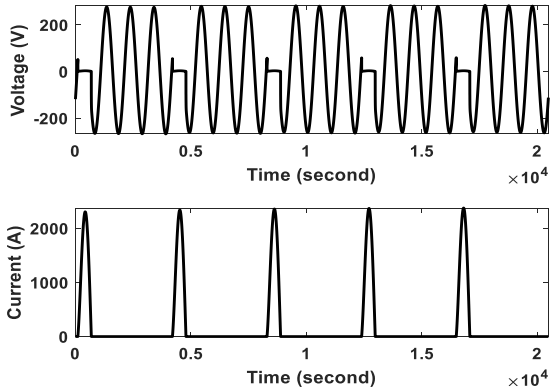

Figure 5.8 Voltage and current waveforms of the thyristor-based signal generator

The system impedances are then estimated by the proposed method with a group of ten samples. The outputted results are shown in Figure 5.9 and Figure 5.10.

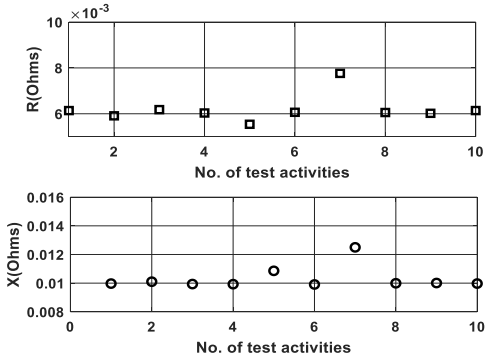

Figure 5.9 Impedance results estimated by positive-sequence quantities

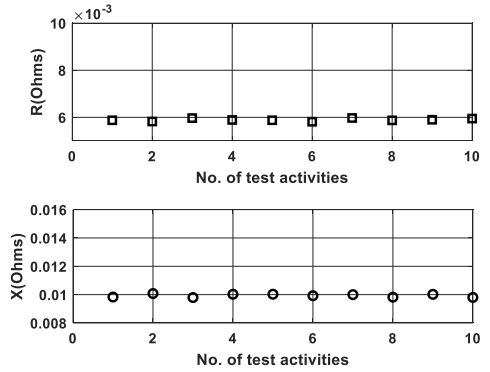

Figure 5.10 Impedance results estimated by negative-sequence quantities

As can be observed from Figure 5.10, the estimation based on negative-sequence quantities leads to better convergence than that based on the positive sequence. After the statistical check is applied, the average values of the estimated impedances are presented in Table 5.7. The reference value derived from the short-circuit test is shown in Table 5.7 as well. The agreement is quite acceptable, and the impedance result estimated by negative-sequence quantities is more accurate.

Table 5.7: System impedance results with one-phase injection mode

Estimated by Positive Sequence	Estimated by Negative Sequence	Reference Value
0.0062+0.0103j (CL 80%)	0.0059+0.0099j (CL 100%)	0.0059 + 0.0101j

5.2.3 Comparative Study

The performance of the proposed method is compared to an existing method proposed in [20]. The one-phase injection mode with the negative sequence is chosen for analysis. The firing angle of the thyristor is increased by 20 degrees to reduce the size of the injected disturbance signals gradually. Error is calculated by computing the difference between the resulting impedance estimates from the two methods and the reference value. Figure 5.11 shows the error level of the proposed method and the existing method.

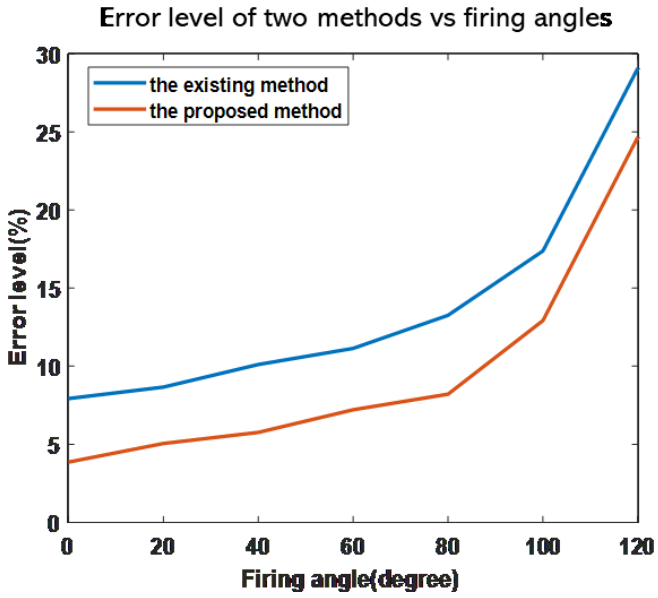

Figure 5.11 Error level of the proposed method vs the existing method

From Figure 5.11, it can be seen that the performance of the proposed method has better accuracy with the lower error level. The reason is that the method in [20] directly subtracts post-disturbance quantities by pre-disturbance quantities by assuming that the system side is constant during two consecutive cycles. Therefore, the existence of system variations will

increase its error level. However, the proposed method takes the fundamental frequency component's variations from the system side into consideration and uses ICA to solve the problem by assuming independent sources on both the system side and the load side. As a result, the error level of the proposed method is lower.

5.2.4 Conclusions and Discussions

Verification studies have been conducted for the proposed active system impedance measurement method using simulation studies. The results show that the proposed method can be used to estimate system impedances with high accuracy. The main findings are summarized and discussed as follows:

- Many parameters in this simulation case are set by the considerations of the worst case. For example, the distance between the socket and the indoor transformer is set as the longest distance in electrical design. If the distance is shorter, the impedance of cables is smaller. In this way, the signal generator could induce larger variations of the voltage and current quantities at the measuring point. As a result, the accuracy of the final results will be better. Therefore, we can conclude that, for practical purposes, the proposed method will be able to meet industry needs.

- In view of the fact that the network positive-sequence impedance is generally equal to its negative-sequence impedance, this research has investigated the use of negative-sequence components as an additional source of data to improve positive-sequence impedance estimation. The results are satisfactory as more reliable estimates are obtained. As negative-sequence quantities are generally more stable in distribution systems, it is recommended to use impedance results based on the negative-sequence components when the impedance results of positive-sequence components and those of negative-sequence components are similar.

- It is possible that there are occasional large fluctuations caused by other electrical components during the measurement period. Therefore, it is recommended to conduct at least ten measurement activities; more measurement activities will lead to more accurate and reliable estimates of the system impedance.

5.3 Summary

This chapter has presented comprehensive simulation studies. The estimated results by the proposed method and reference values are generally close to each other. In addition, it is found that estimating system impedance based on negative-sequence quantities may have much better performance than that of the positive sequence. This is mainly due to the small variation of the negative-sequence voltage at the system side. Overall, the performance of the proposed active system impedance method is satisfactory, and it can serve as a backup method to deal with systems consisting of stable loads.

Chapter 6 An Integrated Impedance Measurement System

A system that integrates both passive and active system impedance measurement methods has been developed. This system mainly consists of software embedded with algorithms and a portable thyristor-based device. The software is called "Zfinder" in this thesis. The algorithms of passive and active methods (i.e., the LD method, the SD method, and the AD method) are integrated into the software along with detection techniques. The portable device is the proposed disturbance generator used for the proposed active method as in section 4.3.1.

In this chapter, the application of software and the portable device are introduced first. Next, how to integrate the algorithms of passive and active methods into the software is explained. Finally, the design of the proposed disturbance generator is clarified.

6.1 Software Application

"Zfinder" software is designed to estimate the supply system impedance at the PCC. The input data required for the software is three-phase voltage and current waveforms measured at the PCC. The outputted results provided by the software are the equivalent impedance of the supply system seen from the PCC.

6.1.1 Hardware and Software Requirement

"Zfinder" software should be installed and run with the following requirements:

- A computer with necessary configurations such as 4-core CPU and 8GB memory. Better configurations can improve the efficiency of the tool.
- Windows 7 or Windows 10 operation system.

- Internet access (to download the software installation package).

6.1.2 Input Data

The input data can be acquired by PQ monitors such as *PQPro*™. The data should meet the following conditions:

- Three-phase voltages and currents at the metering point whose upstream impedance needs to be estimated. The line-to-line voltage and line-to-ground voltage are both accepted. The current should be line current.
- The data are in the form of waveforms with a sampling rate of at least 64 points per cycle.
- The duration of the data should be at least 120 minutes with gapless measurement. For long-duration data such as ten hours, it is recommended to break the data into several blocks that each contains 120 minutes.
- There is no restriction on the storage sequence of voltage and current quantities.
- The data file formats supported by the software are ".TSQ," ".mat," and ".xlsx."

6.1.3 Instructions

After downloading and installing "Zfinder" software, users can double click to run "Zfinder." "Active mode" and "Passive mode" are displayed on the user interface. The "Passive mode" does not need any additional device. However, a disturbance generator is required to use the "Active mode" feature. The disturbance generator will be introduced in the next section.

After selecting "Active mode" or "Passive mode," measured three-phase voltage and current waveforms are required to be inputted. Users can load the data file of supported formats and click the "run" button when finished. Then the estimated system impedance will be displayed with the corresponding confidential level if the algorithm yields results. Otherwise, "N/A" will be shown on the user interface.

Please note that it is strongly recommended to try “Passive mode” first. If it does not work on the target system (i.e., “N/A” is displayed), the disturbance generator can be used and the “Active mode” feature of “Zfinder” software should be selected to run.

6.1.4 Additional Device

A disturbance generator is provided to support the “Active mode” feature of “Zfinder.” It consists of two parts: a disturbance generator with a single-phase plug and a single-phase to three-phase plug adaptor. If single-phase sockets (120 V) are available, the disturbance generator can be directly plugged in. Then the disturbance generator will automatically inject the designed disturbances after the “run” button is pressed. The disturbances can be injected several times, but the time interval of two button-press actions should be at least ten seconds. If three-phase sockets (208 V) are available, the plug adaptor can be used to convert the single-phase plug of the disturbance generator to the three-phase plug, and then the disturbance generator can be used in the same way.

6.2 The Design of “Zfinder” Software

In this section, the internal structure of “Zfinder” software will be introduced to explain how to integrate the algorithms of passive and active methods.

The internal structure of “Zfinder” software is illustrated in Figure 6.1. The “Zfinder” software processes the recorded waveform data obtained from measurement activities. When “Passive mode” is selected, the proposed detection scheme will automatically identify the type of disturbances, and corresponding algorithms of passive system impedance measurement methods (i.e., the SD method or the LD method) are selected to analyze the recorded waveform data. Next, according to the results of algorithms, the estimated system impedance with a confidential level or “N/A” will be outputted and displayed. When “Active

mode" is selected, the proposed algorithm of the active system impedance measurement method (i.e., the AD method) will be used to analyze the recorded waveform data. Next, the estimated results of the supply system impedance will be outputted and displayed with a confidential level.

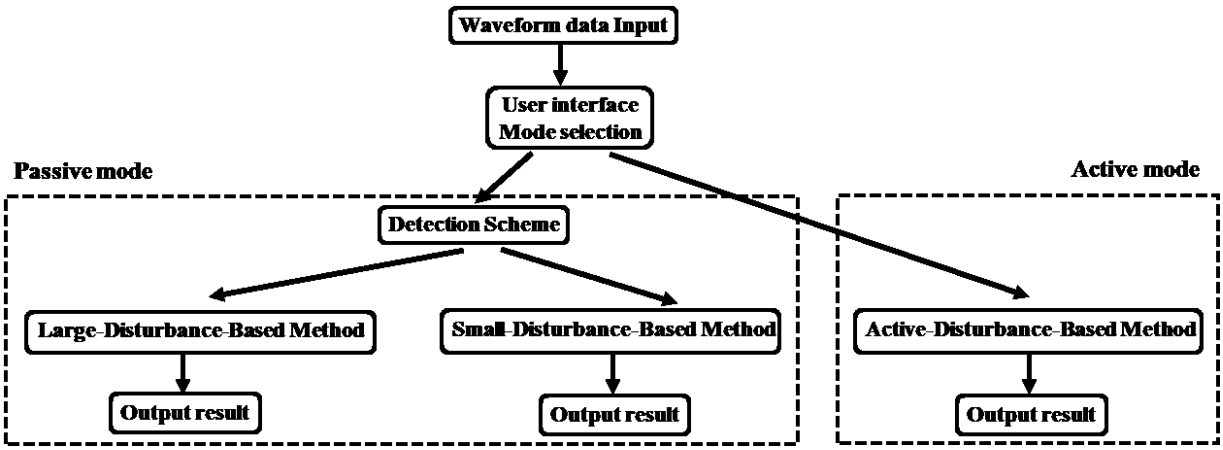

Figure 6.1 The structure of "Zfinder" software

It is useful to note that the active method is not recommended if a system has a lot of small disturbances that are sufficient for impedance determination. This is because (1) the signal produced by the active method may be buried in the small disturbances so there are no results for the active method. (2) if the signal can be detected, the small disturbances might interfere with that active signal, resulting in wrong estimation results. Further research is still needed to clarify the above issues. Therefore, the proposed procedure for impedance measurement, for now, is to use the passive method first. If there are no results, the active method can then be used.

6.3 The Design of the Proposed Disturbance Generator

In this section, the internal structure of the proposed disturbance generator will be introduced to clarify how it works.

If “Passive mode” always outputs “N/A,” it means that the measured power system has relatively stable loads, and passive methods cannot yield reliable results. In this way, active methods can be used by plugging the proposed device of the disturbance generator into one of the downstream sockets to inject specific disturbances. The structure of the proposed device is illustrated in Figure 6.2.

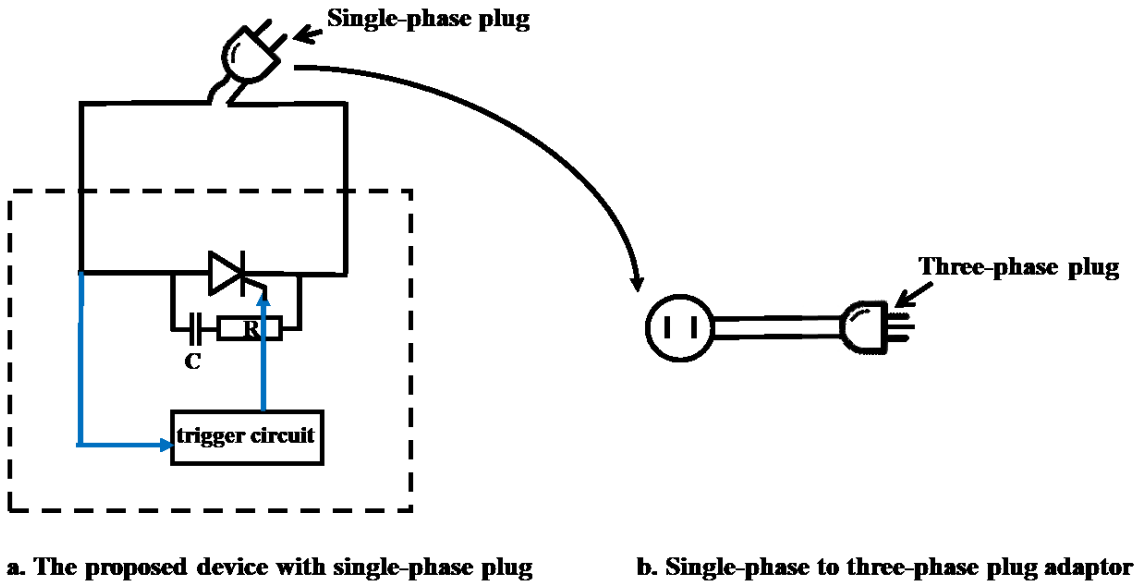

Figure 6.2 The topology for the proposed device

The proposed device mainly consists of the trigger circuit, the thyristor, and the plug. The trigger circuit will track the phase angle by PLL and trigger the thyristor by the firing angle of ten degrees. When the “run” button is pressed once, the thyristor will be triggered 50 times in ten seconds and then untriggered until the next button-press action. The thyristor is designed in the voltage level of 208 V for the use of both one-phase injection mode (suitable for single-phase sockets) and two-phase injection mode (suitable for three-phase sockets). As for the plug, a single-phase plug is connected to the thyristor along with an optional plug adaptor. As shown in Figure 6.2a, the single-phase plug is designed for single-phase sockets (120 V). Also, the plug adaptor shown in Figure 6.2b can convert the single-phase plug to

the three-phase plug for the use of three-phase sockets (208 V). Therefore, the use of the proposed disturbance generator is quite flexible.

6.4 Summary

An integrated impedance measurement system, combining both passive and active methods into “Zfinder” software along with a portable thyristor device, has been developed. The application of this software was introduced first. The integration of the proposed algorithms into “Zfinder” software was then demonstrated, and the topology of the proposed devices was presented as well.

Chapter 7 Conclusions and Future Work

This chapter summarizes the main findings of the thesis and provides suggestions for extending and improving this research.

7.1 Thesis Conclusions and Contributions

With the rapid development of renewable energy and distributed generators, new power electronic devices and other electrical equipment are being introduced into power systems. The modern power system has become more complicated than ever. The increasing significance of stability and power quality issues has led to the development of system impedance measurement techniques in recent years. However, the existing system impedance measurement methods are still far from perfect, and can be divided into two categories: passive methods and active methods. Passive methods do not need additional hardware, but accuracy and reliability are concerns. Active methods have better performance on accuracy and efficiency, but the devices needed for injecting disturbances are costly. Meanwhile, safety and power quality issues are also other concerns for active methods. Therefore, the objective of this thesis is to propose solutions that would be easy to implement and adaptive to different conditions.

In this thesis, several algorithms are proposed for the system impedance measurement. The main conclusions and contributions of the thesis are summarized as follows:

- A technique of estimating the system impedance using natural disturbances is proposed. It consists of two methods where each of them deals with large disturbances and small disturbances, respectively. This technique increases the efficiency and expands the application scope of passive system impedance measurement methods.

- A technique of estimating the system impedance using intentional disturbances is proposed. It uses a portable thyristor-based device to create a controlled short-circuit downstream and extract the impedance based on this unique disturbance. This technique improves the flexibility of active system impedance measurement methods, and it can work as a backup method for customer facilities that have very little load fluctuations.

- An integrated impedance measurement system is proposed by combining the previous two techniques. It consists of software embedded with algorithms and a portable thyristor-based device. This system can estimate the supply system impedance at the PCC by inputting the waveform data collected by PQ monitors.

7.2 Suggestions for Future Work

The research work presented in this thesis can be extended in the following directions:

- As discussed in section 4.4.2, in practical use, the firing angle of the proposed disturbance generator should be gradually reduced to increase the resulting pulse current until the corresponding threshold is reached. Therefore, a current threshold should be determined according to the standards or requirements of the proposed device's target market as a stop criterion, and a module should be designed to measure the resulting pulse current. How to achieve these goals still need further research.

- As discussed in section 6.2, the "Passive mode" is designed for customers with sufficient downstream natural disturbances, and the "Active mode" should work as a backup method for customers having stable loads. There is a need to research and clarify if the active method can still be used when the system has a lot of small disturbances.
- The supply system impedance measurement can be extended to harmonic impedance measurement. The information of harmonic impedances can be used to estimate the harmonic contribution of harmonic generating loads at the point of common coupling.

- The algorithms of the proposed method can be further improved; it is theoretically possible to realize the real-time monitoring of the system impedance.

Bibliography

[1] S. A. Arefifar, "Online Measurement and Monitoring of Power System Impedance and Load Model Parameters," Ph.D dissertation, University of Alberta, Edmonton, 2010.

[2] M. Nagpal, W.Xu, and J. Sawada, "Harmonic impedance measurement using three-phase transients," *IEEE Trans. Power Del.*, vol. 13, no. 1, pp. 272–277, Jan. 1998.

[3] W. Xu, E. E. Ahmed, X. Zhang, and X. Liu, "Measurement of network harmonic impedances: Practical implementation issues and their solutions," *IEEE Trans. Power Del.*, vol. 17, no. 1, pp. 210–216, Jan. 2002.

[4] R. Langella and A. Testa, "A new method for statistical assessment of the system harmonic impedance and of the background voltage distortion," presented at the Int. Conf. Probabilistic Meth. Appl. Power Syst., Stockholm, Sweden, Jun. 2006.

[5] S.A. Arefifar and W. Xu, "Online Tracking of Power System Impedance Parameters," *IEEE Trans. Power Del.*, vol. 24, no.4, October 2009, pp.1781-1788.

[6] S.M. Abdelkader and D.J. Morrow, "Online Tracking of Thevenin Equivalent Parameters Using PMU Measurements," *IEEE Transactions on Power Systems*, vol. 27, no.2, May 2012, pp.975-983.

[7] Hui, J., Yang, H., Lin, S., et al., "Assessing utility harmonic impedance based on the covariance characteristic of random vectors," *IEEE Trans. Power Del.*, 2010, 25, (3), pp. 1778–1786.

[8] H. Jin, W. Freitas, J.C.M. Vieira, H. Yang, "Utility Harmonic Impedance Measurement Based on Data Selection," *IEEE Trans. Power Del.*, vol. 27, no.4, October 2012, pp.2193-2202.

[9] F. Karimzadeh, S. Esmaeili, S. H. Hosseinian, "A novel method for noninvasive estimation of utility harmonic impedance based on complex independent component analysis," *IEEE Trans. Power Del.*, vol. 30, no. 4, pp. 1843-1852, Aug. 2015.

[10] F. Karimzadeh, S. Esmaeili, S. Hossein Hosseinian, "Method for determining utility and consumer harmonic contributions based on complex independent component analysis," *IET Generation Transmission & Distribution*, vol. 10, pp. 526-534, Feb. 2016.

[11] Robert, A., Deflandre, T., Gunther, E., Bergeron, R., Emanuel, A., Ferrante, A., Finlay, G.S., Gretsch, R., Guarini, A., Gutierrez Iglesias, J.L., Hartmann, D., Lahtinen, M., Marshall, R., Oonishi, K., Pincella, C., Poulsen, S., Ribeiro, P., Samotyj, M., Sand, K., Smid, J., Wright, P., and Zhelesko, Y.S., "Guide for assessing the network harmonic

impedance," Proc. 14th Int. Conf. Electricity Distribution, Brussels, Belgium, June 1997, Part 1. Contributions, pp. 3/1–310.

[12] W. Wiechowski, "Validation techniques of network harmonic models based on switching of a series linear component and measuring resultant harmonic increments," presented at the 9th Int. Conf. Elect. Power Qual. Utilisation, Barcelona, Spain, 2007.

[13] M. Sumner, B. Palethorpe, D. W. P. Thomas, "Impedance measurement for improved power quality—Part 1: The measurement technique," *IEEE Trans. Power Del.*, vol. 19, no. 3, pp. 1442-1448, Jul. 2004.

[14] Bendel, C., Nestle, D., and Viotto, M., "Safety aspects of decentralized net-coupled electrical generators," [Online]. Available: http://www.iset.uni-kassel.de/abt/FB-A/publication/2004/Safety%20Aspects%20of%20NetCoupled%20DER%20Bendel%20Nestle%20Viotto%20Press.pdf.

[15] Sumner, M., Abusorrah, A., Thomas, D., and Zanchetta, P., "Improved power quality control and intelligent protection for grid connected power electronic converters, using real time parameter estimation," Proc. IEEE/IAS Annual Meeting, Florida, USA, October 2006, vol. 4, pp. 1709–1715.

[16] W. Wang, E. E. Nino, W. Xu, "Harmonic Impedance Measurement using a Thyristor-Controlled ShortCircuit," *IET publication on Generation Transmission Distribution*, vol. 1, no. 5, pp. 707-713, 2007.

[17] D. Borkowski and A. Bien, "Improvement of Accuracy of Power System Spectral Analysis by Coherent Resampling," *IEEE Trans. Power Del.*, vol. 24, no. 3, pp. 1004-1013, July 2009.

[18] M. Karimi-Ghartemani and M. R. Iravani, "Measurement of harmonics/inter-harmonics of time-varying frequencies," *IEEE Trans. Power Del.*, vol. 20, no. 1, pp. 23-31, Jan. 2005.

[19] B. Li, Y. Jing, W. Xu, "A Generic Waveform Abnormality Detection Method for Utility Equipment Condition Monitoring," *IEEE Trans. Power Del.*, vol. 32, no. 1, pp. 162-171, Feb. 2017.

[20] W. Wang, "Power-Electronics-Based Online Signaling Techniques and Their Applications to Power Systems," Ph.D dissertation, University of Alberta, Edmonton, 2008.

[21] Hyvarinen, A., Oja, E., "Independent component analysis: algorithms and applications," *Neural Netw.*, 2000, 13, (4–5), pp. 411–430.

[22] Sioe T. Mak, Thomas G. Moore, "TWACS, A New Viable Two-Way Automatic Communication System for Distribution Networks. Part II: Inbound Communication", *IEEE Transactions on Power Apparatus and Systems,* vl03, n8, pp.2141-2147, Aug. 1984.

[23] Sioe T. Mak, "A new method of generating TWACS type outbound signals for communication on power distribution networks", *IEEE Transactions on Power Apparatus and Systems*, vl03, no. 8, pp.2134-40, Aug. 1984.

[24] F. Karimzadeh, S. Esmaeili, S. Hossein Hosseinian, "Method for determining utility and consumer harmonic contributions based on complex independent component analysis", *IET Generation Transmission & Distribution*, vol. 10, pp. 526-534, Feb. 2016.

[25] E. Bingham and A. Hyvärinen, "A fast fixed-point algorithm for independent component analysis of complex-valued signals," *Int. J. NeuralSyst.*, vol. 10, pp. 1–8, 2000.

[26] E. Gursoy, "Independent Component Analysis for Harmonic Source Identification in Electric Power Systems," Ph.D dissertation, Drexel University, 2007.

[27] Karimzadeh Farzad, S. Esmaeili, S. H. Hosseinian, "A Novel Method for Noninvasive Estimation of Utility Harmonic Impedance Based on Complex Independent Component Analysis", *IEEE Trans. Power Delivery*, vol. 30, pp. 1843-1852, Aug. 2015.

[28] Y. Wang, "Investigation, Identification and Mitigation of Harmonic Distortions in Power Systems," Ph.D dissertation, University of Alberta, Edmonton, 2017.

[29] Zhao Xi, H. Yang, "A New Method to Calculate the Utility Harmonic Impedance Based on FastICA", *IEEE Trans. Power Delivery*, vol. 31, pp. 381-388, Feb. 2016.

[30] M. R. Spiegel, L. J. Stephens, *Schaum's Outlines Statistics*, 4th ed., US: McGraw Hill, 2008.

[31] M. M. William, L. S. Terry, *Statistics for Engineering and the Sciences*, 5th ed., US: CRC Press, 2007.

[32] S. A. Glantz, B. K. Slinker, T. B. Neilands, *Primer of Applied Regression & Analysis of Variance*, 3rd ed., US: McGraw Hill, 2016.

[33] K. A. Aho, *Foundational and Applied Statistics for Biologists*, 1st ed., US: CRC Press, 2014.

[34] L. B. Robert, *Electronic Devices and Circuit Theory*, 11th ed., US: Pearson Education, 2012.

[35] H. John, B. Keith, I. M. Smith, *Electrical and Electronic Technology*, 10th ed., US: CRC Press, 2008.

[36] M.V. Chellappan, M.H. Todorovic and P.N. Enjeti, "Fuel Cell Based Battery-Less UPS System," Industry Applications Society Annual Meeting, 2008, IAS'08, pp. 1-8.

[37] IEEE 13 bus test case, [Online]. Available: http://sites.ieee.org/pes-testfeeders/resources/.

[38] Test System 4: A 10-Node Unbalanced Commercial Distribution System, [Online]. Available: http://grouper.ieee.org/groups/harmonic/simulate/download.htm.

[39] T. A. Short, *Electric Power Distribution Handbook*, 2nd ed., US: CRC Press, 2014.

[40] Ralph Baeza, Selecting sizing transformers for commercial buildings, 2011, [Online]. Available: https://www.csemag.com/articles/selecting-sizing-transformers-for-commercial-buildings/.

[41] CANDURA Instrument, PQPro™& PQPro™-HAUser's Guide, 2018, [Online]. Available: https://www.candura.com/files/PQPro_Users_Guide.pdf.

[42] J. Eriksson and V. Koivunen, "Identifiability, separability, and uniqueness of linear ICA models," *IEEE Signal Processing Letters,* Vol. 11, Issue 7, Jul 2004, pp. 601-604.

[43] J. Eriksson and V. Koivunen, "Complex random vectors and ICA models: Identifiability, uniqueness, and separability," *IEEE Transactions on Information Theory,* Vol. 52, Issue 3, Mar 2006, pp. 1017-1029.

[44] A. Papoulis and S. U. Pillai, *Probability, random variables, and stochastic processes*, 4th ed. Boston: McGraw-Hill, 2002.

[45] P. Comon, "Blind identification and source separation in 2 x 3 under-determined mixtures," *IEEE Transactions on Signal Processing,* Vol. 52, Issue 1, Jan 2004, pp. 11-22.

[46] P. Comon and M. Rajih, "Blind identification of complex under-determined mixtures," *Independent Component Analysis and Blind Signal Separation,* Vol. 3195, 2004, pp. 105-112.

[47] T. W. Lee, M. S. Lewicki, M. Girolami, and T. J. Sejnowski, "Blind source separation of more sources than mixtures using overcomplete representations," *IEEE Signal Processing Letters,* Vol. 6, Issue 4, Apr 1999, pp. 87-90.

Appendix

Appendix A Determination of Impedance's True Value in Experiments

To obtain a relatively accurate true value of the added impedance, 2 PQ pro instruments are used to measure quantities of three-phase voltage and current at point A and point B.

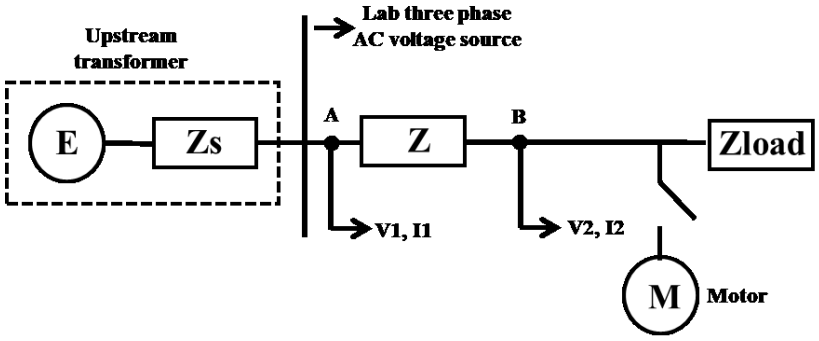

Figure A.1

In this way, we can get respective positive-sequence voltage phasor V_1, V_2 and current phasor I_1, I_2. Then, we can calculate the added impedance Z by the following equations:

$$\begin{aligned} Z + Zload &= \frac{V_1}{I_1} \\ Zload &= \frac{V_2}{I_2} \end{aligned} \tag{A.1}$$

Then we can get:

$$Z = \frac{V_1}{I_1} - \frac{V_2}{I_2} \tag{A.2}$$

When the induction motor is not connected, Z is (93.3900 + 4.8805i) - (86.7655 + 3.0439i) = 6.6245 + 1.8366i Ohms. In fact, 6 Ohms slide resistance is used for Z and 83 Ohms slide resistance for *Zload*. Note that 6 Ohms and 83 Ohms are obtained by the multimeter, which

is not very accurate. Meanwhile, the existence of mutual inductance is reasonable for this kind of old slide resistance.

When the induction motor is switched on, Z is (7.8562 +10.3322i) - (1.7517 + 9.4894i) = 6.1045 + 0.8428i Ohms. The reason for the impedance difference is that the current is larger when the induction motor is connected. Then the temperature is increased, and the impedance is reduced.

As the algorithm of system impedance measurement uses both the pre-disturbance and post-disturbance quantities, the reference value of the added impedance can be estimated by averaging these two impedances: (6.6245 + 1.8366i+6.1045 + 0.8428i) / 2 = 6.3645 + 1.3397i Ohms. The magnitude is abs(6.3645 + 1.3397i) = 6.5040 Ohms.

Appendix B Error Analysis of Phase Lock Loop

As the LD method is assuming a constant system side, the estimated results of the system impedance are very sensitive to the phase difference and frequency variation. Therefore, the PLL function in PQ monitors (e.g., *PQPro*™) will lead to significant errors in this algorithm.

To illustrate this issue, 2 *PQPro*™ instruments are used to measure three-phase voltage and current at point A and point B.

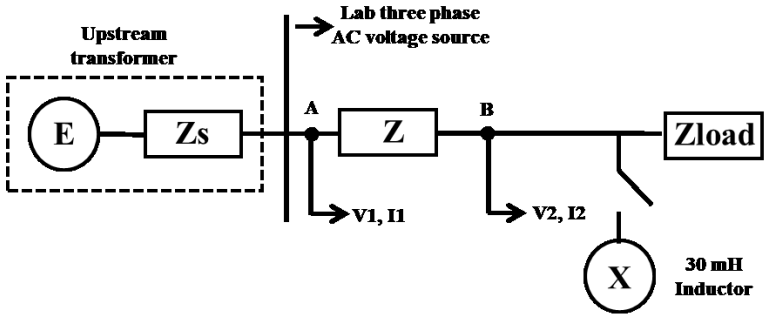

Figure B.1

When the induction motor is not connected, the measured positive-sequence voltage phasor V_1 is $111.7602 \angle 32.45°$ V and the measured positive-sequence current phasor I_1 is $1.2881\angle 30.36°$ A for point A. Meanwhile, the measured positive-sequence voltage phasor V_2 is $89.1232\angle 30.8730°$ V and the measured positive-sequence current phasor I_2 is $9.2933\angle -48.6654°$ A for point B.

When the induction motor is switched on, the measured positive-sequence voltage phasor V_1 is $111.7602 \angle 32.4511°$ V and the measured positive-sequence current phasor I_1 is $1.2881\angle 30.3634°$ A for point A. Meanwhile, the measured positive-sequence voltage phasor V_1 is $89.1232\angle 30.8730°$ V and the measured positive-sequence current phasor I_1 is $9.2933\angle -48.6654°$ A for point B.

As shown in Table B.1, we can see that the PLL function of the PQ pro instrument is using voltage phasor as the reference. In this way, the phase of voltage phasors is locked. Two different *PQPro*™ are used for the measurement, so the locked phase is different: one is around 30 degrees and the other is about -22 degrees.

Table B.1

	Point A		Point B	
	Voltage (V)	Current (A)	Voltage (V)	Current (A)
Pre-disturbance	111.76∠32.45°	1.29∠30.36°	120.16∠-22.71°	1.29∠-25.77°
Post-disturbance	89.12∠30.87°	9.29∠-48.67°	119.48∠-22.43°	9.29∠-75.04°

To better illustrate the errors caused by the PLL function, the measured data is modified by correcting the difference of the locked phase between two *PQPro*™ as shown in Table B.2.

Table B.2

	Point A		Point B	
	Voltage (V)	Current (A)	Voltage (V)	Current (A)
Pre-disturbance	111.76∠32.45°	1.29∠30.36°	120.16∠32.45°	1.29∠29.39°
Post-disturbance	89.12∠30.87°	9.29∠-48.67°	119.48∠30.87°	9.29∠-21.74°

The basic idea is that point A and point B are series-connected, so the current phasor should be the same. As shown in Figure B.1, the current phasors of point A and point B are almost the same for pre-disturbance. However, there is a large phase difference (around 27 degrees) between current phasors of point A and point B for post-disturbance. It is not reasonable in both theory and practice. In addition, the calculated results of system impedance are presented to clarify the error level. Without phase compensation, the system impedance can be calculated as follows:

$$Z1 = \left| -\frac{V1_{pre} - V1_{post}}{I1_{pre} - I1_{post}} \right| = \left| -\frac{111.76\angle 32.45° - 89.12\angle 30.87°}{1.29\angle 30.36° - 9.29\angle -48.67°} \right| = 2.4972 \qquad \text{(B.1)}$$

It can be seen that the calculated system impedance is much smaller than the reference value. The error level is about 61.61%.

With rough phase compensation, we can anticlockwise shift pre-disturbance quantities by 27 degrees. Then, the system impedance can be calculated as follows:

$$Z1 = \left| -\frac{V1_{pre} - V1_{post}}{I1_{pre} - I1_{post}} \right| = \left| -\frac{111.76\angle 59.45° - 89.12\angle 30.87°}{1.29\angle 57.36° - 9.29\angle -48.67°} \right| = 5.58 \qquad \text{(B.2)}$$

It can be seen that the calculated system impedance is much closer to the reference value. The error level is about 14.21%.

In this way, the PLL function is recommended to be closed during measurement and to compensate the phase difference caused by frequency variation using the method in section 2.1.2.

Appendix C Monte-Carlo Simulation

As discussed in previous chapters, system variation level ρ_E and the size of voltage change ρ_V both have an influence on the error level of system impedance measurement error. To evaluate this influence, a Monte-Carlo simulation is conducted as follows.

As discussed in [19], noise in power systems can be modelled by utilizing Gaussian distribution. Load impedance is changed to create a disturbance with ρ_V=βρ_E voltage change. The pre-disturbance load impedance is marked as Z1, and the post-disturbance load impedance is marked as Z2. The detailed parameters in the simulation are listed in Table C.1.

Table C.1: Parameters of components in simulation

Sign	Name	Parameter
E0	Base voltage level	25 kV
ρ_E	System variation level	Variable (0.1%-1%)
β	Voltage-system ratio	Variable (0.2-5)
E	System source voltage	E0+normrand(0, ρ_EE0)
Zs	System impedance	0.2+2j Ohms
Z1	Pre-disturbance load impedance	26+5j Ohms
Z2	Post-disturbance load impedance	(1-βρ_EE0)×Z1×Zs/(Z+ βρ_EE0×Z1)

As seen from the above table, there are two possible factors (ρ_E and β) affecting the error level of system impedance measurement. To evaluate their influence separately, one variable is fixed and the other varies.

When β is fixed, the error level of system impedance measurement is not affected by system variation level ρ_E. For example, when β is fixed as 3, the relationship between error level and ρ_E is shown in Figure C.1.

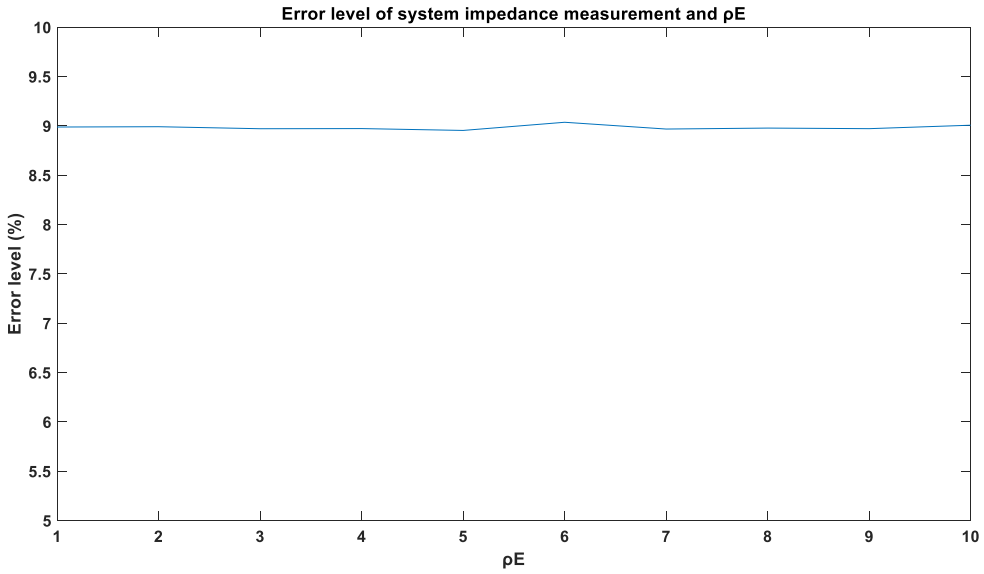

Figure C.1 The relationship between the error level and ρ_E

When ρ_E is fixed, the relationship between error level and voltage-system ratio β is shown in Figure C.2.

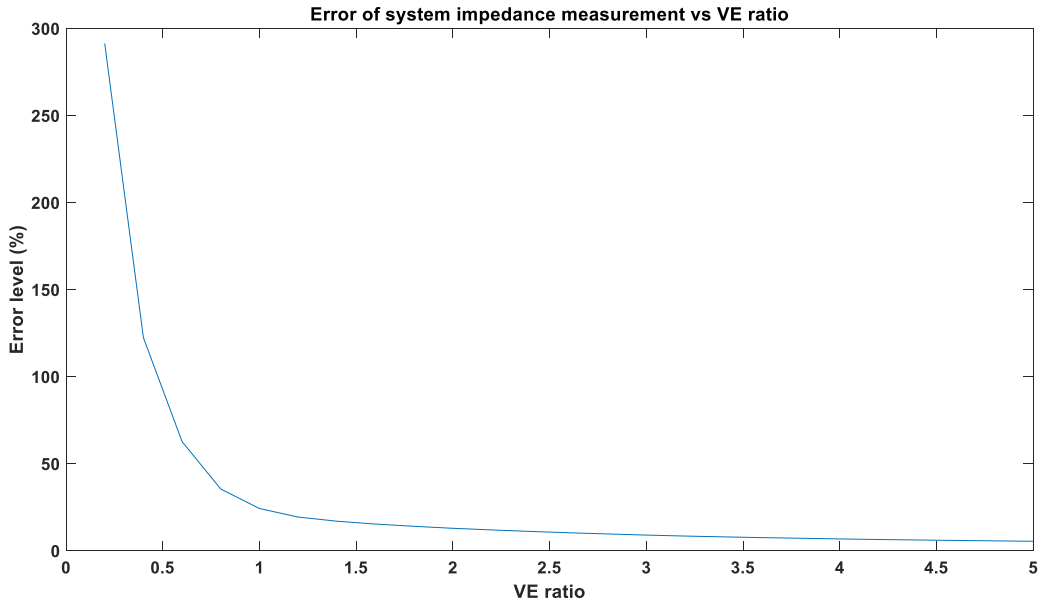

Figure C.2 The relationship between the error level and VE ratio

Using a curve-fitting tool in MATLAB, this relationship can be expressed by (C.1) with the goodness of fit in Table C.2.

$$Error\ level\ (\%) = \frac{29.79\beta^2 - 40.6\beta + 20.45}{\beta^3 - 1.097\beta^2 + 0.5127\beta - 0.02026} \quad (C.1)$$

Table C.2: Goodness of fit

No.	Name	Value
1	SSE	0.6744
2	R-square	1
3	Adjusted R-square	1
4	RMSE	0.1884

Please note that the above relationship is obtained by setting the system's voltage level as 25 kV. To evaluate the impacts of the voltage level on this relationship, other cases with different voltage levels are investigated.

The relationship obtained by setting the system's voltage level as 14.4 kV is presented as follows:

$$Error\ level\ (\%) = \frac{29.71\beta^2 - 40.68\beta + 20.38}{\beta^3 - 1.107\beta^2 + 0.5159\beta - 0.02084} \quad (C.2)$$

The relationship obtained by setting the system's voltage level as 4.16 kV is presented as follows:

$$Error\ level\ (\%) = \frac{29.89\beta^2 - 41\beta + 20.84}{\beta^3 - 1.099\beta^2 + 0.5196\beta - 0.02048} \quad (C.3)$$

As we can see, the values of parameters in the relationship are very close. So the voltage level almost has no impact on the proposed relationship. The main reason is that ρ_V, β, ρ_E are all dimensionless quantities, the voltage level has no impact on these values.

Appendix D Fuse time-current curves

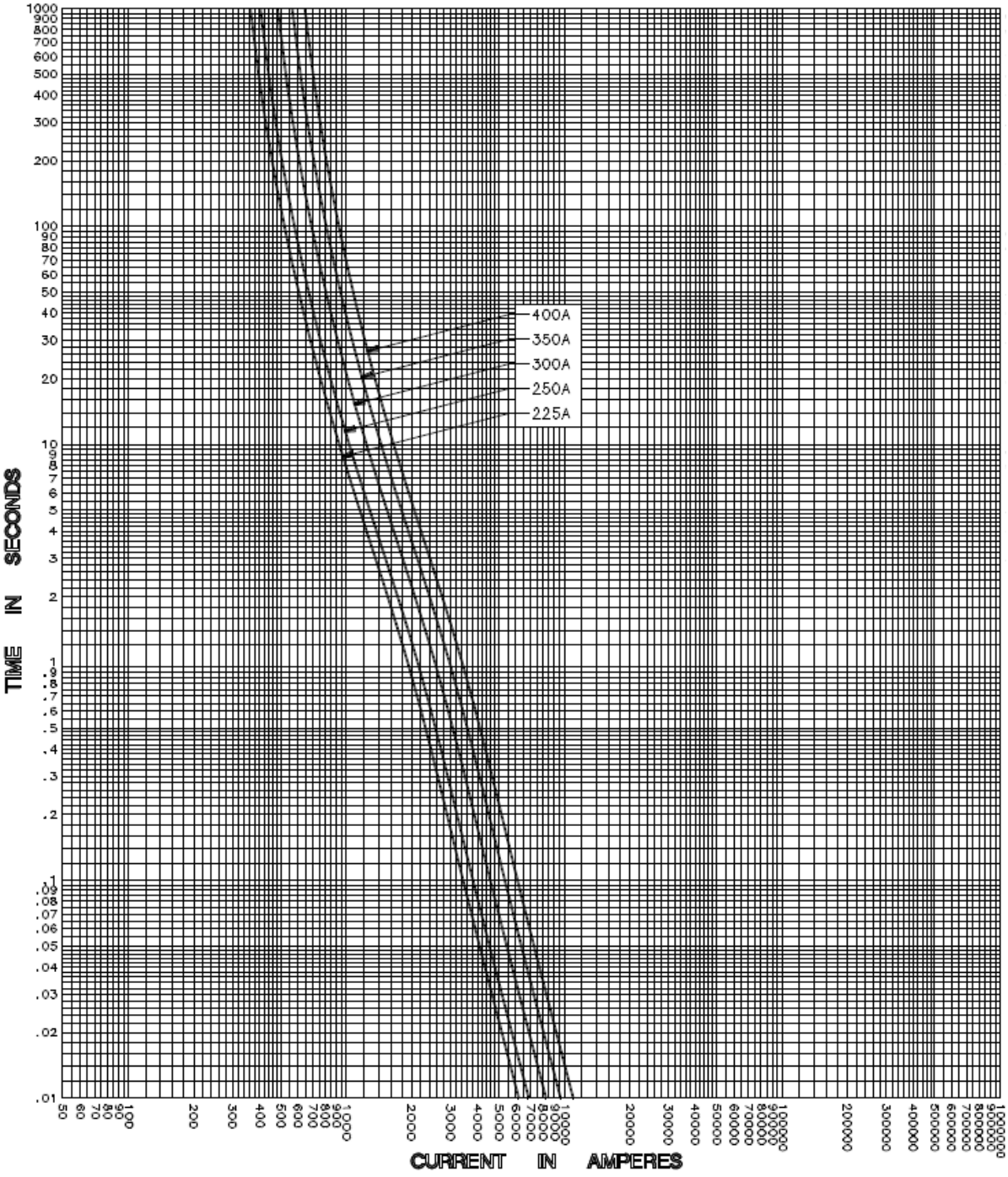

Appendix E Impedances of Single-Conductor Copper Power Cables

TABLE 3.16

Impedances of Single-Conductor Copper Power Cables

Conductor Size	R_1	X_1	R_0	X_0	R_S	X_S
Flat spacing with a 7.5-in. separation						
2	0.2083	0.1029	0.5108	0.4401	0.3092	0.2153
1	0.1671	0.0991	0.4718	0.4267	0.2687	0.2083
1/0	0.1334	0.0965	0.4405	0.4115	0.2358	0.2015
2/0	0.1082	0.0938	0.4171	0.3967	0.2112	0.1948
3/0	0.0871	0.0911	0.3975	0.3794	0.1906	0.1872
4/0	0.0705	0.0884	0.3816	0.3626	0.1742	0.1798
250	0.0607	0.0862	0.3719	0.3471	0.1644	0.1732
350	0.0461	0.0823	0.3558	0.3181	0.1493	0.1609
500	0.0352	0.0782	0.3411	0.2891	0.1372	0.1485
750	0.0272	0.0732	0.3241	0.2490	0.1261	0.1318
1000	0.0234	0.0699	0.3104	0.2196	0.1191	0.1198
Triplex						
2	0.2032	0.0508	0.5707	0.4642	0.3257	0.1886
1	0.1619	0.0477	0.5301	0.4480	0.2846	0.1811
1/0	0.1281	0.0460	0.4966	0.4295	0.2509	0.1738
2/0	0.1028	0.0442	0.4709	0.4116	0.2255	0.1667
3/0	0.0816	0.0426	0.4485	0.3910	0.2039	0.1587
4/0	0.0649	0.0409	0.4299	0.3713	0.1866	0.1510
250	0.0551	0.0398	0.4175	0.3532	0.1759	0.1442
350	0.0403	0.0377	0.3962	0.3202	0.1589	0.1319
500	0.0292	0.0355	0.3765	0.2882	0.1450	0.1197
750	0.0211	0.0333	0.3524	0.2450	0.1315	0.1039
1000	0.0173	0.0322	0.3336	0.2142	0.1227	0.0929

Note: Impedances, Ω/1000 ft (× 5.28 for Ω/mi or × 3.28 for Ω/km). Resistances for a conductor temperature = 90°C and a shield temperature

Appendix F Theory of ICA

ICA is the statistical signal processing technique to recover the latent variables or source signals from observed mixtures without knowing the way the source signals are mixed [24]. It can be extended to the separation of complex-valued signals, which facilitates the power system analysis in the frequency domain [25].

In the complex ICA model, the observed signals based on complex values are expressed as a linear combination of source signals based on complex values as follows.

$$\boldsymbol{O} = \boldsymbol{MS} \tag{F.1}$$

Where $\boldsymbol{O}$ is the observed signals matrix with $m \times k$ dimensions, $\boldsymbol{S}$ is the source signals matrix with $n \times k$ dimensions, and $\boldsymbol{M}$ is an unknown constant mixing matrix. Generally, k is the number of measured samples, m is the number of measured channels, and n is the number of the latent independent source signals.

Before applying the complex ICA, three basic assumptions should be satisfied [26]:

1. The source signals are mutually statistically independent.
2. At maximum, one source is Gaussian distributed.
3. The mixing matrix has full column rank.

The detailed explanation of these three assumptions can be found in [44]-[47]. Actually, the most important thing in estimating the ICA model is nongaussianity [21]. The aim of the ICA technique is to search a separating matrix $\boldsymbol{W}$ that maximizes the nongaussianity of $\boldsymbol{W^T O}$. And then, the source signals can be recovered as follows.

$$\widehat{\boldsymbol{S}} = \boldsymbol{W}^T \boldsymbol{O} \tag{F.2}$$

where matrix $\widehat{\boldsymbol{S}}$ is the estimation of source signals, and superscript T stands for Hermitian transpose. The detailed iterative process to maximum the nongaussianity of the original sources can be found in [25].

Before searching a separating matrix $\boldsymbol{W}$, the preprocessing of the observed signals $\boldsymbol{O}$ is required. The preprocessing steps mainly consist of centring and whitening [24]. The centring process makes the observed signals zero-mean, and the whitening process linearly transforms the observed variables such that the transformed variables are uncorrelated and their variances equal unity. The whitening process can be done by the following equation.

$$\widetilde{\boldsymbol{O}} = \boldsymbol{\Lambda}^{-1/2}\mathbf{V}^{\mathrm{T}}\boldsymbol{O} \tag{F.3}$$

where $\widetilde{\boldsymbol{O}}$ is the whitened observed signals, $\boldsymbol{\Lambda}$ is the diagonal matrix of eigenvalues of $\mathrm{E}\{\boldsymbol{O}\boldsymbol{O}^{\mathrm{T}}\}$, and $\boldsymbol{V}$ is the orthogonal matrix of eigenvectors of $\mathrm{E}\{\boldsymbol{O}\boldsymbol{O}^{\mathrm{T}}\}$ where symbol E denotes the statistical expectation.

After estimating the separating matrix $\boldsymbol{W}^{T}$ with whitened observed data, the source signals can be calculated from the following equation.

$$\widehat{\boldsymbol{S}} = \boldsymbol{W}^{T}\widetilde{\boldsymbol{O}} \tag{F.4}$$

For better illustration, the mixing and separation process of ICA is presented in Figure F.1.

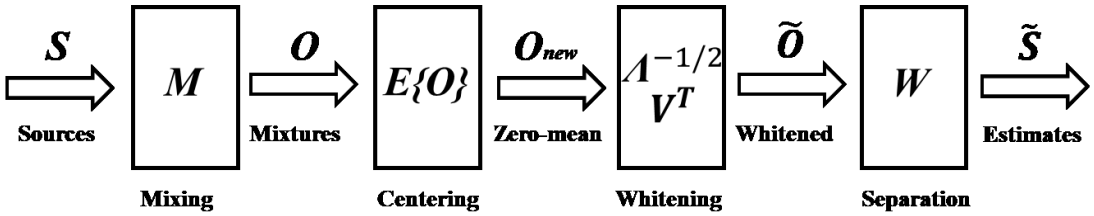

Figure F.1 The mixing and separation process of ICA

There are two indeterminacies in the estimation of the ICA model. These indeterminacies are due to the fact that both the sources $\boldsymbol{S}$ and the way the sources are mixed, $\boldsymbol{A}$, are unknown. Estimation by ICA is unique up to a scaling and permutation [42]-[43].

1. Scaling Indeterminacy. A non-singular diagonal matrix $\boldsymbol{K}$ and its inverse $\boldsymbol{K}$-1 can be multiplied by the mixing matrix $\boldsymbol{M}$ without changing the measurement matrix $\boldsymbol{O}$.

$$\boldsymbol{O} = \boldsymbol{M}\boldsymbol{K}\boldsymbol{K}^{-1}\boldsymbol{S} = \boldsymbol{M}'\boldsymbol{S}' \tag{F.5}$$

Equation (F.5) shows that the magnitudes of the sources cannot be estimated uniquely.

Scaling indeterminacy can be removed by setting all the sources with the same magnitude, i.e. unit variance or using prior information about the sources or the mixing matrix [26].

2. Ordering Indeterminacy. The order of the sources can be changed and labelled differently (first, second …) without affecting the estimation result. Multiplying the mixing matrix $\boldsymbol{M}$ by a permutation matrix $\boldsymbol{P}$ and its inverse $\boldsymbol{P}$-*1*, which has only one nonzero element of value 1 in each row and column, will not change the measurement matrix $\boldsymbol{O}$. In the complex case, the non-zero element is a unit length complex number, and this indeterminacy pertains to the phases [26].

$$\boldsymbol{O} = \boldsymbol{MPP^{-1}S} = \boldsymbol{M''S''} \tag{F.6}$$

Appendix G Simulation Block of System Variations

To simulate the variations of voltage quantities, we can use breakers to switch on/off some loads at the measuring point. The switch-on events of loads will lead to a decrease in voltage quantities and the switch off events of loads will lead to an increase in voltage quantities. For example, the positive-sequence voltage's RMS value of cycle 2 decreases by 0.03% compared to that of cycle 1, and negative-sequence voltage's RMS value of cycle 2 increases by 0.01%. Then, we can switch on a 1.97 KVA single-phase load and a 3.94 KVA three-phase load. The equivalent circuit of the simulation case is shown in Figure G.1, and calculations are explained as follows.

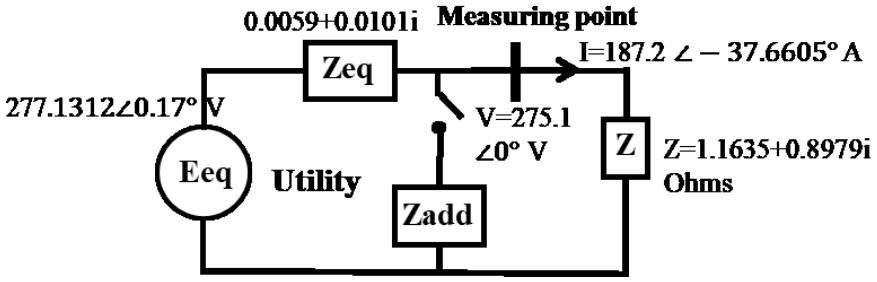

Figure G.1 Equivalent circuit

As shown in Figure G.1, the switch on/off event of the load will decrease/increase the current, and then the voltage drop across Zeq will decrease/increase respectively. A single-phase load is added first to meet the requirements of negative-sequence variations, and then a three-phase load is added to meet the requirements of positive-sequence variations.

Single-phase load calculation is presented as follows:

$$V = 275.1\angle 0°V \times (1-0.01\%) = 275.0725\angle 0°V$$

$$I = \frac{E_{eq}-V}{Z_{eq}} - \frac{V}{Z} = \frac{277.1312\angle 0.17°V - 275.0725\angle 0°V}{0.0059+0.0101i\Omega} - \frac{275.0725\angle 0°V}{1.1635+0.8979i\Omega} = (1.2311\text{-}2.0889\text{i})A$$

$$S_{Zadd} = 3\times(1.2311\text{+}2.0889\text{i})A \times 275.0725\angle 0°V = (1.016+1.724i)KVA$$

The three-phase load calculation is presented as follows:

$$V = 275.1\angle 0°V \times (1-2\times 0.01\%) = 275.045\angle 0°V$$

$$I = \frac{E_{eq}-V}{Z_{eq}} - \frac{V}{Z} = \frac{277.1312\angle 0.17°V - 275.045\angle 0°V}{0.0059+0.0101i\Omega} - \frac{275.045\angle 0°V}{1.1635+0.8979i\Omega} = (2.4327\text{-}4.1318\text{i})A$$

$$S_{Zadd} = 3\times(2.4327\text{+}4.1318\text{i})A \times 275.045\angle 0°V = (2.0073+3.4093i)KVA$$

Then the single-phase load and three-phase load are switched on by a breaker at the beginning of the fourth cycle. The resulting variations of positive-sequence voltage and negative-sequence voltage are plotted in Figure G.2.

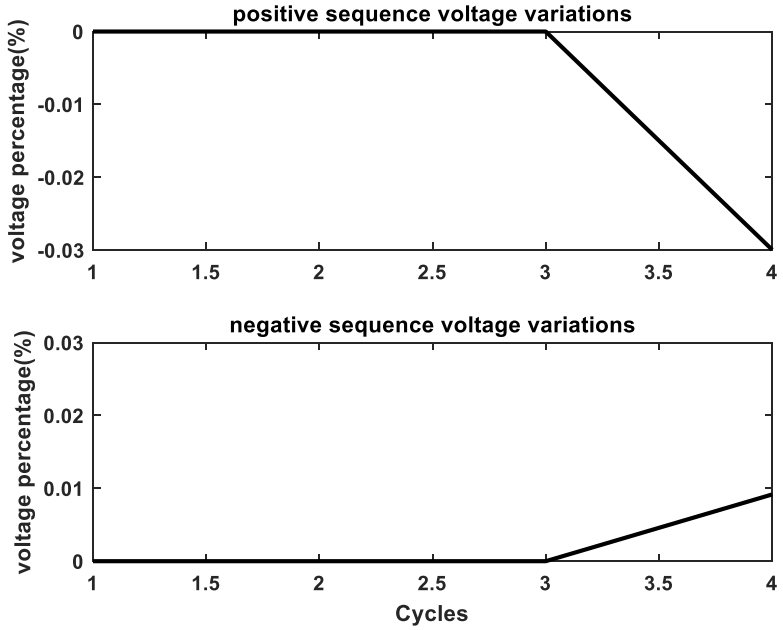

Figure G.2 Variations of positive-sequence voltage and negative-sequence voltage

In conclusion, two breakers and two loads are needed to simulate the variations of one cycle, which is called one unit, as shown in Figure G.3. For the simulation case in this thesis, the simulation lasts for 200 cycles, so 200 units are added.

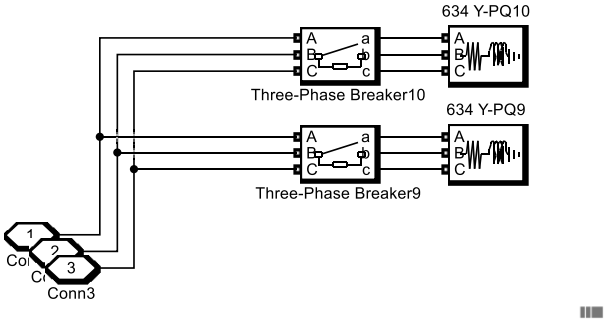

Figure G.3 One unit